BIOPRINTED CARDIAC PATCH COMPOSED OF CARDIAC PROGENITOR CELLS AND EXTRACELLULAR MATRIX FOR HEART REPAIR AND REGENERATION

A Dissertation
Presented to
The Academic Faculty

by

Donald Bejleri

In Partial Fulfillment
of the Requirements for the Degree
Doctor of Philosophy in Biomedical Engineering in the
Wallace H. Coulter Department of Biomedical Engineering

Georgia Institute of Technology and Emory University
December 2020

BIOPRINTED CARDIAC PATCH COMPOSED OF CARDIAC PROGENITOR CELLS AND EXTRACELLULAR MATRIX FOR HEART REPAIR AND REGENERATION

Approved by:

Dr. Michael E. Davis, Advisor
School of Biomedical Engineering
Georgia Institute of Technology

Dr. Johnna S. Temenoff
School of Biomedical Engineering
Georgia Institute of Technology

Dr. Manu O. Platt
School of Biomedical Engineering
Georgia Institute of Technology

Dr. Hee Cheol Cho
School of Biomedical Engineering
Georgia Institute of Technology

Dr. Julie A. Champion
School of Chemical and Biomolecular Engineering
Georgia Institute of Technology

Date Approved: [August 14th, 2020]

This thesis is dedicated to my fiancé, family, and friends, as well as all the people who are struggling in the face of disease and injustice.

ACKNOWLEDGEMENTS

I would like to thank my fiancé Lisa, my parents Mirela and Ilir, my brother Eric, and all my friends and family for their continued support.

I would like to thank my advisor, Dr. Michael E. Davis, for supporting me throughout my graduate studies, in regards to moving my project forward, helping me grow as a scientist/engineer by allowing me to independently work while providing critical feedback, and finding ways forward in achieving goals when things did not go as planned.

I would like to thank my committee members, Dr. Johnna Temenoff, Dr. Manu Platt, Dr. Julie Champion, and Dr. He Cheol Cho, for providing informative and effective feedback on improving the project. I would also like to thank Dr. Karen Christman and her lab, particularly Dr. Roberto Gaetani, for providing critical biomaterials used in this work and expertise in working with extracellular matrix biomaterials. Additionally, I would like to thank all the past and present members of the Davis lab for their immense support throughout my project, both intellectually and physically. This project would not have been completed without my fellow lab members supporting the work by discussing results, developing protocols, and running experiments/data acquisition.

Thank you all!

TABLE OF CONTENTS

LIST OF TABLES

LIST OF FIGURES

LIST OF SYMBOLS AND ABBREVIATIONS

ACTA-2	α-Smooth muscle actin
CAD	Computer-aided design
CD31	Platelet endothelial cell adhesion molecule
CDC	Cardiosphere-derived cell
cECM	Cardiac extracellular matrix
cFB	Cardiac fibroblast
CHD	Congenital heart defect/disease
Cx43	Connexin 43
CXCR4/7	C-X-C chemokine receptor type 4/7
dECM	Decellularized extracellular matrix
EC	Endothelial cell
EDD	End diastolic dimension
EdU	5-Ethynyl-2'-deoxyuridine
EF	Ejection fraction
EGF	Epidermal growth factor
ESC	Embryonic stem cell
ESD	End diastolic dimension
FGF	Fibroblast growth factor
FLT-1	Vascular endothelial growth factor receptor 1
GelMA	Gelatin methacrylate
HBSS	Hanks balanced salt solution
hCPC	Human cardiac progenitor cell

HGF	Hepatocyte growth factor
HIF-1	Hypoxia-inducible factor 1
HLHS	Hypoplastic left heart syndrome
HUVEC	Human umbilical vein endothelial cell
iPSC	Induced pluripotent stem cell
LV	Left ventricle
LVAD	Left ventricular assist device
MEF2C	Myocyte enhancement factor 2C
MI	Myocardial infarction
MMP	Matrix metalloproteinase
MSC	Mesenchymal stromal cell
MYH	β-Myosin heavy chain
NVP	1-Vinyl-2-Pyrrolidione
PAB	Pulmonary artery band
PCL	Polycaprolactone
pECM	Pericardical extracellular matrix
RA-Area	Right atrium area
RV	Right ventricle
Sca-1	Stem cell antigen 1
SDF-1	Stromal cell-derived factor 1
sECM	Skeletal extracellular matrix
sGAG	Sulfated glycosaminoglycan
SIS	Small intestinal submucosa
SMC	Smooth muscle cell
SSEA-1	Stage-specific embryonic antigen 1

TAPSE	Tricuspid annular plane systolic excursion
TEOA	Triethanolamine
TIMP	Tissue inhibitor of metalloproteinases
TMR	Transmyocardial revascularization
TNF-α	Tumor necrosis factor-α
UBM	Urinary bladder matrix
VE-Cad	Vascular endothelial cadherin
VEGF	Vascular endothelial growth factor
WGA	Wheat germ agglutinate

SUMMARY

Congenital heart defects (CHDs) are present in 8 of 1000 newborns, and palliative surgical therapy has increased survival rates. Despite improved outcomes, many children develop reduced cardiac function and go on to heart failure and transplantation. Human cardiac progenitor cell (hCPC) therapy has the potential to repair the pediatric myocardium through reparative factor release but suffers from limited hCPC retention and functionality. Decellularized cardiac extracellular matrix hydrogel (cECM) has been shown to improve heart function in adults while also improving CPC functionality in 2D and 3D culture. This work focuses on developing a bioprinted cardiac patch composed of native cECM and pediatric hCPCs, for use as an epicardial device in repairing the damaged myocardium. Cardiac patches are printed with bioinks composed of cECM, hCPCs, and gelatin methacrylate (GelMA). GelMA-cECM bioinks print uniformly with a homogeneous distribution of cECM and hCPCs. hCPCs maintain above 75% viability, and incorporation of cECM within patches results in a 30-fold increase in cardiogenic gene expression of hCPCs compared to hCPCs grown in pure GelMA patches. Conditioned media from GelMA-cECM patches show improved angiogenic potential over GelMA alone, as seen by improved endothelial cell tube formation. To further tailor the reparative potential of cardiac patches, we evaluate modifying patch components, particularly cell age, matrix composition, and oxygen growth conditions. While tailoring the patch composition to represent fetal matrix composition and hypoxic growth conditions does not improve the angiogenic potential of neonatal hCPC-cECM patches, child hCPCs show an improved reparative potential when grown in cECM laden patches and hypoxic conditions compared

to child hCPC-GelMA patches. Finally, we evaluate the implantation of patches *in vivo* towards improvements to cardiac function in a rat model of right ventricular heart failure, compared to sham controls and cell-free patches. By incorporating hCPCs within patches (both GelMA and cECM), cells are retained throughout four weeks of therapy. Neonatal hCPC-cECM patches show the greatest improvements in right ventricular function, along with improvements in tissue vascularization and reduction in cardiomyocyte hypertrophy, compared to all other groups and controls. However, cell-free cECM patches demonstrate a nearly equivalent improvement in secondary cardiac functionality and tissue remodeling, indicating that cell-free cECM patches may be just as effective as neonatal hCPC-cECM patches for cardiac repair. While cECM laden patches show improvements over GelMA patches throughout all functional and tissue analysis methods and across all groups, incorporation of hCPCs does not present differences compared to cell-free patches. Also, child hCPC-cECM patches present improvements in right ventricular function compared to controls, although this trend is not seen in further functional analysis. However, the incorporation of cECM within child hCPC patches is necessary to facilitate functional and tissue improvements over child hCPC-GelMA patches, indicating that cECM may be a strong modulator of child hCPC reparative functionality. Altogether, the incorporation of cECM into hCPC-laden and bare patches results in significant cardiac repair in an animal model of pediatric heart failure, paving the way for clinical trials in treating congenital heart diseases using the bioprinted hCPC-GelMA-cECM patches developed in this work.

CHAPTER 1. INTRODUCTION

Congenital heart defects (CHDs) affect 35,000 newborns annually, resulting in significant impairments in cardiac function and increased patient morbidity and mortality.[1,2] Although surgical treatment methods have improved outcomes, many children end up with right-ventricular (RV) dysfunction due to increased RV load.[1,2] This chronically elevated load leads to increased fibrosis and hypertrophy, resulting in RV failure.[1] In cases where RV dysfunction persists, 18-month survival rates are 35%.[3] The only restorative treatment for patients is transplantation, which is limited by the availability of donor hearts and transplant rejection.[2,3] Even in cases where there is not critical RV dysfunction, RV output remains reduced, leading to poor quality of life.

Reparative therapies for improvement of cardiac function are critical, and although limited in pediatric populations, new treatments are being explored.[4-9] While there have been hundreds of stem cell trials in adults, very few address pediatric populations.[4,5,6] A recent study showed that intracoronary infusion of cardiosphere-derived cells could improve RV function in children, and follow up studies have been promising.[7] Also, bone marrow stem cells and cord blood-derived mononuclear cells improved RV function following intramyocardial injection.[8] We have recently shown that progenitor cells (CPCs) could improve the failing RV of juvenile rats subjected to pulmonary banding, and a clinical trial is now underway (NCT03406884).[9] Despite this enthusiasm, similar concerns exist in children that have been shown in adults. While CPC therapy demonstrated modest improvements in adult therapy, most CPCs were lost to circulation immediately

after injection into the myocardium.[10,11] Also, cells are being injected into a diseased microenvironment that may not provide healthy cues for optimal CPC function.[11]

To increase retention and modify the local microenvironment, researchers have used both synthetic and natural biomaterials.[12,13] The inclusion of appropriate cues can both direct the fate of the implanted cells and improve the release of paracrine factors, a major mechanism of cellular therapy.[14,15] Several studies have shown that a decellularized cardiac extracellular matrix hydrogel (cECM) is a promising biomaterial used in the repair of myocardial dysfunction in adults, as well as for the delivery of stem cells.[16-21] In prior studies, cECM increased the differentiation of rat CPCs compared to either collagen or adipose ECM alone.[16,20] Moreover, cECM is currently in clinical trials for adults post-myocardial infarction (MI) (NCT02305602) and thus, combined with human pediatric CPCs, could rapidly advance to human testing. In adults, the material is delivered invasively through a catheter, which can present certain challenges.[19] For one, the local structure of the material cannot be controlled during injection, a property that may alter stem cell phenotype.[22] While MI is a localized disease, heart failure due to CHDs may be more global, and local delivery may not be sufficient.[1,2,3]

One powerful method of generating controlled 3D structures for cardiac therapy is bioprinting, which has been used extensively to produce highly defined geometries of biomaterials and cells.[23-28] Bioprinting is effective in generating polymeric scaffolds but can be problematic for naturally-derived materials.[24,25] For the case of bioprinting ECM-derived materials, current methods rely on creating non-degradable polymeric support scaffolds or require high concentrations of poorly printed ECM.[26,27,28] The inclusion of polymers produces device-tissue and cell-material mechanical mismatch and imposes

degradation limitations.[29] Further, finding materials that are compatible with ECM printing is not trivial.[30,31] A bioprinting methodology that prints both cells and ECM without using non-degradable components is key in generating functional heart patches with high design control.

This work focuses on developing a bioprinted cardiac patch composed of native cECM and pediatric human CPCs (hCPCs), for use as an epicardial device that releases paracrine factors into the dysfunctional myocardium. The patch overcomes problems seen in cell therapies by retaining viable hCPCs in naturally-derived cECM, allowing for improved paracrine release from hCPCs through the bioactive cECM inducing guiding effects on cells, and incorporating the pro-reparative cECM biomaterial.[10,16,20] Additionally, the bioprinting approach allows for the generation of highly defined patches with uniform component distribution.[23] After development, we evaluate the implantation of patches *in vivo* towards improvements in cardiac function in a rat model of right ventricular heart failure, compared to sham controls and cell-free patches. Ultimately, the findings of this work may point towards hCPC-cECM patch implantation as therapy for pediatric patients suffering from RV failure, or perhaps even in an allogeneic manner for adult cardiac dysfunction.

CHAPTER 2. SPECIFIC AIMS

The **overall hypothesis** of this work is that a bioprinted cardiac patch composed of native cECM and pediatric hCPCs would allow for the improved repair of damaged myocardium when implanted as an epicardial device, compared to cell-free patches, cECM-free patches, and sham controls. This hypothesis will be tested by the following **specific aims**:

2.1 Development and *In Vitro* Assessment of a Bioprinted Patch Composed of cECM and hCPCs

Patches will be bioprinted using bioinks composed of cECM and CPCs, through the incorporation of secondary bioactive materials to allow for printing of solid patches and shape retention. The printability of the bioinks will be assessed through strand analysis, cECM fiber formation, and cell homogeneity throughout constructs. Cellular function within the cECM-incorporated patches will be assessed through measurements of viability, proliferation, differentiation, and paracrine release profiles, compared to cellular function in cECM-free patches. Finally, cECM-incorporated patch mechanics will be assessed through swelling ratio, viscoelastic moduli, and patch degradation in cell growth media and fibroblast conditioned media.

2.2 Evaluation of Modified Patch Parameters (Biomaterial Composition, Oxygen Growth Conditions, and Cell Age) on *In Vitro* Reparative Potential of hCPC-cECM Patches

While cECM-CPC interactions may improve the paracrine release of hCPCs, additional CPC modulation in patches may prove to further improve paracrine release

profiles of patches grown *in vitro* before *in vivo* implementation. The effect of variations in cell age (neonatal, child), additional ECM components, and oxygen concentration in growth chambers will be assessed through measurement of cell viability, differentiation, proliferation, and paracrine release profiles, both in 2D culture and 3D bioprinted patches.

2.3 Assessment of *In Vivo* Reparative Potential of hCPC-cECM Patches Delivered to Failing Right Ventricular Myocardium

Patches will be evaluated in rat models of RV failure to assess the therapeutic potential of the devices in repairing damaged myocardium and restoring cardiac function. Patch attachment will be assessed to determine how the patches will be incorporated onto the epicardium for sustained retention, through simple placement, sutures, or pericardial implantation. Cellular retention during surgery will be evaluated both *in vivo* and through tissue analysis. Cardiac improvements will be assessed through changes in tricuspid annular plane systolic excursion, end cardiac dimensions, and atrial area, while tissue-level effects will be assessed through evaluating vessel density, cardiomyocyte hypertrophy, and tissue remodeling in the myocardium. The therapeutic outcomes will be compared to sham controls, pulmonary artery banding controls, and cell-free patches.

The **results of this study** will address the development and *in vivo* evaluation of hCPC-cECM patches towards device effectiveness in treating heart failure, with hopeful progression towards the clinic.

CHAPTER 3. LITERATURE REVIEW

3.1 Pediatric Heart Disease

3.1.1 Overview

Congenital heart defects and diseases (CHDs) are malformations and structural modifications to human hearts that occur during fetal development.[1-3, 32-36] CHDs are some of the most common types of birth defects, affecting over 35000 newborns annually in the US.[1,2,32] CHDs can be malformations of any region of the heart, such as the large vessels, ventricles, atria, septum, pacing components, or any combination of defects. [1,2,33] Since these defects can affect one or more areas of the heart, there are many types of CHDs. Examples of CHDs can include atria septal defects, coarctation of the aorta, double-outlet right ventricle, transposition of the great arteries, hypoplastic left heart syndrome (HLHS), pulmonary atresia, single ventricle, tetralogy of Fallot, tricuspid atresia, or ventricular septal defects, to name a few. [3,33-36] All of these conditions modify and inhibit how the heart pumps blood through the body, resulting in symptoms that can range from transient ischemia to death. Also, 1 in 4 infants born with CHD is diagnosed with a critical CHD condition, which defines all of the example conditions listed above besides the septal defects.[1-3] Non-critical CHDs may result in mild effects on infant heart function, and surgical advancements have greatly improved the quality of life of many patients. For example, septal defects, which are small holes in the septum that result in blood flowing between atria or ventricles, may result in minor or no symptoms and can be remedied with basic tissue or synthetic patches.[32] However, critical CHDs, such as HLHS or tetralogy of Fallot, result in significant malformations throughout the entire heart and can be life-

threatening immediately after birth.[3,34] Patients with critical CHDs require multiple major surgeries within the first year of life, relating to over 25% of CHD patients. [3,35] Fortunately, the mortality rate of CHDs in the United States has been in a state of decline due to increased surgical effectiveness and intervention. [1,2,35] Even with surgical interventions, critical CHD patients experience a high degree of morbidity and mortality. CHDs are the most common cause of infant death from birth defects, accounting for 25% of infants who die from birth defects.[1,2] Patients that survive after intervention and medical treatment continue to exhibit a low quality of life in addition to neurological and cognitive impairments. [1,2,36]

3.1.2 Right Ventricle Failure and CHD Surgery

As described in section 3.1.1, there is a large variation in CHD types and malformations, which results in difficulties with producing singular effective therapies. However, a common result of critical CHDs is right ventricle (RV) dysfunction and failure. RV dysfunction occurs in over 40% of infants and over 65% of adults with CHD, either by inherent malformations of the RV, blockage of the RV outflow tract, increased RV load due to diminished left ventricle (LV) functionality, or a variety of other reasons. [1,2,32,37-40] As an overview, many children end up with right-ventricular (RV) dysfunction due to chronically increased RV load, leading to increased fibrosis and hypertrophy, and ultimately resulting in RV failure.[1,2] This progression can be described through the function of RV and related CHD malformations and surgical treatments implemented to treat CHD.

The progression of RV failure is similar to tissue failure of other areas of the heart, where a physiological feedback loop that would normally allow the RV to adjust functionality in response to stress results in a continued reduction in RV function.[37] The healthy RV functions to pump deoxygenated blood from the systemic circulation, through the RV, into the pulmonary circulation for reoxygenation. While the stroke volume of the RV and LV is similar, the RV stroke work is 25% that of the LV.[37,38] This is due to the low resistance of the pulmonary circulation compared to the systemic circulation, requiring the RV to perform less work and a weaker contraction. The lower work required by the RV results in longitudinal contraction without rotation or twisting while holding a greater volume and being more compliant then the LV. [37,38] Also, the RV is much thinner than the LV, reflecting the lower number of cardiomyocytes that are required to perform the low stroke work. The RV is effective in adjusting to changes in preload but is ineffective in adjusting to changes in afterload. This functionality poses the greatest problem in cases of RV tract obstruction or RV malformations (common in cases of critical CHD) or when the LV functionality is diminished (common in cases of CHD after surgical intervention), ultimately resulting in chronic increased pressure and load on the RV. [37-40] This pressure overload results in progressive failure of the RV through a feedback loop. As the RV experiences excessive load, the tissue adapts to stress by upregulating cytokine activation, cardiomyocyte genetic expression, hormonal activation, and tissue remodeling. [37,38] Cardiomyocytes, unlike many other tissue cell types, do not proliferate and therefore undergo hypertrophy to facilitate increased contractile force. When this feedback is applied to remedy brief or small perturbations in myocardial load, the system allows for increased RV cardiomyocyte functionality through transient cardiomyocyte hypertrophy and tissue

interactions. In cases of chronic load, the upregulation of the remodeling state results in excessive cardiomyocyte hypertrophy, increased tissue fibrosis, and decreased vasculature density. [37,38] One a larger scale, the RV remodeling is not enough to normalize wall stress, resulting in dilatation. Increased filling pressure, decreased unified contractile force, increased RV size, and decreased cardiac output ultimately result in RV failure. [37-40]

The progression towards RV failure is directly set off from malformations seen in CHDs (as described earlier), leading to RV failure in untreated cases. This poses a large problem for patients, and interventions are required. However, surgical interventions that are employed to fix other problems caused by CHD also result in increased load on the RV. [1-3,39,40] The goal of surgical intervention for CHD is to reform the malformed sections of the heart by moving tissue sections, reducing pressure/flow in specific areas of the heart, closing holes, or using synthetic grafts and materials. For example, in transposition of the great arteries (which is also seen in complex CHDs like tetralogy of Fallot), an atrial switch operation is conducted by constructing an atrial baffle to redirect blood from coming into the atria and restoring the systemic – pulmonary blood flow by using patient-derived pericardium or a synthetic material.[3,41] However, this causes RV outflow tract obstruction, leading to RV failure through pressure overload. Similar pressure-overloads are induced by treatments for other CHDs. For example, in the case of HLHS, the hypoplastic LV is remedied by developing a single systemic RV, leading to RV pressure-overload. RV failure can also occur from volume overload, specifically in cases of valvar regurgitation and septal defects. [3]

Although these surgical interventions improve outcomes and limit infant death, they commonly lead to RV dysfunction in aging patients. In cases where RV dysfunction

persists, 18-month survival rates are only 35%.[3] Even in cases where there is not critical RV dysfunction, RV output remains reduced, leading to poor quality of life. Standard management of RV dysfunction post-surgery is limited due to the patient-specific nature of CHD. Patients are routinely administered medications such as inotropes, ACE inhibitors, beta-blockers, or vasodilators.[42] However, these treatments have found no conclusive beneficial effect, and patients continue to suffer.[42] To remedy this, most patients who experience RV failure only have one option for survival – heart transplantation.[43,44] Heart transplantation is fraught with limitations mainly driven by limited donor availability, high transplant rejection (upwards of 70% after three months), and infection (upwards of 70% after one year). [43,44] As mentioned, 18-month survival rates are only 35% for patients with RV dysfunction, which does not allow patients much time to wait for transplants to be available. [1, 2, 43] While there are devices that may allow patients to survive while waiting for a transplant, such as extracorporeal bypass with membrane oxygenator or left ventricular assist devices (LVADs), patients are often waiting longer for the transplant then they can remain on these devices and therefore need a longer timeline to bridge to transplantation. [43,44] Even after successful transplantation, the overall 15-year survival in CHD patients is 41%.[43,44]

Altogether, these considerations point to a critical need in more effective therapies for treating RV failure in pediatric and adult CHD patients, through complete improvement or by slow RV degeneration to bridge patients to transplantation. The majority of novel cardiac therapies in development focus on treating adults with LV damage (post-ischemia or infarction), with limited research into treating the RV. However, general therapies for

restoring myocardial function may also be applied to RV restoration or improving transplantation outcomes, leading to ultimate survival.

3.1.3 Cardiac Therapy Directions Overview

Reparative therapies for improvement of myocardial function are critical in both adult and pediatric populations. For adult patients, therapy is focused on repairing or replacing the LV post-ischemia, such as after MI or its eventual outcome of heart failure in aging populations.[4,45] While therapeutic methods are limited in pediatric populations, new treatments are being explored and are common extensions of effective therapies found for adult patients, and instead geared towards the repair of damaged RV muscle or slowing degeneration to bridge patients towards transplantation.[4-9] Most methods of tissue repair are focused on incorporating or controlling critical components of endogenous regeneration, by specifically using tools such as tissue cells (stem cells or primary cells), biomaterials (natural, synthetic, or combination materials), and molecules (proteins, genetic components, and combination materials).[4,11,12,14] To truly restore tissue function, scientists and engineers have found the greatest success when directly using or recapitulating native tissue components. For cardiac repair and regeneration, recent work focuses on a subset of the general tools described above, specifically stem cells, natural biomaterials, and exosomes.[9,10,11,18] In this work, we will focus on advances and implementation in employing a subset of the cellular and biomaterial approaches – cardiac progenitor cells and extracellular matrix.

3.2 Cardiac Progenitor Cells

3.2.1 Cardiac Progenitor Cell Biology

Human cardiac progenitor cells (hCPCs) are endogenous progenitors found in the myocardium.[46-49] During development, CPCs are thought to give rise to several cardiac cell types, particularly cardiomyocytes and endothelial cells (ECs).[46,47] This differentiation towards a cardiomyocyte lineage is driven by evolutionally conserved transcription factors that include Nkx2.5, GATA4, myocyte enhancement factor 2C (MEF2C), and many others.[46-48] CPCs progress from immature, non-contractile progenitors into functional cardiomyocytes by the development of cellular junctions such as connexion 43 (Cx43), contractile proteins such as myosin heavy chain (MYH), and calcium handling proteins such as L-type Ca^{2+} channels. The development of the heart is a complex process, as is seen with any fetal organ, and has been the subject of many reviews.[46-48] Soon after birth, the heart becomes a terminally differentiated organ, and any new cardiomyocytes are primarily derived from existing cardiomyocytes. It is now accepted that the differentiation potential and population sizes of hCPCs quickly diminish after birth, to the point that hCPCs may be non-existent in the adult myocardium.[9,46,50] Also, several critical markers have been discovered to identify hCPCs, which overlap with many other classical stem cell or hematopoietic progenitor cell markers.[46-49] These markers include c-kit, stem cell antigen 1 (Sca-1), Islet 1, and stage-specific embryonic antigen 1 (SSEA-1), among others, in addition to heterogeneous populations of CPCs such as cardiosphere derived cells (CDCs) and side population cells. Of specific note, c-kit+ hCPCs have been of key interest as they originally were thought to differentiate into functional cardiomyocytes after isolation and culture, and several clinical trials have been implemented using c-kit+ cells for cardiac therapy in adults and children.[4,6,7] However, lineage-tracing studies and a large body of research has pointed to the fact that the

differentiation potential of c-kit+ CPCs is extremely limited when isolated after birth.[50,51] This is further complicated by controversy over the original studies conducted using c-kit+ cells towards their differentiation potential.[52] However, there have been several clinical trials and beneficent therapeutic results using injectable hCPCs.[6,7,15,46] These studies point to the fact that neonatal derived hCPCs or engineered hCPCs may have a potential therapeutic effect via the release of pro-reparative paracrine components, rather than differentiation towards cardiomyocyte replacement, which will be discussed in section 3.2.2.[15] hCPCs may also require modulation and engineering to improve and control their reparative potential, especially for aging cell populations, which will be discussed in section 3.2.3.

3.2.2 Cardiac Cell Therapy and Clinical Advances

As stated in section 3.2.1, there have been attempts to study the therapeutic potential of CPCs, which have led to several clinical advances and an understanding of the therapeutic benefit of CPCs.[15,53] The basic methodology for classical cardiac cell therapy focused on harvesting stem or progenitor cells, expanding the cells by *in vitro* culture, and injecting the expanded cells into a diseased or damaged tissue. As stated in the previous section, the original goal of cardiac cell therapy was the replacement of diseased of hypertrophic cardiomyocytes and other tissues cells with new, functional cardiomyocytes derived from the injected cells.[46,52] However, modern cell therapy was built upon discoveries that unmodified primary cells do not differentiate into functional cardiomyocytes.[15,46,47] As a note, it may be possible to generate immature, unorganized, and partially functional cardiomyocytes used reprogrammed cells (specifically induced pluripotent stem cells, or iPSCs), which can eventually lead to functional cardiac tissue

implants.[54] This topic will be discussed further in section 3.4. However, a focus of modern cell therapy is harnessing the pro-reparative paracrine release profile of injected cells to promote endogenous regeneration. These pro-reparative factors can include soluble factors such as growth factors, chemokines, cytokines, and matrix remodeling enzymes.[15] Stem cells release these factors in response to tissue damage in their native state, which can drive endogenous regeneration and repair. In the myocardium, soluble paracrine factors can affect native cardiomyocytes, ECs, smooth muscle cells (SMCs), cardiac fibroblasts (cFBs), resident and circulating immune cells, and even cardiac progenitors if existent.[15] These cells respond to paracrine mediators by improving survival, contractile protein function, vessel replication, differentiation, and deposition/degradation of native extracellular matrix (ECM).[15,46,53] In turn, regeneration can occur through myocardial protection, increased cardiac metabolism, improved contractility, reduction in cardiomyocyte hypertrophy, neovascularization, and cardiac remodeling.[55]

While this methodology of paracrine function is the basis of modern research into cardiac cellular therapy, there have been many early-stage clinical trials to date that use injected cells in treating the damaged myocardium.[5-8,57,58] Over 5000 patients have received some type of stem cell therapy for cardiac dysfunction over the past ten years. Several cell types have been explored for therapy, which includes mesenchymal stromal cells (MSCs), CDCs, CPCs, embryonic stem cells (ESCs), iPSCs, and umbilical cord cells, among others. While there have been hundreds of stem cell trials in adults, very few address pediatric populations, and fewer cell types have been investigated for this direction.[4,5,6] Bone marrow stromal cells (ELPIS trial) and cord blood-derived mononuclear cells (NXT011883078) improved RV function following intramyocardial injection, although

long term functional improvements were limited.[8] A recent study showed that intracoronary infusion of cardiosphere-derived cells could improve RV function in children (TICAP), and follow up studies have been promising (PERSEUS134 and APOLLON).[7,57,58] The work in our lab has recently shown that progenitor cells (CPCs) could improve the failing RV of juvenile rats subjected to pulmonary banding, and a clinical trial is now underway (NCT03406884).[9] This phase 1 trial delivers autologous CPCs to HLHS patients at 4-6 months during stage II repair, and the study is still ongoing. Although both CDC and CPC therapy has the potential to be beneficial for cardiac patients, CDCs are heterogeneous cell populations with limited potential for controlled and improved therapy. CDCs are isolated from tissue explant cultures and contain a variety of cells, such as cFBs. These combinations make the cellular therapy heterogeneous in terms of outcome, in addition to difficulty in developing an FDA approved and reliably manufactured cell system. Even in an autologous or allogeneic case, CDCs from specific patients are difficult to characterize and replicate in terms of identifying which patient samples are effective in therapy. CPCs may potentially provide a unified, homogenous, easy to isolate, and reliably modulated cell source for application to children. Also, variations in patient-derived hCPCs can be analyzed using computation methods to optimize cell source and functionality for specific disease types.[59] Additionally, CPCs derived from neonatal patients may be more reparative then CDCs derived from adult hearts when targeted to the pediatric population.[6,9]

Despite this enthusiasm, similar concerns exist in children that have been shown in adults. While CPC therapy demonstrated modest improvements in adult therapy, most CPCs were lost to circulation immediately after injection into the myocardium.[10,11,22]

Cells are injected into a diseased microenvironment that may not provide healthy cues for optimal CPC function.[11] Also, studies from our lab and others have shown that CPCs have a significantly reduced therapeutic potential as early as one year after birth. Engineering CPCs and their delivery environment may improve CPC therapeutic benefits in treating both adult and pediatric populations and will be discussed in the next section.

3.2.3 Modulation of CPC Functionality

While CPCs have found potential therapeutic benefits in adult and pediatric patients when directly injected into the damaged or failing myocardium, the benefits may not be significant enough for true restorative therapy or for bridging patients to transplantation. Cellular therapy involves the injection of cells into diseased tissues, which are hostile environments that may reduce injected cellular therapeutic functionality. Furthermore, over 90% of injected cells can be lost to the circulation within hours of injection, reducing the number of cells that can perform repair and ultimately increasing the number of cells required for therapy, which may be difficult to produce in culture.[11] For CPCs, the biological problem of reduced therapeutic potential with increasing cell age remains a challenge in using autologous cells for patients older than one year.[9] Child derived cells show minor therapeutic benefits when injected in animal models of heart failure. However, the average age of children enrolled in clinical trials for treating CHD is greater than one year. For example, the TICAP trial treated children age 1-3 years old.[8] Even neonatal CPCs show reduced therapeutic potential compared to fetal CPCs, especially after *in vitro* culture for sustained periods as required to expand cell populations for injection. Methods to improve CPC functionality before injection or by incorporating additional reparative components during therapy are of key interest. Several methods have been employed with

success both *in vitro* and in small animal models.[16,17,59-63] These methods include clustering CPCs into spheres, pacing CPCs with electrical stimulation, growing CPCs in hypoxia, and combining CPCs with biomaterials. The latter two methods are of interest in this work, particularly in how CPCs interact with hypoxic growth conditions or biomaterials to improve CPC paracrine effects and therapeutic potential.

Hypoxia is characterized as physiologically low oxygen, usually in the range of 0.1-5% oxygen, compared to normoxic conditions at 14-20% oxygen required for cell growth *in vitro*.[64] While most tissue cells require a constant supply of oxygen to perform physiological functions, a growing body of studies indicates that hypoxic conditions when culturing stem cells *in vitro* may improve therapeutic potential.[65-69] This trend is similarly seen for CPCs, although the number of studies is more limited compared to studies on other stem cell types.[62,63,67-69] One early study on stem cell-oxygen interactions by Ceradini et al. evaluated low oxygen conditions on circulating endothelial progenitor and bone marrow cells.[66] They found that hypoxia facilitates the hypoxia inducible factor (HIF-1) pathway that regulates the release of stromal cell-derived factor 1 (SDF-1) from endothelial progenitors. The increased SDF-1 gradient causes the mobilization of progenitor cells by SDF-1 binding to C-X-C chemokine receptor type 4 (CXCR4). This system is seen *in vivo*, where the release of SDF-1 from tissue-resident stem cells during disease results in progenitor cells to mobilize towards the damaged tissue and induce repair.[66] This pathway induction is also seen in CPCs, although they are already tissue-resident cells. A study by Tang et al. using CDCs in 0.1% oxygen showed that CXCR4 expression is low in native CDCs, which became upregulated after 8 hours in hypoxia.[67] Expression of the CXCR4 receptor increased cell honing to the cardiac tissue after intravenous injection in a model

of murine ischemia. The cells showed expression of endothelial markers (Von Willebrand Factor), cardiac markers (cardiac troponin I), and smooth muscle markers (smooth muscle actin) after one month *in vivo*, although the *in vivo* environment may be a confounding variable towards the hypoxic effect conclusions. Oorschot et al. grew Sca1+ cells in either 20% or 1% oxygen for six days (short term) or nine days (long term).[68] They found that short term exposure to hypoxia increased migration and invasion of CPCs using *in vitro* mobilization assays. Long term exposure increased cellular proliferation, reduced expression of cellular remodeling and migration, decreased growth factor released, and increased angiogenesis. These results are conflicting with one another, and show the need for more standard models of hypoxic exposure. However, stem cell migration seems to be improved in CPCs grown in hypoxia by controlling the HIF-1/SDF-1/CXCR4+7 pathway. Additional studies, such as by Chen et al., further showed that the effect of hypoxia on rat CPCs might be directed towards mobilization and proliferation of cells, which is critical in response to injury.[69] A potential mechanism could be explained by hypoxia commonly seen in damaged tissue. Cells respond to hypoxia by upregulating SDF-1 and related receptors to drive cellular migration to areas of damage. Cellular proliferation is also required to increase physiologically low progenitor numbers and respond accordingly to the need for repair, moving cells from a state of senescence during homeostasis to a state of self-renewal to promote repair.[46,69]

However, the need for cellular migration is part of the classical idea of CPC therapy, where the goal was to induce CPCs to differentiate into functional cardiomyocytes. Studies that focus on the paracrine potential of CPCs and CPC-derived exosomes have been of interest recently.[61,62] A study from Gray et al. investigated the

therapeutic potential of exosomes derived from rat CPCs grown in either hypoxic or normoxic environments for 3 or 12 hours in culture, both *in vitro* and *in vivo* in a model of rat cardiac ischemia.[62] While exosomes derived from cells grown for 3 hours in hypoxia showed no difference *in vitro* compared to normoxic exosomes, exosomes derived from cells grown for 12 hours in hypoxia saw improved angiogenic potential and reduction in myofibroblast expression. When injected at high concentrations (10 μg/mL) into ischemic rats, only exosomes derived from hypoxic CPCs resulted in improvements in fractional shortening and decreased myocardial fibrosis 21 days after injection. While injections of hypoxic CPCs did not result in any functional improvements, it is important to note that injected cells would likely not produce high concentrations of exosomes, although a similar concentration of exosomes may be produced if cells are retained over a longer timeframe. A follow-up study by Agarwal et al. investigated the effect of hypoxia on exosomes derived from CPCs taken from patients of different ages, specifically neonatal, infant, and child cells.[63] In a rat model of MI, only normoxic neonatal hCPC exosomes saw improvements in ejection fraction (EF) similar to sham values, while no other normoxic group saw improvements over sham groups. In evaluating fibrosis, vascularization, and cardiomyocyte hypertrophy, neonatal exosomes improved hypertrophy regardless of hypoxia, while only hypoxic neonatal exosomes improved vascularization and fibrosis. For child and infant derived exosomes, hypoxia was required to improve cardiac ejection faction, fibrosis, hypertrophy, and angiogenesis compared to sham and normoxic exosome groups. Altogether, these studies point towards the need for hypoxic growth conditions to generate any therapeutic functionality from paracrine factors derived from exosomes expressed by child and infant CPCs, while neonatal CPCs may not be as affected by

hypoxia. Neonatal hCPCs are already be exposed to hypoxia in the fetal and neonatal heart, indicating that they may not be as responsive to hypoxic culture as longer-lived cells.[46,62]

Altogether, hypoxia may induce CPC proliferation and mobilization, although the exosomes studies indicate that paracrine factor release may also be affected. It is important to keep in mind that many of the studies mentioned use rat CPCs, not human CPCs. Rat CPCs may be inherently regenerative since they are multinuclear even upon isolation and expansion, while human CPCs are not and maybe less reparative accordingly. However, hCPCs may more readily respond to environmental stimuli in terms of their reparative potential, as seen in the case of child hCPCs in the latter study.

While hypoxia is a powerful growth condition, the use of biomaterials to modulate stem cell therapeutic benefit has also been extensively explored in many cell types. Cells rely heavily on interactions with native ECM in tissues to provide structural support and chemical cues.[10,14,15,16] Biomaterial therapy alone has been used extensively in many regenerative medicine contexts, such as for restoring bone, muscle, and vascular function.[14] Additionally, biomaterials may provide an effective vehicle for cell transplantation to improve cell retention and modulate cell effects *in vivo*. In 2D culture, where cells are grown on substrates coated with specific natural biomaterials, CPC therapeutic potential has been investigated with natural materials such as laminin, fibronectin, collagen I, fibrin, and collagen IV, and a variety of synthetic materials such as polycaprolactone (PCL), silicone, and glass, although most materials are only studied in one to two papers.[16,17,20,70-75] While all studies showed that CPCs upregulate cardiac tissue cell markers when cultured on biomaterials, stiffer materials, such as PCL, and materials that are in higher abundance in adult tissue compared to fetal tissue, such as collagen I,

showed a trend towards endothelial and smooth muscle differentiation compared to materials found in the fetal ECM, such as fibronectin, which showed a trend towards cardiac differentiation.[17,71-75] Also, materials that are found in the fetal ECM, particularly fibronectin, induced a higher degree of CPC differentiation and release of paracrine components such as vascular endothelial growth factor (VEGF) than other materials, with increased expression of cell-material receptors such as α5β1 integrin.[17,71-75] In 3D materials and gels, CPC interactions with gelatin, hyaluronic acid, polyethylene glycol, and agarose have been investigated, as single materials or combination materials.[70,76-80] While all materials showed a trend towards cardiac differentiation, natural biomaterials such as hyaluronic acid improved expression of cardiac markers over synthetic materials. Moreover, hyaluronic acid showed higher release of paracrine components such as VEGF, hepatocyte growth factor (HGF), fibroblast growth factor (FGF), and remodeling components such as matrix metalloproteinase (MMPs). [70,76-80] Also, complex materials composed of multiple natural biomaterials, such as hyaluronic acid and gelatin, showed the highest degree of cardiac expression of CPCs. [70,76,77] These results point towards multi-component natural biomaterials as the strongest modulators of CPC therapeutic potential. To this end, a growing body of research is pointing towards improved stem cell function when cultured on or within full ECM.[21,81] A major disadvantage of the materials described in this section is that they lack the complexity and specificity of native myocardial extracellular matrix (cECM), which is required to generate tissues during development and repair processes in the myocardium. This work is not only focused on implementing hCPCs for cardiac repair, but also on incorporating cECM with hCPCs to improve the functionality

of both components. An overview of cECM function, specificity, material types, stem cell-cECM interactions, and clinical advances will be covered in the next section.

3.3 Cardiac Extracellular Matrix

3.3.1 cECM Chemical, Physical, and Mechanical Properties

Organs and tissues are the combinations of multiple cell types and biochemical components such as soluble factors and ECM proteins.[82-90] The ECM is critical in establishing tissue structure, transducing signals from cells to cells or from the ECM to cells, and maintaining homeostasis.[83] In most tissues and the heart, the ECM is composed of a complex combination of proteins, sugars, and soluble factors.[85-90] Quantification of decellularized adult human cECM by Johnson et al., among others, has determined that approximately 70% of human cECM is composed of fibrillar collagens, mainly collagen types I and V.[86] The basement membrane comprises 20% of human cECM, composed mainly of collagen IV, but with additional proteins such as laminin, agrin, perlecan, and nidogen. Structural ECM comprises 4% of cECM, which include mainly proteoglycans such as biglycan and decorin, and fibrous glycoproteins such as fibrillin 1, all of which play a key role in secondary structural support and induction of intracellular signaling. Matricellular components compose roughly 3% of cECM, including collagen VI, fibronectin, dermatopontin, emilin 1, fibulin 5, lumican, periostin, prolargin, and thrombospondin 2. cECM is a complex system of matrix components that play a role in cardiac function, with the relative concentrations of matrix components within cECM being highly conserved and regulated in homeostasis.

The cECM components found in cardiac tissue are organized in a specific manner to support cells and maintain tissue function.[88,89,90] In healthy adult cardiac tissue, the ECM is organized as a heterogeneous structure, with areas of formed collagen fibers, basement membrane, and large spaces where clusters of cardiomyocytes reside.[90] While uninterrupted interactions and cell junctions between cardiomyocytes are critical for contraction, the ECM also dictates cardiomyocyte contractility and endothelium-cardiomyocyte coupling.[91] These requirements result in ECM components surrounding mature cardiomyocytes, seen by intertwined collagen nanofibrils in an organized manner with cardiomyocyte alignment. Cells also rest on homogenous and matured basement membranes with honeycomb-shaped areas of laminin and site-specific collagen IV. The basement membranes of cECM show complete assembly of laminin and collagen IV in thick microfibers, possibly due to the basement membrane forming around vasculature. While the mechanical properties of both solid and soluble dECM (decellularized ECM) are much different than native myocardium, the mechanical modulus of healthy myocardium has been measured anywhere from 3-100 kPa, based on the method of analysis and location of measurement within the myocardium itself.[92-96] This heterogeneity in tissue mechanics is seen within dECM as well, and studies are needed to better understand how changes in various ECM and cellular components, such as collagen and titin, modulate myocardial stiffness.[97,98]

3.3.2 Changes in cECM due to Age, Disease, and Damage

cECM undergoes both physiological and pathological changes driven by cells and matrix remodeling enzymes such as cathepsin K, MMPs, and tissue inhibitors of metalloproteinases (TIMPs). As cardiac tissue forms during development, cECM

composition changes drastically as cells differentiate from proliferative, immature CPCs to mature, contractile cardiomyocytes.[88] There are substantial differences in macrostructure and biochemical composition between fetal, neonatal, and adult cECM, which has been investigated by Silva et al. and Williams et al. through tissue decellularization, summarized in **Table 1**.[89,90,99] Fibronectin and periostin substantially decreased in aged compared to young cECM, as both proteins drive expansion and differentiation of neonatal cardiomyocytes.[89] Components such as collagen IV, collagen VI, fibrillin 1, and perlecan also decreased in abundance with age, but not as substantially as fibronectin and periostin. Emulin-1 and fibrillin two were only found in fetal and neonatal cECM, while collagen III and V were only found in adult cECM. Collagen I and laminin were substantially increased in older compared to younger cECM, indicating the formation of a supporting system for mature cardiomyocytes. The differences in ECM with aging is further demonstrated when comparing the structural changes between collagen IV, laminin, fibronectin, and collagen I in fetal and adult decellularized hearts.[90] Fetal cECM had extensive fibronectin in fibrillar arrangements, while adult cECM had less fibronectin with discrete distributions. Fetal cECM was composed a loose meshwork with a thin and irregular basement membrane, while adult cECM had thick basement membranes with complete assembly of laminin and collagen IV. While the overall fiber percent in both tissues was similar, fetal scaffolds mainly consisted of nanofibers and slender microfibers, while adult cECM had intertwined nanofibrils where mature cardiomyocytes resided. These changes in biochemical profiles and structural expression represent changes to cardiac function and growth related to modulation of cellular phenotype and expression. Aging seems to represent the production of mature tissue and the formation of a stiff

collagenous matrix with a mature basement membrane. Change in the matrix may be a factor in the inability of aging myocardium to repair, with stiffer components in aged myocardium and lack of factors such as fibronectin or periostin, which would otherwise push cardiomyocytes towards a proliferative phenotype.

Table 1. Differences in cECM due to Age and Disease

Condition	ECM Composition	Structural Properties	References
Adult (Healthy)	High collagen I and laminin Uniquely contains collagen III and collagen V	Intertwined nanofibrils and thick microfibers Thick/mature basement membrane Complete laminin/collagen IV assembly in honeycomb-shape Discrete distribution of fibronectin	[88, 89, 90]
Fetal/Neonatal	High fibronectin, periostin, collagen IV, collagen VI, fibrillin 1, perlecan Uniquely contains emulin-1, fibrillin 2	Loose meshwork of nanofibers and slender microfibers Thin/irregular basement membrane Fibrillar fibronectin	[89, 90, 99]
Post-MI	Increase in collagen overall Initial increase in collagen IV and periostin Decrease in collagen IX	Change in stiffness (possible decrease) Increased fiber alignment Decreased crosslinking	[98,107]

There are extensive changes to cECM after ischemia or damage.[87,91,100,101] The balance of normal cECM turnover in the heart is disrupted with disease and causes accumulation of collagen (fibrosis), which impairs cardiac function, increases myocardial stiffness, and drives heart failure.[102] ECM regulatory factors, growth factors (GFs) such as tumor necrosis factor-α (TNF-α) and transforming growth factor-β (TGF-β), and cells such as myofibroblasts drive ECM changes and hinder cardiac function in pathological situations. Fibroblasts and myofibroblasts become hyperactive and excessively deposit ECM with reduced production of MMPs and increased production of TIMPs, resulting in

less ECM turnover.[103,104,105] Cardiovascular disease also affects other heart cells, including cardiomyocytes, ECs, CPCs, SMCs, and transient and tissue-resident immune cells.[106] Fibroblasts dynamically interact with these cells, by modulating the ECM itself, as well as through cell-cell coupling and paracrine effects.

Studies by Sullivan et al. and Quinn et al. on solid decellularized cECM have attempted to elucidate the post-MI changes on the biochemical and macrostructure level, comparing healthy cECM to cECM after 1-8 weeks following infarction, summarized in **Table 1**.[98,107] Although stiffness changes to decellularized myocardium after infarction seems to have conflicting values based on measurement technique used, optical measurements show a decrease in stiffness post-infarct, which may be more supported since the methodology overcomes errors in mechanical measurements by non-destructively evaluating tissue stiffness.[98,107] Collagen content was significantly increased at 4 and 8 weeks compared to the healthy cECM. The infarcted cECM showed an increase in fiber alignment and a decrease in crosslinking, which supports a decrease in myocardial stiffness and indicates that crosslinking plays a key role in stiffness along with total collagen content following infarction. Collagen III, collagen V, collagen VI, fibronectin, laminin, and elastin content did not change from healthy to 8 weeks after infarction. Collagen IV seemed to increase between 1 to 2 weeks after infarction, then decreased again at 4 and 8 weeks, possibly due to initial upregulation of basement membrane formation that was reduced as the tissue remodeled. Collagen XV decreased significantly in the infarcted cECM at all time-points compared to the healthy cECM. Finally, periostin content increased one week after infarct but then decreased to pre-infarct levels after 4 and 8 weeks, possibly indicating that the tissue was in a reparative state after infarction, although further studies are

necessary. Studies on decellularized cECM show a substantial change in cECM mechanics and composition following infarction, pointing towards pathological changes that result in hindrance to cardiac function, which may be remedied with replacement or addition of healthy dECM.

3.3.3 Properties and Function of cECM Compared to dECM from Secondary and Non-Human Sources

In addition to cECM, other types of dECM from different sources have been used for heart-based applications, summarized in **Table 2**.[108] The sourcing of tissue can be separated based on species and tissue (primary cardiac or secondary tissue) variance. Decellularized human skin, porcine small intestinal submucosa (SIS), and porcine urinary bladder matrix (UBM) were investigated in the late 2000s, with a focus on restoring cardiac function through the use of solid dECM, modulated with GFs, stem cells, or additional polymers.[109-112] Since 2008, methods to directly decellularize heart tissue have shifted dECM research and applications towards using heart-specific dECM.[113,114] Although there have been recent advances using various dECM sources for cardiovascular engineering, the question remains as to the ideal sourcing for dECM-based therapies for cardiovascular tissue. Secondary dECM sources, such as SIS and UBM, may be easier to obtain and process then cECM, with improved batch-to-batch variability for clinical application, as seen in commercial products such as MatriStem® and AlloDerm™.[115] Primary cardiac-derived dECM, both as cECM and pericardial ECM (pECM), may have a tissue-specific biochemical profile and structure composition that induces more effective cardiac repair compared to secondary dECM, where batch to batch variability is improving as these therapies move towards the clinic.[116]

Table 2. Comparison of Various dECM vs. cECM

Form	Tissue	Species	Differences compared to cECM	Reference
Solid Sheet	Skeletal	Murine	Similar fiber structure	[117]
	Liver	Murine	Lower fibrilin-1, microfibrillar-associated protein 2/5	[118]
			Higher collagen II, arginase-1	
			Decreased ESC cardiac commitment	
	Pericardium	cECM - porcine	Similar microstructure	[119]
		pECM - human	Larger pore size	
			Better cell infiltration	
			pECM expressed 25 unique components	
			cECM expressed 14 unique components	
Hydrogel	Adipose	Porcine	No change in cardiac and fibroblast commitment of CPCs compared to collagen	[16]
	Skeletal	Porcine	sECM uniquely expressed heparin sulfate, decorin	[120]
			cECM uniquely expressed collagen IV, elastin, fibrinogen, fibrillin-1	
	Lung	Porcine	Lung ECM uniquely expressed collagen II and collagen IX	[123]
			cECM uniquely expressed collagen VII, fibrinogen, heparan sulfate	
Milled Powder within Fibrin	Liver	Murine	Promoted *in vivo* fibroblast migration, neovascularization, cell infiltration	[122]

The review of the numerous sources and implementations of dECM solid scaffolds until 2009 by Badylak et al. shows that many companies have attempted to commercialize dECM as solid dry or hydrated sheets, generated through natural processing or crosslinking methods.[115] An example of dECM that moved towards clinical use is bovine pericardium-derived heart valves, which are often cross-linked to improve mechanical functionality as valves. The implementation of solid dECM for myocardial repair has been limited, and although clinical functionality is being assessed, most companies have moved forward with valve, vasculature, or pericardial patches rather than myocardial replacement or repair.

Direct comparisons of differences in composition and function between tissue source, species, and decellularization method of dECM for cardiovascular applications have not been explored, and recent solid dECM studies have mainly focused on whole heart decellularization and recellularization. Since SIS, UBM, and other tissues are commercially available, their applications may be best compared in clinical systems.[115] Hong et al. decellularized murine cECM and skeletal ECM (sECM) solid scaffolds and found that both cECM and sECM had similar fiber structure after decellularization.[117] Higuchi et al. compared solid scaffolds of cECM and liver dECM in terms of their relative protein concentrations and cellular responses to ESCs.[118] cECM had lower collagen II and arginase-1 content and higher fibrillin-1, microfibrillar-associated protein 2, and microfibrillar-associated protein five than liver dECM. ESCs showed higher cardiac differentiation when cultured on cECM compared to liver dECM. Perea-Gil et al. compared two decellularized scaffolds based on either porcine cECM or human pECM repopulated with adipose tissue-derived MSCs.[119] The general structure and mechanical properties of the two grafts were preserved after decellularization and recellularization, although the decellularized cECM was stiffer than the native myocardium. The decellularized pECM showed much higher expression of major ECM components, better cell infiltration and retention, and larger pore size. The study evaluated the protein expression of both scaffolds, with 14 distinct components found in the human cECM (such as fibrillin-2 and nidogen-2) and 25 distinct components found in porcine pECM (such as galectin-1, biglycan, and GFs). It is important to mention that since both tissue and species sources were variables in the study, it was difficult to determine which factor influenced the cellular effects.

Soluble porcine cECM has moved towards translation, with clinical trials completed and ongoing in post-MI patients (NCT02305602). While human, rat, and goat myocardium, human and ovine pericardium, and porcine omentum have undergone *in vitro* analysis or histological assessment for soluble hydrogels, they are the least therapeutically evaluated using *in vivo* models.[108] Human placenta, porcine SIS, and porcine pECM have undergone functional studies, but maybe lacking *in vitro* analysis or biocompatibility and histological assessment.[108] An analysis of the general soluble dECM hydrogels towards *in vivo* implementation is seen in the review by Spang and Christman.[108] There are, however, limited studies as to the differences in the effectiveness between types of soluble dECM towards heart repair. French et al. showed that CPCs grown on cECM significantly increased proliferation and expression of cardiac markers and decreased expression of fibroblast markers, compared to CPCs grown on collagen or adipose dECM.[16] These results suggest that tissue-specific cECM may drive CM differentiation of CPCs more effectively. DeQuach et al. characterized differences in the biochemical composition of sECM and cECM through mass spectrometry.[120] While there was overlap in component expressions, such as collagen I and V, fibrinogen, and fibrillin-1, there were marked differences, with cECM expressing collagen IV, elastin, fibronectin, and laminin exclusively, while sECM expressed several unique collagens, heparin sulfate, and decorin. Ungerleider et al. showed that similar methods could be used to develop soluble porcine sECM and cECM, although the difference in protein expression was not qualified.[121] Tabuchi et al. compared rat liver dECM and cECM milled powders within injectable fibrin material for the treatment of acute MI in rats.[122] They found that both dECM powders, especially liver dECM, promoted fibroblast migration into the materials *in vitro*. While

both dECM powders induced neovascularization in the infarct area and cell infiltration into the materials *in vivo*, the liver powder was more effective, although there was limited direct comparisons on dECM composition and function. Merna et al. grew heart and lung fibroblasts on cECM and lung ECM and found that fibroblast source and integrin expression were more important than dECM source in myofibroblast differentiation potential.[123] They also characterized the differences in dECM composition, where lung ECM expressed collagen II and IX exclusively, and cECM expressed collagen VII, fibrinogen, and heparan sulfate proteoglycan. Overall, tissue quantification of dECM scaffolds compared to cECM seem to be contradictory, and more sophisticated techniques such as proteomics are required to better elucidate differences.

Both tissue and species variances may be important characteristics of dECM that drive effective regeneration and repair. Johnson et al. investigated the differences between human and porcine sourcing of cECM. Both soluble cECM materials could gel and spread *in vivo* after injection.[124] In terms of biochemical composition, both matrices were similar, where porcine cECM had a higher sulfated glycosaminoglycan (sGAG) content, while human cECM had components such as periostin, fibulin-2, and differential collagens. Most importantly, generating human cECM was problematic due to difficulty in obtaining healthy human myocardium, patient-to-patient variability in composition due to age, and increased difficulty in processing human tissue. This patient variably was assessed in further studies by the same laboratory, which showed marked differences in pECM composition and mechanical properties between patients.[116] It seems that overall it is much more difficult to scale human cECM towards clinical application, while porcine

cECM is easier to obtain and process and is composed of similar components as human cECM.

While these studies have attempted to compare differences in tissue and species sourcing between cECM and other dECM through quantification of chemical composition or assessments in cellular responses, a comparison between implementing dECM from different sources in the treatment of cardiovascular diseases is critical in determining which sourcing allows for the most effective therapy.[115-124] The studies discussed in this section point towards diverse differences between dECM sources based on tissue or species source. It may turn out that the sourcing is not as important as the method of decellularization, functional modification, cell sourcing, or any other factor involved in dECM therapy. Alternatively, tissue-specific dECM may be the most critical factor in cardiac regeneration and repair. Regardless, progress towards the clinic is promising.

3.3.4 Types of dECM for Cardiac Tissue Engineering

3.3.4.1 Solid dECM

Many methods have focused on developing dECM that can be used in cardiac therapy as solid dECM scaffolds, which are not solubilized into dECM powder or liquid and are used directly after decellularization. This methodology preserves the native tissue structure and vasculature while expressing dECM components in their tissue-specific location. Therapies that use this method of solid decellularization focus on direct use of the material as a solid patch or attempt to recellularize the dECM towards functional tissue development. A goal of generating whole decellularized hearts is the ultimate recellularization of the hearts to produce functional off-the-shelf organs for transplantation

into patients. Although many recent studies have attempted to recellularize whole hearts with a variety of cell sources and bioreactor setups, these studies are not the focus of this work, and the technologies have been recently reviewed by Taylor et al.[125,126,127-131] Cardiac patches derived from sections of the decellularized heart tissue may be just as effective as whole hearts in repairing damaged myocardium, without the need for full transplantation. Studies that focus on cardiac patches follow classic tissue engineering methods, where 3D scaffolds are generated from decellularized cECM followed by seeding with stem cells or differentiated cells generated from stem cells. A summary of these studies is seen in **Table 3**. Solid dECM will not be discussed further in terms of *in vitro* applications or cell-solid dECM interactions, and will only be discussed in the clinical advances section.

Table 3. Solid dECM Scaffolds with Cells

dECM Source	Cell Source	Findings	References
Human cECM	Human MSCs, CPCs, HUVECs, cardiomyocytes	MSCs – infiltrated, no alignment CPCs – no infiltration HUVECs – grew around vessels Cardiomyocytes – attached in matrix, aligned with fibers	[132]
	Human iPSC-derived cardiomyocytes, ESCs	Improved cardiac commitment, conduction velocity, decreased calcium upstroke, ion channel formation of cardiomyocytes in cECM compared to Matrigel	[133]
	Human iPSC-derived cardiomyocytes	Sarcomere formation, cell/matrix deformation, contractile force, electrical conduction	[134]
	Murine ESCs, iPSCs, MSCs	Improved proliferation, cardiac commitment of ESCs and iPSCs only compared to Matrigel/Geltrex	[135]
Human cECM and Fibrin Hydrogel	Human MSCs	Improved angiogenic GF release, enhanced vascular formation in a murine infarction model	[136]
Porcine cECM treated with HA	Human MSCs, HUVECs	Thick scaffolds showed high cell density, survival, angiogenesis, vascular formation	[137]
Porcine SIS	Porcine MSCs	MSC addition reduced immune response following pericardial/epicardial implantation compared to SIS alone	[138]
Murine cECM	Human iPSC-derived cardiomyocytes, iPSC-derived CD90+ cells	Improved cardiac commitment, higher myofilament width of cells in patches compared to cardiomyocyte aggregates	[139]
Murine cECM (Fetal)	Murine neonatal cardiomyocytes and CPCs	Improved cell migration, cardiac commitment, paracrine release, adhesion in fetal compared to adult cECM	
Murine sECM	Murine ESCs and ESC-derived cardiomyocytes	Adherence, survival, proliferation, electrical response, cardiac commitment of both cell types Cardiomyocytes formed gap junctions and synchronized contraction	[117]

3.3.4.2 Soluble dECM

Another form of dECM biomaterials used in cardiac therapy is soluble dECM scaffolds derived from myocardium, pericardium, or secondary sources such as SIS or omentum. These dECM materials have been decellularized, followed by additional steps to break down the ECM structure and solubilize the complex ECM material into liquid form. The solubilized dECM can form 2D and 3D hydrogels either *in vitro* or *in vivo* after injection into the myocardium. Studies using dECM for cardiac tissue engineering

applications either focus on generating and modifying pure dECM for direct injection into damaged myocardium or by combining dECM with cells or additional biomaterials to produce bioactive and cell-laden injectable gels or cardiac patches. Soluble dECM is much more versatile than solid dECM scaffolds, maintaining ECM composition but lacking structural and mechanical similarity to solid dECM scaffolds. Unlike the section on solid scaffolds, where literature was summarized in a table, soluble dECM for cardiac tissue engineering has been investigated more in-depth in terms of cellular interactions and will be used directly in this in this work. Studies evaluating the cellular responses to soluble dECM for cardiac therapy will be the focus of the next section.

3.3.5 Cellular Responses to Soluble dECM

3.3.5.1 2D Coatings and Hydrogels

Platforms using dECM scaffolds through 2D coating or hydrogel systems provide an excellent method to evaluate cellular responses to different dECM, allowing for high-throughput analysis of multiple parameters and evaluation of rare or difficult to obtain pathological dECM. Tissue-specific dECM can be used to coat cell culture dishes in similar methods employed for coating dishes with natural materials such as collagen or can be polymerized as a thin hydrogel for cell seeding on top of the scaffold.[120] These soluble dECM platforms have been used in modeling biological niches, infarct environments, matrix stiffness, and cell-matrix binding, while also evaluating how dECM modulates stem cell phenotype and matrix binding.

Sarig et al. grew human umbilical vein endothelial cells (HUVECs) and human MSCs on porcine cECM and evaluated tissue properties and phenotypic changes during

cell growth through mechanical testing, molecular biology assays, and principal component analysis.[140] They found that MSCs remodeled the cECM, HUVECs improved the tissue-specific recognition of differentiation, and co-culture improved tissue integration, angiogenesis, and differentiation. Stem cells grown on tissues at different ages can help understand factors involved in cardiac development, such as mechanotransduction. Gershlak et al. grew MSCs on cECM scaffolds derived from fetal, neonatal, or adult myocardium, which was further modified with polyacrylamide gels of varying stiffness as a system to evaluate contractile forces of MSCs across cECM development.[98] MSC responses to varying stiffness were different based on cECM age, and MSC differentiation induced toward early cardiomyogenesis was only seen in stiff neonatal substrates.

Modulations to cardiac ECM properties after infarction can change therapeutic outcomes for cell therapy compared to testing with healthy tissue. Sullivan et al. decellularized and solubilized healthy and infarcted cECM at 1 and 4 weeks after infarct, which was then combined with hard and soft polyacrylamide gel to grow MSCs in 2D culture.[97] MSC differentiation towards the cardiac lineage, based on Nkx2.5 expression, was only evident on soft healthy and soft 1-week infarct cECM. Interestingly, MSC-induced release of GFs such as HGF and SDF-1 were highest in 4-week infarct cECM. In follow-up work, Sullivan et al. modified the *in vitro* model to more accurately replicate an *in vivo* infarct environment by increasing dECM stiffness, decreasing oxygen tension, removing serum from culture media, and incorporating common GFs found in infarct environments such as FGF and TGF-β.[141] The model determined that the expression of Isl-1 by CPCs was the main factor required for differentiation in an infarct environment.

In vitro systems using cardiac-specific cells or stem cells on cardiac-specific dECM have also been used to determine the biology of cell-ECM binding in the heart. Merna et al. grew human cardiac and lung fibroblasts on intact cECM, collagen gels, and coatings of cECM, lung ECM, and ECM components.[123] cFBs had higher expression of β3 and β4 integrins compared to lung fibroblasts, and inhibition of only β3 integrin resulted in substantial increases to myofibroblast differentiation of cFBs cultured on either lung ECM, cECM, or fibronectin. The integrin profile and source of fibroblasts were more important than dECM type in generating myofibroblast phenotypes, although dECM and fibronectin-binding through β3 integrin seem to reduce the instance. A similar study by Gershlak et al. investigated how MSCs interact with cECM scaffolds to modulate traction forces.[142] They found that once again, MSCs grown on cECM did not respond to changes in substrate stiffness, although MSCs grown on single ECM components such as collagen did modulate traction forces based on stiffness. When β1 integrin was inhibited, the MSCs grown on cECM responded to substrate stiffness by modulated traction forces similarly to cells grown on single ECM components.

Stem cell-ECM interactions in modulating stem cell differentiation and reparative potential are of most interest in quantifying cellular modifications through dECM materials on 2D substrates. CPC differentiation towards a reparative phenotype, whether by improved differentiation, paracrine release, or both, has been studied with many materials. French et al. grew rat neonatal CPCs on collagen, porcine cECM, and adipose dECM substrates to evaluate the CPC's differentiation potential.[16] Compared to collagen and adipose dECM, CPCs grown on cECM expressed an increase in early CM markers and protein expression, improved proliferation, resistance to apoptosis, and improved adhesion.

The CPCs expressed an increased profile of MMP and TIMP production compared to cells grown on collagen. A follow-up study by French et al. evaluated the effects on CPCs on cECM or single ECM components with cyclic strain.[143] The study found that strain improved VEGF production and decreased Cx43 expression of CPCs grown on cECM, indicating that combined strategies may improve CPC release profiles. Baghalishahi et al. grew human adipose-derived stem cells on rat cECM with and without a cardiac inductive cocktail to analyze cardiac differentiation potential after three weeks in culture.[144] Expression of cardiac genes was significantly increased when adipose-derived stem cells were grown on cECM compared to standard tissue culture or addition of the inductive cocktail, with a combination of both cECM and cocktail further driving cardiac differentiation.

3.3.5.2 3D Hydrogels

In therapy, cells are exposed to 3D scaffolds and environments, which may significantly alter cell properties and reparative potential compared to 2D growth. CPCs and iPSCs have been investigated within pure cECM and pECM scaffolds, summarized in **Table 4**. Gaetani et al. encapsulated human fetal and adult CPCs in porcine cECM for up to 1 week in culture.[20] Adult and Fetal CPCs had an increased gene expression for cardiac and endothelial lineages up to 1 week in culture, remained viable, proliferated more, and survived more effectively after H_2O_2 treatment compared to cells grown in collagen. Fetal CPCs seemed to proliferate more than adult CPCs, and adult CPCs seemed to survive in higher numbers then fetal CPCs when grown in cECM. Rajabi-Zeleti et al. grew human CPCs in human pECM gels and found that CPCs were able to migrate, survive, proliferate, and differentiate towards a cardiac phenotype more effectively than cells grown on 2D

pECM membranes or 3D collagen scaffolds, mirroring the results seen in cECM materials.[145] Fong et al. grew human iPSC-derived cardiomyocytes on 2D and 3D cECM scaffolds derived from fetal or adult bovine cECM.[146] While both 3D cECM scaffolds induced cardiomyocyte expression of calcium-handling genes, Cardiomyocytes grown in 3D adult cECM had higher expression of these genes in comparison to 3D fetal cECM, although there was no significant difference when comparing fetal and adult 2D cECM. The cardiomyocytes in 3D adult cECM showed increase calcium signaling and kinetics compared to cardiomyocytes grown in 2D and were more responsive to calcium inducing drugs. Jeffords et al. used genipin crosslinking to modulate the mechanical properties of porcine cECM hydrogels for the induction of human MSC endothelial differentiation.[147] Genipin crosslinking increased cECM hydrogel storage modulus, decreased swelling ratio, and prolonged degradation. MSCs showed maintained viability, downregulation of early EC markers, and upregulation of mature EC markers. These studies show that 3D cECM and pECM scaffolds are effective in driving stem cell differentiation towards cardiac lineages and may be more effective than 2D cardiac dECM models.

Table 4. Pure dECM-Stem Cell Interactions

dECM Source	Formulation	Cell Source	Findings	References
Porcine cECM	2D Coating	Rat Neonatal CPCs	Improved cardiac commitment, proliferation, adhesion, reduction in apoptosis compared to collagen or adipose dECM	[16]
			Improved production of MMPs/TIMPs compared to collagen	
	2D Coating	Rat Neonatal CPCs	Improved VEGF production, decreased Cx43 expression with strain	[143]
	3D Hydrogel	Human Fetal and Adult CPCs	Improved cardiac commitment, endothelial commitment, proliferation, survival compared to collagen	[20]
	3D Hydrogel with Genipin	Human MSCs	Improved mature EC commitment, reduced early EC commitment with genipin crosslinking	[147]
Murine cECM	2D Coating	Human ADSCs	Improved cardiac commitment compared to standard tissue culture, further improved by combination of inductive cocktail and cECM	[144]
Human pECM	3D Hydrogel	Human CPCs	Improved migration, survival, proliferation, cardiac commitment compared to 2D pECM or 3D collagen	[145]
Bovine cECM (Fetal and Adult)	2D Coating and 3D Hydrogel	Human iPSC-derived cardiomyocytes	Improved expression of calcium-handling genes in 3D adult cECM compared to fetal	[146]
			Improved calcium signaling and kinetics in 3D adult cECM compared to 2D adult cECM	

3.3.6 Clinical Advances

There are a large number of murine and large animal studies conducted using dECM for cardiac applications, which has been recently reviewed.[81] Clinical applications of dECM materials for cardiovascular treatment have generally been limited to repair or replacement of heart valves, large vasculature, and CHDs.[148,149] These applications rely on patches and valves such as PhotoFix®, CryoValve®, SJM™ pericardial patch, and Tutopatch®, with many additional products implemented extensively in clinical treatment. In contrast, tissue-engineered dECM scaffolds and injectable materials have been studied extensively *in vitro* since 2008, with a modest number of *in vivo* rat studies of MI, and even

less large animal studies. Two main dECM technologies are being evaluated in clinical testing – injectable cECM (VentriGel™) and SIS cardiac patches (CorMatrix®).

Injectable cECM therapy is the only soluble dECM therapy that has moved from *in vitro* analysis, to *in vivo* testing, and finally to clinical studies. This work has been developed since the original paper by Singelyn et al., which was followed immediately by several studies on cECM hydrogel analysis *in vitro*.[150] *In vivo* success through rat models (Singelyn et al., Wassenaar et al.) and porcine pre-clinical models (Singelyn et al., Seif-Naraghi et al.) have paved the way for a phase 1 clinical trial (NCT02305602) that evaluated the safety and feasibility of VentriGel™ in treating MI.[151,153,153] Results from the trial support the safety and feasibility of VentriGel™ injection in post-MI patients with LV dysfunction. Also, patients across the entire cohort showed improvements in walking test distance and decreases in functional heart class assessment. Improvements in LV remodeling were also seen in patients that were treated within one year post-MI compared to patients treated after 1-year post-MI. These results show the effectiveness of porcine cECM in treating adult patients post-MI, where faster treatment may be more beneficial. Alternatively, the SIS based solid dECM patch, CorMatrix®, has found commercial use in carotid repair, pericardial reconstruction, and cardiac tissue repair, although cardiac closure is the most common use of the product. Studies by Mewhort et al. on both rat and porcine pre-clinical models have shown success in treating MI in animal models, with phase 1 clinical trials completed in 2017 (NCT02887768), although results have not been published.[154,155,156]

Two studies on individual human patients have recently been published that use dECM materials for the treatment of cardiovascular dysfunction. Avery et al. used human amniotic fluid-derived MSCs loaded within a micronized human liquid matrix derived from amniotic membrane for treatment of a 59-year-old male patient with refractory angina, heart failure, and ischemic cardiomyopathy from chronic diabetes.[157] Laser-guided transmyocardial revascularization (TMR) was performed on the LV walls, and the MSC-liquid matrix was added to several of the TMR channels in the infarct. On day six post-operation, there was a large, stable, transmural infarct, and the patient showed a reduction in LV EF. On day 27 post-operation, the patient showed improvement in LV wall thickness and EF of 34%. By day 91, the patient showed a decrease in angina, and MRI showed confluence areas of healthy myocardium with improved wall thickening and EF of 40%. Thallium imaging of the infarct showed new areas of thallium labeling in the LV, suggesting the formation of new, viable myocardium and ventricular remodeling. Ferng et al. implanted CorMatrix® in a 62-year-old male with a history of diabetes, atrial fibrillation, class IV heart failure, and hypertension.[158] The patient underwent removal of an LVAD due to persistent infection, at which point a single CorMatrix® scaffold was used to reconstruct the aortic graft anastomosis site and LV apex defect. After three months, the patient had worsening heart failure and underwent implantation of a new LVAD, at which time the CorMatrix® graft was removed and evaluated histologically. The apex graft showed striations like native myocardium, presence of mature cardiomyocytes, and fibrotic stroma, possibly due to the resolution of initial inflammation. Sections of the apex graft stained positive for HOP, a gene important in the developing heart. These results may support the hypothesis presented in the studies by Mewhort et al., where CorMatrix® was

thought to promote cardiac repair through remodeling. Regardless, these clinical studies have shed interesting findings on dECM based materials for heart repair, whether by an improvement of cardiac function using MSC-loaded amniotic membrane or by evaluation of remodeling potential, but possibly limited therapeutic potential, of solid SIS grafts. With time, the results from current and future clinical trials may be most helpful in understanding how dECM can be used in cardiovascular tissue engineering for the treatment of cardiovascular disease.

3.4 Cardiac Patch Therapy

3.4.1 Limitations of Injectable Therapy

Many of the applications of CPCs and dECM (specifically cECM) for cardiac therapy rely on injecting cells or matrix through intravenous or intrathoracic injection into the myocardium. While this approach allows for ease of application by not requiring open-heart surgery, many limitations can hinder therapeutics effects of CPCs or cECM.

Over 90% of cells are lost to circulation immediately after injection into the myocardium, reducing their beneficial effect.[10,11] Irrespective of cell type, cell therapy remains limited by the survival, proliferation, and engraftment of transplanted cells. Cell injections force cells into confined areas of damaged tissues, where they are exposed to a complex array of pro-necrotic factors, remodeled matrix, hostile immune cells, and destructive enzymes.[10,11,22] This hostile environment can cause high degrees of implanted cell death, which in turn limits engraftment and benefit. The complex cytokine and chemokine profiles found in damaged tissues result in heterogonous effects on implanted cells, making them difficult to control after injection and reducing optimal cellular

function.[11] In addition to cell source, the ideal delivery time, method, and dosage have yet to be identified. As discussed in previous sections, CPCs may show reduced therapeutic potential when grown in *in vitro* culture for sustained periods as required to expand cell populations for injection.[46,62,159] Methods to improve CPC functionality by incorporating additional reparative components during therapy are of key interest. The delivery of cells alone may prove insufficient, and many ongoing studies pair a biomaterial with cells to improve their successful transplantation and regeneration of host tissue.

Biomaterials have their own sets of limitations towards therapy when injected, compared to cellular therapy.[14,22] One aspect is the lack of complexity of implemented biomaterials, such as polymers, to facilitate effective cardiac repair. This limitation is overcome by using natural biomaterials, and specifically in using tissue-specific and complex cECM. However, pure cECM gels are very soft (as described in section 3.3) with a stiffness 1000-5000 times lower than native myocardium.[92-96,108] A mechanical mismatch between the injected cECM and native myocardium post-injection can result in reduced functionality through effects such as contractile complications and induction of local immune responses.[108] Immune responses can also occur due to the xenogeneic aspect of injected biomaterials, particularly in the case of non-human derived cECM, although this effect was shown to be limited in clinical trials. Also, small islands of cECM gels within a larger, organized myocardium can create pockets where cardiac electrical signals do not propagate, increasing chances of arrhythmia. Natural biomaterials may also quickly degrade post-injection due to high concentrations of MMPs and other remodeling enzymes, limiting therapeutic timelines, or requiring multiple injection times.[86,108] One benefit of cellular therapy is that cells may respond dynamically to changes in tissue status, producing

a wide range of paracrine effectors based on the repair condition of the cell. Biomaterials by themselves do no exhibit this dynamic temporal effect, and multiple injections may be required throughout therapy. CHD is a global disease of the myocardium, which affects large areas of the RV, compared to MI, which affects smaller areas of the LV. Even in the case of MI, patients require multiple injections within the damaged site to facilitate effective biomaterial delivery. This need for many injections is further amplified when applied to CHD treatment and may reduce the feasibility of an injectable approach.

Altogether, the limitations of injectable cell and biomaterial therapies alone are numerous and present a large barrier to therapeutic mechanisms of action. Injecting both biomaterials and cells may overcome cellular problems by the biomaterial acting as a vehicle for cells and providing a suitable microenvironment to facilitate therapeutic benefit. However, many of the problems with injection overall are still barriers to therapeutic outcome in a combined cell-biomaterial injection.[10,160,161] Cardiac patches, which are solid devices containing cells and biomaterials, may overcome all of the problems associated with cell therapy and will be discussed in the next section.

3.4.2 Cardiac Patches – Overview

Cardiac patches are solid structures that contain cells or drugs supported in biomaterials. Cardiac patches can be surgically manipulated to be implanted directly on the targeted area, such as the epicardium that covers the myocardium in cases of LV or RV repair. The therapeutic target of patches can follow one of two paths, for replacement of myocardial tissue (beating patches) or for use as a reservoir of pro-reparative components for sustained endogenous repair (paracrine cell or drug delivery patches).[160,161] Cardiac

patches were classically employed for closure or merging of heart tissue sections in CHD or adult defects. While the "patch" term has remained, modern patch design is now geared towards generating patches that regenerate, repair, or replace damaged contractile myocardium in a tissue engineering approach, rather than simple passive devices.[10,160,161] There are several reviews on the development of reparative patches for the myocardium, with patches having found success (based on design) in animal models.

While some patches have employed methods of catheter-based implantation and delivery, the major drawback of most patch therapies is the need for opening the thoracic cavity for myocardial implantation. Moreover, patch surgery may require the use of sutures or surgical adhesive to attach patches onto the target tissue throughout therapeutics timescales. However, all of these drawbacks may be minor compared to the benefits of cardiac patch therapy over injectable biomaterial/cell therapy. On the cellular side, patches can contain cells within a biomaterial that results in an effective cellular microenvironment for the promotion of target cell functionality. Cells can be retained while in biomaterial scaffolds compared to pure cell injection *in vivo*. Cells delivered within biomaterial patches are shielded from the hostile environment of the damaged tissue, allowing the cells to grow, proliferation, and produce guided functional improvements without exposure to destructive conditions.[160,161] Also, the type of biomaterial used in patch design is a critical factor in modulating cellular phenotype and functionality, which is important for cells that may benefit from support such as hCPCs. On the biomaterial side, patches can be designed to incorporate a large amount of biomaterial for direct treatment of a large area of the heart. This aspect is especially important for treating global CHDs. Biomaterial (and cell) patch treatment would only need one implantation surgery to provide a large therapeutic benefit.

Also, patch devices can be designed to match the mechanics of the myocardium and reduce the potential of arrhythmia formation, although beating patches provide their own set of challenges in terms of patch-tissue integration.[160,161] As with injectable combined biomaterial/cell therapy, the benefits of both cells and biomaterials can be incorporated through a patch system. Furthermore, degradation can be highly tailored to allow for both biomaterial retention during required therapeutic timescales and biomaterial degradation to allow for only patient myocardium to remain by using degradable materials such as cECM.[161]

Design considerations for cardiac patches include ultimate function/patch use, cell type, biomaterial type, and fabrication method.[10,160,161] These design considerations will be discussed in the next sections.

3.4.3 Patch Design – Function

The majority of cardiac patch development is geared towards the development of a fully contractile, beating patch for replacement of damaged tissue.[160-166] Alternatively, drug delivery patches that release pro-reparative factors from either direct loading or from cells that produce factors are in development but represent a growing field.[160,161]

Beating patches are based on a classic paradigm of tissue engineering, where cells and solid supports are grown in bioreactors to generate functional tissue. The functional cardiac tissues should beat spontaneously and in sync with the native myocardium after implantation, effectively replacing the damaged, non-functional tissue. Many reviews have been written about approaches to developing beating patches.[161,162] Riegler et al. employed an engineered heart muscle ring composed of human ESC derived

cardiomyocytes in a model of rat MI, and saw that transplantation of engineered heart tissue increased engraftment rate and led to long term survival and progressive maturation of ESCs.[162,163] Menasche et al. employed human ESC-derived Isl-1+ SSEA-1+ cardiac cells within a fibrin patch to treat one human patient exhibiting ischemic heart failure from diabetes.[164] After three months, the patient saw improved walking, increased myocardial wall motion, and improved LV ejection EF. Ye et al. grew human iPSC-derived cardiac trilineage progenitors (towards cardiomyocytes, ECs, and SMCs) in a fibrin patch, which improved LV EF and improved and ventricular wall stress with no arrhythmia formation in a porcine model of MI.[165] Finally, Weinberger et al. loaded human iPSC-derived cardiomyocytes and ECs into a fibrin patch to treat MI in Guinea pigs.[166] After four weeks, the engineered heart tissue displayed engraftment with the host tissue and electrically coupled with the myocardium, although evaluation was performed post-explanation of host tissue. These are only a few examples of a large body of work being investigated in generating beating patches.

From these studies, the main workhorses of generating a functional cardiac patch are iPSCs and ESCs. In other tissue applications, resident tissue stem cells may have the ability to form new different tissue cells to create functional tissue.[4,46,167] However, resident CPCs do not form new cardiomyocytes, and native cardiomyocytes are extremely difficult to culture and expand into new tissue. Therefore, a pluripotent stem cell type must be implemented to develop new cardiomyocytes. While groups are attempting to develop functional cardiomyocytes from iPSCs and ESCs, the cardiac progenitors and cardiomyocytes developed from iPSCs and ESCs are immature and do not exhibit adult cardiomyocyte phenotypes, although studies are promising.[10,160,161] Once a functional

patch can be developed with mature cardiomyocytes, many additional problems may arise.[10,160,161] Importantly, myocardial tissue requires a high vasculature density to supply nutrients to constantly beating cells.[10,14,161] Generating a patch that contains functional cardiomyocytes, sufficient vasculature, robust ECM for force propagation, and fibroblasts for matrix control will be challenging. Another critical problem is patch integration with the native tissue. Cardiac contraction is a highly organized system that relies on pacemaker cells and secondary cells of the cardiac conduction system to work in complete unity and drive contraction through action potential propagation.[168] Pacing fibers must be included in the engineered cardiac patch to incorporate conduction if the tissue being replaced is large. Also, integrating the contractile frequencies of the new and native tissues will be challenging and may cause significant problems such as arrhythmias and lack of organized contractile function.[10,160] Finally, tissue replacement inherently introduces significant immune responses from the host tissue, which can improve or reduce therapy depending on response.[10] Current studies focus on critical aspects of developing a cardiac patch *in vitro*, such as perfusion bioreactor systems, mechanical/electric stimulation, maturation via secondary signaling molecules, vasculature fabrication, and methods to speed up tissue growth *in vitro*.[10,160,169] Advanced technologies also focus on even more sophisticated engineering approaches, such as adding synthetic electronic components to patches, fabricating tissues by layers, engineering whole ventricles, and employing epicardium/endocardium dynamics for integration.[169]

Drug delivery patches, in contrast, rely on the release of pro-reparative components to drive endogenous regeneration of damaged or diseased tissues. Acellular patches loaded with various reparative factors, such as growth factors, exosomes, miRNA, or immune

modulations, represent a classical method of drug delivery to damaged tissues.[10,160,161] A growing body of works is pointing towards exosome and molecular drug release as a powerful method of cardiac repair (although not the focus of this work).[62,63,170] Similarly, cellular patches rely on cells to provide a continuous release of pro-reparative factors towards the damaged tissue. As mentioned in earlier sections, the use of cells allows for continuous, dynamic expressions of complex reparative factors, compared to single or combination acellular drug delivery systems. The goal of implementing cellular patches is the release of reparative factors over the timescale of endogenous repair, after which the patch will degrade and allow for only the native patient tissue to remain. This application is particularly necessary for pediatric patients.[3,4] While post-MI myocardium represents dead tissue, the failing RV of pediatric patients represents a dying tissue with endogenous repair potential. Cardiac patches for treating pediatric patients is also geared towards slowing the progression of RV failure until the patient can receive a transplant, or improve the patient's quality of life. Moreover, the patches must be minimally invasive in terms of tissue integration, as not to elicit an immune response. The development of paracrine patches relies heavily on the cell and biomaterial type and will be reviewed in the next sections.

3.4.4 Patch Design – Cell Type

Cell types used in cardiac patches are numerous. Common types employed are iPSCs, ESCs, MSCs, native cardiomyocytes, endothelial progenitors, CPCs, skeletal myoblasts, and many others.[10,160,171-177] While the generation of beating patches is a significant research direction, the focus of this work is the development of a paracrine

factor-releasing patch. Skeletal myoblasts, MSCs, and hCPCs have been considered effective cell types for paracrine factor release.

Skeletal myoblasts are one of the classical cell types used in cardiac tissue engineering.[171] Physiologically, skeletal myoblasts are progenitor cells that respond to muscle damage or degeneration, which are activated by disease state cytokines and differentiation into multinucleated myotubes, although their paracrine profile appears to drive *in vitro* benefits. Skeletal myoblasts have been studied over the past 30 years for their therapeutic effect on heart repair, with many clinical trials implemented.[171,172] For example, autologous skeletal myoblasts grown in a cell sheet-type patch improved LV EF after six months in patients with ischemic cardiomyopathy.[172] This cell sheet approach has proved effective in small animal models and a few clinical trials. However, skeletal myoblasts have fallen out of focus due to the results of phase II trials such as MAGIC and SEISMIC, where injections resulted in no improved cardiac outcomes and instead increased arrhythmia occurrence.[171] Due to these findings, other cell types have been explored.

MSCs have found success in tissue repair through the effective release of immunomodulatory, angiogenic, and mitogenic factors in a wide variety of applications.[169,171,173-177] These factors make MSCs an interesting possible cell source for cardiac patch development. As an example, human umbilical cord matrix-derived MSCs have been implemented in rabbit and murine models of heart failure via fibrin patches, resulting in improved LV EF, LV fractional shortening, and improved LV remodeling after four weeks.[173,174,175] The beneficial effect of MSCs is also based on reparative factor release from the cells in association with electrophysiological coupling between MSCs and

native cardiomyocytes.[176,177] However, MSCs may not provide a cardiac-specific release profile in terms of types and concentrations of various pro-reparative factors when incorporated within cardiac patches. While effective, MSCs may require large cell numbers and high degrees of tailoring to be truly beneficial for cardiac therapy.

In contrast to skeletal myoblasts and MSCs, CPCs represent a cardiac-specific progenitor cell lineage that has proven effective in treating both adult and pediatric patients suffering from heart disease. Several clinical trials have used CPCs in treating a variety of cardiovascular diseases, as discussed in section 3.2.[169] Clinical results show that CPCs can improve LV ejection faction and decrease infarct size in patients with ischemic cardiomyopathy (SCIPIO trial) and MI (CADUCEUS trial).[5,6,169] Since CPCs have been shown not to differentiate into cardiomyocytes, functional improvements are directed towards factor release. Recent studies have attempted to understand through genomic sequencing and computation models how CPC release profiles repair the myocardium and which factors are most important.[59-63] Within patches, material alignment and composition towards modulating CPC release profiles have also been explored. Gaetani et al. developed a cardiac patch composed of hCPCs within 5-10% alginate-Matrigel scaffolds to improve cell retention and survival.[20] hCPCs remained over 89% viable after 1-7 days post-patch fabrication *in vitro*. Also, hCPCs showed increased expression of early cardiac transcription factors (Nkx2.5, GATA4, MEF-2C) and structural protein Troponin-T. Furthermore, cells migrated from alginate layers to Matrigel layers in printed patches and formed tubular-like structures, showing that hCPCs preferentially survive in complex biomaterials and that multicomponent patches can be generated for defined cell delivery and functional outcomes. Streeter et al. developed a patch of aligned nanofibers to align

CPCs within solid structures successfully.[178] While gelatin and fibronectin incorporation into patches showed improved CPC metabolic activity, the aligned nanofiber patch did not affect the potential for CPC conditioned media to reduce fibrotic gene expression or angiogenesis compared to random nanofiber patches. Regardless, CPCs represent a patient-specific cell source that also produces cardiac-specific paracrine effects. The specific of CPCs may allow for more effective therapy, particularly within a cardiac patch system where CPCs can be controlled and modulated effectively.

3.4.5 Patch Design - Biomaterial Type

Biomaterial type and source is a critical factor in designing effective therapeutic patches. As with any other biomaterial application, a wide variety of natural, synthetic, and combination materials have been implemented in cardiac patches.[10,160,169] Material design considerations involve material degradation, porosity, cell interactions, stiffness, and reactive sites, among others.[10,169] For cardiac regenerative medicine in general, very few materials have moved past evaluation in small animal models towards the clinic.[152,179] Natural materials, particularly alginate and cECM, have moved the farthest in treating adult patients after MI, with cECM hydrogels moving farthest in success (as described in section 3.3). While several reviews have evaluated material choices in cardiac patches, the focus of this work is the implementation of dECM (specifically cECM) materials to promote myocardial repair. dECM shows advantaged over other materials due to its complex formulation of natural biomaterials, intrinsic cell-dECM interactions, and effective degradation for endogenous repair, all of which have been discussed in section 3.3. However, the applications previously discussed implement dECM materials as an injectable therapy due to its soft hydrogel formation after polymerization, which cannot be

easily manipulated for surgical placement as a patch.[10,81,180] Composite materials of dECM and additional biomaterials allow for effective patch formation, and studies investigating dECM composite patches are summarized in **Table 5**.

Table 5. Combinatorial Soluble dECM-Biomaterial Scaffolds

dECM Source	Additional Material	Cell Source	Findings	References
Porcine cECM	Collagen I	Human ESCs	Higher cECM content improved cardiac commitment	[181]
	Chitosan	Murine cardiomyocytes	Improved cardiac commitment, retention, conduction velocities, contractile stress compared to gelatin-chitosan	[20]
	Chitosan, PCL Core	None	Induced M2 macrophages *in vivo*	[184]
	Silk	Human ESCs and ESC-derived cardiomyocytes	Anisotropic, aligned fibers formed via oriented freezing	[187]
			Improved cardiac commitment compared to aligned or isotropic silk	
			cECM inclusion improved cell infiltration and vascularization *in vivo*	
	Silk	Murine Cardiac Fibroblasts	Silk/cECM concentration tailors mechanical properties and fibroblast proliferation, viability, integrin expression	[188]
	PEG-acrylate	Murine Fibroblasts	Increased cECM scaffold modulus	[189]
			Fibroblasts remained viable with the inclusion of PEG	
	PLGA	Human MSCs	Tissue papers induced MSC proliferation	[190]
	PCL and VEGF	Human CPCs and MSCs	Patterned patches improved angiogenesis and ejection fraction in rat MI model	[191]
Human cECM	Amniotic Membrane	Human Cardiac Fibroblasts, Epicardial Cells, cardiomyocytes	Cardiomyocytes showed improved adhesion and survival compared to pure amniotic membrane	[182]
			Reduced monocyte secretion of inflammatory cytokines and induction of M1 macrophages	
Murine cECM (Fetal and Adult)	Fibrin and Transglutaminase	Human CPCs	CPCs remained viable and showed cardiac commitment	[183]
Bovine cECM	Chitosan	Human CPCs	Higher cECM ratio improves CPC viability	[185]
Porcine pECM	Chitosan	Human MSCs	Cardiac preservation and increase in cardiac function 8 weeks post-injection in MI model	[186]
Ovine pECM	CNTs	Murine cardiomyocytes	CNTs suppressed cardiomyocyte cytotoxicity	[192]
			Improved proliferation, gap junction expression, and contraction compared to pECM hydrogels or gelatin-fibronectin coated plates	

3.4.5.1 Natural ECM Component – dECM Cardiac Patches

Several groups have attempted to augment the bioactivity or device fabrication properties of dECM by adding single ECM components such as collagen to maintain the

developed patches as fully bioactive devices composed of only natural materials. Duan et al. developed hydrogels composed of cECM and collagen I at varying ratios to evaluate the material effectiveness in inducing ESC cardiac differentiation, with and without FGF and VEGF.[181] ESC embryoid bodies grown in 75% cECM with no GFs expressed higher levels of cTnT, compared to hydrogels with 25% cECM or 0% cECM with GFs. The high cECM content hydrogels induced the formation of striated cardiac troponin and expression of Cx43, although the effect may be due to the varying storage modulus of the low (8 Pa) and high (60 Pa) cECM scaffolds rather than the cECM composition. Instead of combining cECM with single ECM components, Becker et al. dry coated cell-free amniotic membrane with cECM, combining two complex natural materials.[182] While the cECM coating did not change the mechanical properties of scaffolds, cardiomyocytes showed improved adhesion and survival on cECM coated substrates compared to the pure amniotic membrane. On cECM coated scaffolds, monocytes secreted less inflammatory cytokines and macrophages polarized towards the pro-inflammatory M1 type. Williams et al. used fibrin, adult or fetal cECM, and transglutaminase to generate CPC loaded injectable hydrogels.[183] Transglutaminase effectively modulated the scaffold stiffness from 2-32 kPa, and CPCs grown in scaffolds remained viable and expressed markers for cardiac tissue differentiation such as titin and calponin 1.

3.4.5.2 Non-mammalian Biomaterial – dECM Cardiac Patches

Non-mammalian matrix components, such as chitosan, alginate, or silk, have found relative success in tissue engineering applications, where alginate has moved towards clinical translation for cardiac treatment. Of these, chitosan and silk have been explored in combination with dECM for cardiovascular applications.

The first chitosan-cECM patch was developed by Pok et al., who combined cECM powder with chitosan, followed by lyophilization to form 3D scaffolds.[20] cECM-chitosan scaffolds had similar porosity and elastic modulus (4-13 kPa) to gelatin-chitosan scaffolds. However, cECM-chitosan scaffolds had higher retention of seeded rat cardiomyocytes compared to gelatin-chitosan scaffolds, in addition to increased α-MYH and Cx43 expression, conduction velocities, and contractile stresses. The patch had the potential for direct use as a thick patch for myocardial replacement. Pok et al. modified the patch by adding a PCL core and tested the therapeutic potential of the patch in a rat infarction model.[184] Pourfarhangi et al. evaluated the optimized ratio of cECM and chitosan for improving CPC function and determined that higher cECM composition in composite patches improved CPC viability.[185] Efraim et al. evaluated pECM with genipin crosslinking and chitosan addition, with the intention of therapeutic injection rather than patch implantation.[186] The combined material system showed improved MSC viability, organization, and remodeling on 2D coated systems compared to non-coated plates. The material was injected into acute and long term chronic infarct rat models, which showed preservation and increase in cardiac function eight weeks post-treatment compared to non-treated animals.

Stoppel et al. developed anisotropic silk-cECM scaffolds using an oriented freezing method to form aligned fibers within the scaffolds.[187] The scaffolds had tailorable structures, degradation rates, and mechanical properties based on alignment and composition. *In vitro*, both primary and ESC-derived CM showed improved expression of cardiac markers cardiac troponin and Cx43 in aligned cECM-silk scaffolds compared to aligned or isotropic silk. The patches were implanted subcutaneously in rats, where the

addition of cECM in silk scaffolds significantly improved cell infiltration and vascularization. A follow-up study by Stoppel et al. showed that changing silk and cECM concentration could modulate mechanical properties of scaffolds and cFB proliferation, viability, and integrin expression.[188]

3.4.5.3 Synthetic Biomaterial – dECM Cardiac Patches

Synthetic materials such as PEG, PCL, and carbon nanotubes have been used in cardiovascular tissue engineering as bioinert scaffolds or as supports for bioactive materials. These materials have been combined with cECM and pECM to improve material properties or provide support through similar methods. Grover et al. used PEG-acrylate materials to modulate the mechanical properties of cECM scaffolds and showed that fibroblast viability was not hindered by polymer inclusion.[189] Jakus et al. used a variety of dECM materials, including cECM, to create thin, large "tissue papers" for use in patching applications via the incorporation of poly-lactic-co-glycolic acid.[190] The cECM derived paper showed effective MSC proliferation, although the technology was not evaluated further in the study. Using the vitamin B2 methodology for bioprinting cECM, Jang et al. generated cardiac patches composed of PCL, CPCs, MSCs, VEGF, and cECM. CPC-cECM strands and MSC-VEGF-cECM strands were printed separately for endothelial induction of MSCs and improved functionality of CPCs.[27,191] Alternating PCL layers were required to form printed patches, which in turn improved mechanical properties and handling of patches for surgical implantation and may significantly increase degradation time of the patch. The methodology of combining cells, GFs, cECM, and PCL into a complex tissue scaffold is a significant step towards multi-component patches for cardiac repair. Roshanbinfar et al. developed a unique application of using dECM via the

incorporation of carbon nanotubes within injectable pECM materials to improve pECM electrical conductivity and mechanical properties.[192] Dispersion of nanotubes within the pECM materials was achieved through carbodihydrazide modification of nanotubes, which also suppressed cytotoxicity of cultured cardiomyocytes. Also, cardiomyocytes in the pECM-carbon nanotube scaffolds had higher proliferation and expression of Cx43 compared to pECM hydrogels or gelatin-fibronectin coated plates.

Combinational devices use a wide variety of materials and methods to modulate or supplement cECM and pECM mechanical, bioactive, or formation properties. While investigations on novel materials may pave the way for enhanced dECM therapy in cardiac repair, *in vivo* analysis in animal models is critical for truly evaluating the effects of differential therapies.

3.4.6 Patch Design - Fabrication Methods

The fabrication method employed in generating a solid patch can be just as important as selecting the optimal cell and biomaterial types.[160,169] The number of fabrication methods is as vast as the number of materials that can be used for device design. Conventional biofabrication techniques include methods such as casting, particulate leaching, layer deposition, electrospinning, and freeze-drying.[23,193] Although effective, these methods may result in limited reproducibility and effectiveness in fabrication. Modern approaches have been developed that combine several of these approaches. Specifically, bioprinting has been employed extensively in cardiac tissue engineering.[23,24,193] Bioprinting involves the fabrication of solid constructs using specifically programmed geometries containing biomaterials and cells within a bioink by

synchronizing material deposition/polymerization with motorized capture area movement, layer by layer. 3D bioprinting allows for high degrees of structural control with high reproducibility and opportunity for automation.[23,193] Types of bioprinting include injection printing, extrusion-based printing, and laser-assisted printing, among others. Bioprinting methodology is heavily intertwined with biomaterial requirements and choices since material polymerization and structural support define how each new layer is formed. For hydrogel systems, which represents many of the formulations in cardiac patches, extrusion bioprinting has been extensively employed.[25]

Extrusion bioprinting relies on the layer by layer deposition of bioink filaments, where each successive layer builds upon the previous layer.[193] Extrusion bioprinting has high shape control down to 100 μm, with highly controllable printer parameters and the opportunity to generate devices based on patient-specific geometries.[25,193] Filament deposition allows for customized fiber alignment, infill shape parameters, and intra-device structures. Extrusion bioprinting requires a bioink that is structurally supported for layer by layer deposition, either by high solution viscosity or material polymerization between successive layers. While this requirement may be simple enough to achieve, the material also has to be bioactive enough to support cellular growth and function.[23,193] These conflicting factors are seen in problems with original systems of bioprinting, where ideal printability materials result in poor cell culture environments, and ideal cell culture materials result in poor printability and shape fidelity. Modern bioinks are moving towards materials that offer both ideal printability/shape fidelity and biocompatibility/cell viability, oftentimes by incorporating both bioactive and bioinert materials to support both cells and structure.[23,24,193]

Examples of bioprinting in cardiovascular tissue engineering are numerous and involve printing vasculature, myocardium, heart valves, and even whole hearts.[23] Vasculature is a critical factor in generating beating tissue and cardiovascular constructs. Mironov et al. deposited vascular tissue spheroids within collagen to form acellular vascular grafts through a bioprinting approach, where graft imaging showed the integration of cells after six days and the formation of a double-layered vascular wall.[194] Similarly, Cui et al. incorporated heating to deliver ECs and thrombin into fibrinogen substrates to form microvasculature constructs of ECs and fibrin.[195] Poldervaart et al. used bioinks composed of VEGF and either Matrigel, alginate, or Matrigel-alginate combination to modulate the release profiles of vascularized bioprinted constructs.[196] Similarly, Kolesky et al. printed heterogeneous structures composed of ECs, gelatin, and Pluronic F127 to form vascular networks.[197] Pluronic F127 was removed by perfusion after printing, resulting in vascularized cellular systems. Studies have also attempted to print entire myocardial replacements or cardiac patches. Gaetani et al. used extrusion methods to print scaffolds of fetal CPCs.[20] Cells cultured within printed scaffolds showed high cell viability, increased proliferation, and expression of integrin. Gaebel et al. used an inkjet printing approach to develop a polymeric patch of multiple cell types between two slides.[198] By using laser pulses with gold evaporation at focal points, human ECs and human MSCs were patterned in specific patterns to promote vessel formation and MSC survival around vessels. Several groups have also attempted to print a functional heart valve. Nachlas et al. printed a PCL-gelatin-PEG heart valve for pediatric applications. By selectively depositing gelatin-PEG-cell layers on bioprinted PCL layers, a mechanically and physiologically relevant heart value was engineered.[199] Finally, studies have

attempted to print entire hearts for complete replacement. While ambitious, bioprinted hearts were developed using alginate and 3D imaging data of embryonic chick hearts, although tissue functionality was not achieved.[200] These examples show the power of bioprinting in generating reproducible, controlled, and customizable devices for cardiac tissue engineering and patch development.

CHAPTER 4. DEVELOPMENT AND IN VITRO ASSESSMENT OF A BIOPRINTED PATCH COMPOSED OF CECM AND HCPCS

4.1 Introduction

The development of a cell-biomaterial composite generated through bioprinting relies heavily on biomaterial polymerization and printing dynamics to achieve a functional form and allow for cellular growth and functionality, as discussed in section 3.4.6. Bioprinting of ECM based materials has mainly been achieved with the inclusion of a filler polymer to allow for proper printing viscosity.[23,25,26] ECM solutions at therapeutic concentrations (6-10 mg/mL) are low viscosity pre-polymers, which do not print effectively due to layers remaining fluid and non-overlapping, while polymerized ECM is a fibrous material that, while more viscous then the pre-polymer, comes out in "chunks" rather than a homogenous stream of print filaments.[18,19,26] Surprisingly, cECM has been printed directly without the use of filler polymer; however, this approach suffers from two main issues.[26,191] The first is that the required concentration for printing pure cECM (20-30 mg/mL) is significantly higher than has been used in treatment studies with cECM and requires extensive harvesting from porcine sources for generation of a limited number of devices. Second, and more pressing, is that the pure cECM printed materials are difficult to handle and risk rupture when potentially used as an epicardial patch, due to their low mechanical modulus and fibrous nature.[18,189] cECM was printed with the use of filler polymers such as PCL in alternating layers to improve patch handling, which then produced mechanical mismatch with the patch and the native myocardium, and rendered

the patch with a degradation time much longer than a natural biomaterial system.[191] Although methods have been employed to modify pure cECM mechanical properties in printed constructs, such as by the inclusion of vitamin B2, it is unclear if this method can be employed as a cell-laden patch without the use of supporting polymer layers.[27,191] In this chapter, we develop a methodology of printing hCPC-cECM patches through the incorporation of a bioactive secondary biomaterial. We evaluate the effectiveness in printing cardiac patches using the developed methodology, followed by cellular analysis in terms of viability and functionality and material analysis in terms of mechanical properties and degradation.

4.2 Materials and Methods

Materials – Gelatin methacrylate (GelMA) was purchased from CellINK (Gothenburg, Sweden). Triethanolamine (TEOA), 1-Vinyl-2-Pyrrolidione (NVP), HEPES sodium salt, bovine gelatin, Triton X-100, sodium dodecyl sulfate, and pepsin were purchased from Sigma-Aldrich (MO, United States). Insulin-Transferrin-Selenium (ITS) media, Hams F-12, Matrigel Matrix Growth Factor Reduced, Dulbecco's Modified Eagle Medium (DMEM), and Penicillin Streptomycin (Pen-Strep) were purchased from Corning Cellgro (NY, United States). Eosin Y sodium salt was purchased from TCI (MA, United States). Nordson EFD 30cc barrels, pistons, and 27-gauge plastic tips were purchased from TEK products (MN, United States). Standard fetal bovine serum (FBS) and RNase-free water were purchased from Hyclone (PA, United States). L-glutamine was purchased from MP Biomedicals (OH, United States). Cell culture dishes and well plates were purchased from Cellstar (PA, United States). Calcein AM, Ethidium homodimer-1 (EtD), DAPI, Vybrant DiD cell solution (DiD), Dynal magnetic beads, Trizol, Power SYBR Green, first

strand buffer, dithiothreitol, Click-iT EdU (5-Ethynyl-2'-deoxyuridine) Microplate Assay, RNaseOUT Inhibitor, M-MLV, and Alexa Fluor 568 Carboxylic acid Succinimidyl Ester (AF568) were purchased from Invitrogen (CA, United States). Phosphate buffered saline (PBS) and hexamers were purchased from Fisher Scientific (NH, United States). Oligo(dT) and dNTP were purchased from Fermentas (MA, United States). Primers were purchased from Integrated DNA Technologies (IL, United States). Human umbilical vein endothelial cells (HUVECs) were purchased from Lonza (Basal, Switzerland). Endothelial cell growth media kits (includes growth factors) were purchased from R&D Systems (MN, United States). Hanks balanced salt solution (HBSS) was purchased from Gibco (OK, United States). Collagenase type 2 (300 U/mL) was purchased from Worthington (NJ, United States). Anti-c-kit H300 antibodies were purchased from Santa Cruz (TX, United States). Bovine fibroblast growth factor (bFGF) was purchased from Stem Cell Technologies (Vancouver, Canada). QIAshredder centrifuge filters were purchased from QIAGEN (Hilden, Germany).

Neonatal Human Cardiac Progenitor Cell Isolation and Culture – The Institutional Review Board at Children's Healthcare of Atlanta and Emory University approved the harvesting of human neonatal c-kit expressing CPCs from the atrial appendage, as previously described.[17,62] In short, right atrial appendage tissue was obtained from pediatric patients aged one week or less undergoing heart surgeries due to congenital heart diseases. The atrial appendage tissue was transported using Krebs-Ringer solution, washed with HBSS, and broken down into small sections. The tissue was then enzymatically degraded using 1 mg/mL of collagenase type II at 37^0C, 5% CO_2 for 30 minutes and passed through a 70 μm filter. The mixture was centrifuged at 1000g for 5 minutes to pellet the

cells. The cells were combined with magnetic beads conjugated with anti-c-kit antibody, allowed to incubate for 2 hours at 37^0C, followed by magnetic sorting and successive washes with cell culture media. Separated c-kit+ cells were expanded, and the expression of c-kit in the cell population was measured by flow cytometry to ensure they were at least 90% positive. Cells from three donors were either pooled at the first passage or cultured separately and combined before bioprinting, for all experiments described in this research. hCPCs were grown in T-75 cell culture treated dishes with culture media for expansion. The media was changed every 2-3 days until bioink preparation. Cell culture media consisted of Ham's F-12 media supplemented with 1x Pen-Strep, 1% L-glutamine, 10% FBS, and 10 ng/mL bFGF.

Cardiac Extracellular Matrix Isolation and Characterization – Decellularized porcine ventricular extracellular matrix (cECM) was generated and processed as previously described.[16,17,18] Briefly, porcine ventricular tissue was separated, sectioned into small pieces, rinsed in PBS, and decellularized using a 1% solution of SDS for 4-5 days. The decellularized cECM was rinsed with water, frozen at -80^0C overnight, lyophilized, and milled into a fine powder. Then, the cECM was processed into liquid form by partial digestion with pepsin (1 mg/mL) in 0.1 M HCl for two days, at a ratio of 10:1 of cECM to pepsin. The cECM was then raised to basic pH by adding 1 M NaOH and salt concentration of 1x PBS, followed by adjustment to pH of 7.4 using HCl and NaOH and diluted to a solution concentration of 8 mg/mL. The solution was aliquoted, immediately frozen at -80^0C overnight, lyophilized for 24 hours, and stored at -80^0C before use.

Rat Cardiac Fibroblast Isolation and Conditioned Media Harvesting – Primary cardiac fibroblasts (cFB) were isolated as previously described.[62] In short, hearts were

excised from adult male rats, shredded, and subjected to digestion with 1 mg/mL trypsin in HBSS at 4ºC for 6 hours. The solutions were digested with 0.8 mg/mL collagenase in HBSS at 37ºC for 15 minutes and then quenched with cell culture media. The cell suspensions were passed through 100 µm filters, followed by cell pelleting and plating for 3 hours to allow for cFB adherence, and then washed to remove non-cFBs. cFBs were grown in fibroblast growth media, which is composed of DMEM supplemented with 1x Pen-Strep, 1% L-glutamine, and 10% FBS. cFB conditioned media was collected every two days from cFBs while they were grown until confluence, at which point the media across the entire culture time was combined and homogenized.

Bioink Preparation – GelMA solutions of 14.432% were created by dissolving lyophilized GelMA in 15 mM HEPES buffer and allowed to dissolve under stirring at 60^0C for 1-2 hours. GelMA solutions were frozen at -20^0C until use. Stock solutions of 13 mg/mL cECM are formed by rehydrating the cECM material with HEPES buffer followed by adjusting the solution to pH 7.4 with HCl immediately before use. All bioinks were prepared immediately before printing. GelMA bioinks were prepared by mixing GelMA (final concentration 5% w/v), Eosin Y (100 µM), NVP (0.75% v/v), TEOA (3% v/v), and HEPES buffer (15 mM). In the case of GelMA-cECM bioinks, the HEPES in the above formulation was replaced by the cECM (final concentration 8 mg/mL) solutions. For the inclusion of cells, neonatal hCPCs (passage 6-10, pooled or combined across at least three donors) were removed from cell culture plates, pelleted at 1000 rpm for 5 minutes, and mixed with 1 mL solution of the bioink solution, producing a final concentration of 3 million cells/mL.

Bioprinting and Patch Formation – All bioink solutions, with or without cells, underwent similar printing protocols. 1 mL of bioink was deposited into sterilized 30 cc printer barrels and pushed towards the barrel head with a sterile loose fit plunger, removing any air bubbles that formed. A sterile 27-gauge plastic needle tip was added to the barrel, and a cap connecting the print head to the barrel as added. The barrels were put in the low-temperature head of the bioprinter (EnvisionTEC 3D-bioplotter Developer Series), which was set to 10^0C, and the bioink was allowed to polymerize for 10 minutes. After initial gelation, the printer head was calibrated and purged at 1.2 bar for 1-3 seconds to ensure free-flowing and uniform filaments. Patches and grids were printed onto a glass slide platform at room temperature, using a pressure 0.7-1 bar and speed of 10 mm/s. Patches were 10 mm in diameter and 0.6 um thick, which printed in 3 layers, with an infill pattern of 90^0 grids with 0.5 mm spacing. Six to eight patches were printed at once. Test grids were 10mm x 10mm boxes with an infill pattern of 90^0 grids with 1 mm spacing. CAD (computer-aided design) models of the patches and grids printed were generated using SOLIDWORKS and imported to the printing control system through the Bioplotter RP program. Following printing, both patches and test grids were exposed to white light (Braintree Scientific) at 4^0C for 5 minutes to allow for radical polymerization. The patches were removed from glass slides and put in 2 mL solutions of cell culture media in 24-well plates. Patches that were being evaluated for paracrine release were put in 2 mL solutions of treatment media in 24-well plates. The treatment media consisted of Hams F-12 media supplemented with 1x Pen-Strep, 1% L-glutamine, and 1x ITS. All patches were kept in cell culture incubators during further experiments, which allowed for cECM polymerization within 1 hour after GelMA radical polymerization. The media was changed

or harvested every two days for each group. The test grids followed a similar protocol after polymerization, with the difference being that the grids were not removed from the slides, and media was added directly over the grids to allow for complete coverage. The test grids were left in the cell culture incubator for 1 hour to allow for the cECM to polymerize fully, washed several times, and removed immediately for imaging.

Imaging Printed Test Grids – Imaging of the printed test grids was performed at 10x magnification with an Olympus 1X71 Inverted Microscope. Bright-field images of both GelMA and GelMA-cECM grids were taken for printability comparison. For evaluating cECM homogeneity throughout the printed structures, cECM solutions were allowed to bind with AF568 at 4^0C for 1 hour, which forms a strong bond to primary amines, at a concentration of 13.3 ug/mL based on modifying a previously described protocol.[60] The cECM solution was used to form test grids as described in the printing section, followed by swelling and incubation for at least 1 hour at 37^0C. Stained GelMA-cECM test grids were imaged at 10x magnification both on an Olympus 1X71 Inverted Microscope and Olympus FV1000 Confocal Microscope. Printed test grids with hCPCs were also imaged at 10x magnification with an Olympus 1X71 Inverted Microscope. hCPCs were incubated with the lyophilic dye DiD according to manufacture protocol to allow for cellular imaging. Briefly, hCPCs were trypsinized from cell culture dishes, counted, and pelleted. The cells were suspended at a density of 1 million cells/mL in serum-free culture media supplemented with 5 uL/mL of DiD solution (1 mg/mL stock) and mixed. hCPCs were allowed to incubate for 20 minutes at 37^0C. The cells were centrifuged at 1000 rpm for 5 minutes, the supernatant was removed, and the cells were resuspended in serum-free media. The wash procedure was repeated twice to remove any unbound DiD,

and the cells were resuspended in the bioink solution for printing, as described above. Printed test grids were again imaged at 10x on the fluorescence microscope. For image analysis of cell homogeneity throughout the printed structure, ImageJ was used to measure several line scans of fluorescence intensity along grid lines, which were then averaged to produce the Figure.

Printability Analysis – The printability analysis implemented in this work looks at the effectiveness of the extruded filaments in the test grids to form square holes between filaments, as previously described.[201] Circularity (C) of an enclosed area is based on the shape perimeter and area, where a perfect circle has a circularity of 1. For a square shape, circularity is equal to $\pi/4$. To this end, and as previously derived and defined, printability is given as Equation 1

$$\mathrm{Pr} = \frac{\pi}{4} * \frac{1}{\mathrm{C}} = \frac{\mathrm{L}^2}{16\mathrm{A}} \quad (1)$$

Where L is perimeter and A is area of a shape. A printability of 1 is equal to a perfect square, and indicates optimal gelation, and thus printing, conditions of a bioink. Bright-field images of test grids were evaluated by measuring the perimeter and area of several holes in each sample, and Pr was calculated using Equation 1, with three technical replicates and 4-6 holes per n.

Rheological Analysis – As the printed patches were too thick to be measured on a rheometer without rupture, disk-shaped hydrogels without cells were made by sandwiching 15 uL of sample solution between two glass slides separated by a thin spacer, allowed to gel at 4^0C for 10 minutes, and polymerized by white light (Braintree Scientific) for 5

minutes at 4^0C. The sample disks were incubated overnight in cell treatment media to undergo cECM polymerization and swelling. The storage and loss moduli of the disks were measured using dynamic oscillatory strain and frequency sweeps performed on an Anton Paar MCR 302 stress-controlled rheometer with a 9-mm diameter 2^0 measuring cone.[70] The disks were loaded in the rheometer, and the system was lowered to a 39 μm gap. Strain amplitude sweeps were performed at $\omega = 10$ rad/s to determine the linear viscoelastic range of the samples. Oscillatory frequency sweeps between 0.5−30 rad/s and 2% strain were then used to measure the storage and loss moduli. Samples were measured at 1, 4, 7, 12, and 21 days for degradation analysis of cell-free samples grown in treatment media and at 1, 7, and 21 days for degradation analysis of cell-laden samples grown in cFB conditioned media. All samples had 3-6 technical replicates per n.

Swelling – Patches were printed without cells as described above and allowed to swell for 24 hours in treatment media. The swollen patches were weighed (wet weight) and put in separate centrifuge tubes. The samples were lyophilized in a Labconvo lyophilizer for two days, and the weight of the dried material was measured (dry weight). All samples had three technical replicates per n. The swelling ratio was calculated as wet weight/dry weight.

Degradation – Patches were printed as described above and allowed to swell for at least 24 hours in treatment media. For measuring of degradation via weight change, the patches were weighed at days 1, 3, 7, 10, 15, and 21 after formation, and degradation via hydrolysis was determined as the change in weight compared to original weight at day 1. For measurement of degradation via mechanics, as described in the Rheological Analysis section, mechanical measurements of the materials were taken at 1, 4, 7, 12, and 21 days

for cell-free samples grown in treatment media, and at 1, 7, and 21 days for cell-laden samples grown in cFB conditioned media. Degradation was determined as the change in storage modulus (measured at 1.61 rad/s) compared to the modulus at day 1. All samples had 3-6 technical replicates per n.

Viability Analysis – hCPC containing patches were grown in cell culture media for 1, 3, or 6 days, changing media every two days. Patches were removed from growth plates and placed in a 250 uL solution of 3 uL/mL Calcein AM (live) and 2 uL/mL EtD (dead) in HBSS in 48 well plates. The patches were left for 30 minutes at 37^0C to incubate, followed by two washed with 1x HBSS for 5 minutes each. The patches were removed and placed on glass-bottom dishes for imaging on an Olympus FV1000 Confocal Microscope. Live/dead images of the hCPCs within the patches were taken at several locations. Several areas of each patch, six patches each, were used as technical replicates to evaluate data expressed as live cells/total cells.

Tube Formation Assay – Conditioned media from empty or hCPC containing patches were grown in treatment media was collected at days 3 and 7. The conditioned media was centrifuged at 10000g for 10 minutes to remove any cell debris or particulate matter, and the supernatant was stored at -80^0C until analysis. HUVECs were grown on 0.1% w/v gelatin-coated T-75 tissue culture plates with endothelial cell growth media until assays were performed. Tube formation assays were implemented as previously described.[62,70] In short, HUVECs were removed from culture using trypsin and added to Matrigel-coated well plates at a concentration of 10000 cells/well. Conditioned media harvested from patches (200 μL) was added to the top of each well. For positive controls, non-conditioned treatment media was added. All HUVECs were allowed to grow for 6

hours. Calcein AM dye (2 mg/mL) was added to each well, and cells were imaged via fluorescence to measure tube formation. The extent of total tube length formed in each well was evaluated by the Angiogenesis Analyzer for ImageJ (Gilles Carpentier), and the total tube length for each sample was normalized to the value of the positive controls.

RNA Isolation, Reverse Transcription, and Quantitative Real-Time PCR – Cell-laden patches were grown in culture media for 3 and 7 days. At each time-point, three technical replicates/n were harvested, added to vials containing 1 mL Trizol to isolate RNA, and homogenized (Fisher Scientific PowerGen 500) for several minutes.[70] The homogenized suspension was centrifuged at 15000g for 1 minute with QIAshredder filters to separate the cellular components from the gel. RNA extraction was performed according to the manufacturer's protocols. RNA quantification and purity were determined by measuring absorbance at 260 and 280 nm wavelength on a spectrophotometer (Thermo Scientific NanoDrop One), followed by running reverse transcription as previously described.[16,17,70] Briefly, 0.5-2 µg RNA was mixed with hexamers, oligo(dT), dNTP, and RNase-free water in a final volume of 12 µL, and samples were heated to 65ºC for 5 minutes to denature the RNA, followed by cooling to 25ºC for 10 minutes to allow for components to anneal. Then, RNaseOUT inhibitor, M-MLV, first strand buffer, and dithiothreitol were added to solutions, heated to 37ºC for 60 minutes to undergo reverse transcription, and heated to 70ºC for 15 minutes for enzyme inactivation. cDNA samples were stored at -80ºC before further measurement. Gene expression was measured using a quantitative real-time PCR system (Applied Biosystems, StepOne Plus Software). cDNA in 1:5 ratio was mixed with Power SYBER Green, RNase-free water, and target primer, heated to 95ºC for 10 minutes, and allowed to run for 40 cycles, as previously

described.[16,17] Each sample was run in triplicate per primer, and $\Delta\Delta C_t$ method was used to obtain fold change values over GAPDH and GelMA control.[62] The primer sequences used are seen in **Table 6**.

Table 6. PCR Primers for Aim 1

Name	Forward 5'-3'	Reverse 5'-3'
Connexin 43 (Cx43)	CAATCTCTCATGTGCGCTTCT	GGCAACCTTGAGTTCTTCCTC
GATA4	TAGACCGTGGGTTTTGCATTG	CATCCAGGTACATGGCAAACAG
Myocyte enhancement factor 2C (MEF2C)	TAACTTCTTTTCACTGTTGTGCTCCTT	GCCGCTTTTGGCAAATGTT
β-Myosin heavy chain (MYH7)	GGCAAGACAGTGACCGTGAAG	CGTAGCGATCCTTGAGGTTGTA
Vascular endothelial cadherin (VE-Cad)	CCGACAGTTGTAGGCCCTGTT	GGCATCTTCGGGTTGATCCT
Platelet endothelial cell adhesion molecule (CD31)	TCTATGACCTCGCCCTCCACAAA	GAACGGTGTCTTCAGGTTGGTATTTCA
Vascular endothelial growth factor receptor 1 (FLT-1)	GACTAGATAGCGTCACCAGCAG	GAAACCGTCAGAATCCTCCTC
α-Smooth muscle actin (ACTA-2)	AATACTCTGTCTGGATCGGTGGCT	ACGAGTCAGAGCTTTGGCTAGGAA

Proliferation - Cell-laden patches were grown in culture media supplemented with 20 μM EdU for 3 and 7 days. At each time-point, patches were harvested and cut into equal size sections to fit in 96 well plates. Click-iT EdU assay was performed according to manufacturer instructions. Briefly, cell-laden samples were fixed and incubated with Click-iT reaction cocktail. Samples were then incubated with anti-Oregon green HRP, followed by incubation in Amplex UltraRed reaction mixture. The reaction was stopped after 15 minutes, the absorbance of each well was measured, and absorbance of the blank was

subtracted from each sample. Absorbance from GelMA-cECM patches was normalized to the absorbance of GelMA patches for each n.

Statistics – Numerical data are the mean ± SEM. All data except for printability were analyzed using one-way ANOVAs with Tukey's multiple comparison post-test. Sample size (n) was 3-6 for all samples. In cases where both days and groups were involved, data were compared across groups within the same day and across days within the same group to determine significant differences. An unpaired t-test was used to compare GelMA and GelMA-cECM in the printability analysis. Control group error for normalized measurements is presented either as SEM of replicates across experiments or SEM of normalized values across n.

4.3 Results and Discussion

To generate a cECM patch that has a high degree of printability, proper mechanical properties for myocardial therapy, and allows for cell viability and paracrine release, we used gelatin methacrylate (GelMA) as a support material. GelMA is a natural biomaterial based on collagen, which has methacrylate groups grafted onto the gelatin structure so that the material can undergo radical polymerization.[202,203] GelMA is used extensively as a bioactive and resorbable material for regenerative medicine applications and in a multitude of tissues such as muscle, liver, and bone.[202,203,204] To limit cell damage, we employed a white light system for gel polymerization after structure formation. This white light system has advantages over UV systems that otherwise induce increased cell death and stress.[205,206,207] We investigated the use of various cross-linking systems in forming solid structures post-printing, such as ruthenium-sodium persulfate or Irgacure 2959, but found

that an Eosin Y system allowed for the most effective formation of structurally reliant and viable patches.[203,206,207] Most importantly for bioprinting, GelMA undergoes polymerization when cooled from physiological temperatures to below 10ºC, and is viscous even at room temperature with concentrations of 10% weight/volume (w/v) and above. This phase transition makes it suitable for bioprinting as a natural material and has been used often for this application.[207] This work utilized 5% w/v GelMA in the bioink formulations so that the bioink was still a significant portion cECM (8 mg/mL), compared to increasing the concentration of GelMA to 10% or higher, which would have produced a bioink that is mostly GelMA with some cECM added. Also, low w/v % GelMA supports more effective cellular outcomes such as viability and proliferation.[208] Our printing strategy involved cooling 5% w/v GelMA to 10ºC for 10 minutes to allow for gelation and enhanced printing viscosity of the cECM/hCPC bioink. An overview of the printing strategy is seen in **Figure 1**.

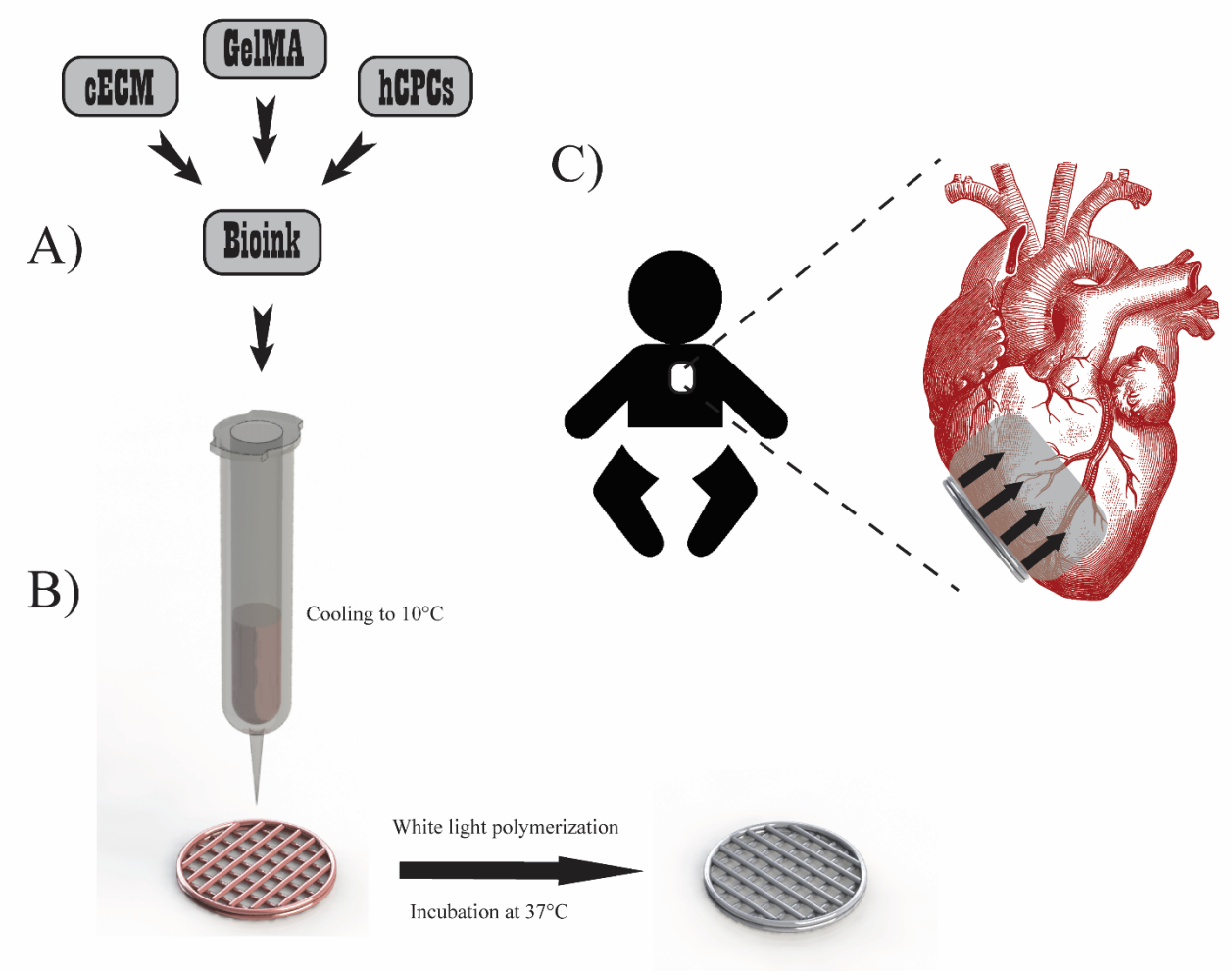

Figure 1 Printing methodology overview. A) Bioink preparation involved combining cECM, hCPCs, and GelMA to form naturally derived and cell-laden materials for printing. B) Printing methodology involved cooling the bioink to 10ºC in the 3D bioprinter barrels to allow GelMA polymerization for improved printability. Patches were printed with infill patterns of 90º intersecting filaments and contour. Patches were polymerized via white light to induce radical polymerization of GelMA, followed by incubation at 37ºC for at least 1 hour to induce cECM polymerization. C) Patch implementation will involve epicardially inserting the patch to the RV of pediatric patients, where the patch will release key pro-regenerative paracrine factors.

The printing methodology allowed for clean and defined extruded filaments when printing either GelMA or GelMA-cECM (**Figure 2A)**. To ensure that the cECM fibers were uniformly distributed in the printed structures, we stained the cECM with AF568 carboxylic acid succinimidyl ester (AF568), which forms a strong bond to primary amines on the cECM proteins. The red staining in **Figure 2B** is the cECM fibers, indicating that the cECM was distributed homogeneously throughout the entire printed structure, rather than in clumped locations such as filament junctions. Higher magnification in 3D of a printed filament in **Figure 2C** shows that the cECM formed homogeneously distributed dense fibers after polymerization at physiological pH and temperature. We quantified the printability of the structures using a parameter based on the extent to which the holes between filaments match a square shape, as previously described and discussed in the materials and methods section.[201] A value of printability close to 1.0 demonstrates ideal gelation, and thus the printing property, of the bioink. This value shows that the holes are close to a perfect square shape due to the filaments being uniform in thickness, homogeneous, and rigidly defined with multiple layers stacking on one another. As can be seen in **Figure 2D**, both GelMA and GelMA-cECM bioinks had printability close to a value of 1.0, and the inclusion of cECM improved the printability of the bioink significantly to achieve a value closest to ideal printing.

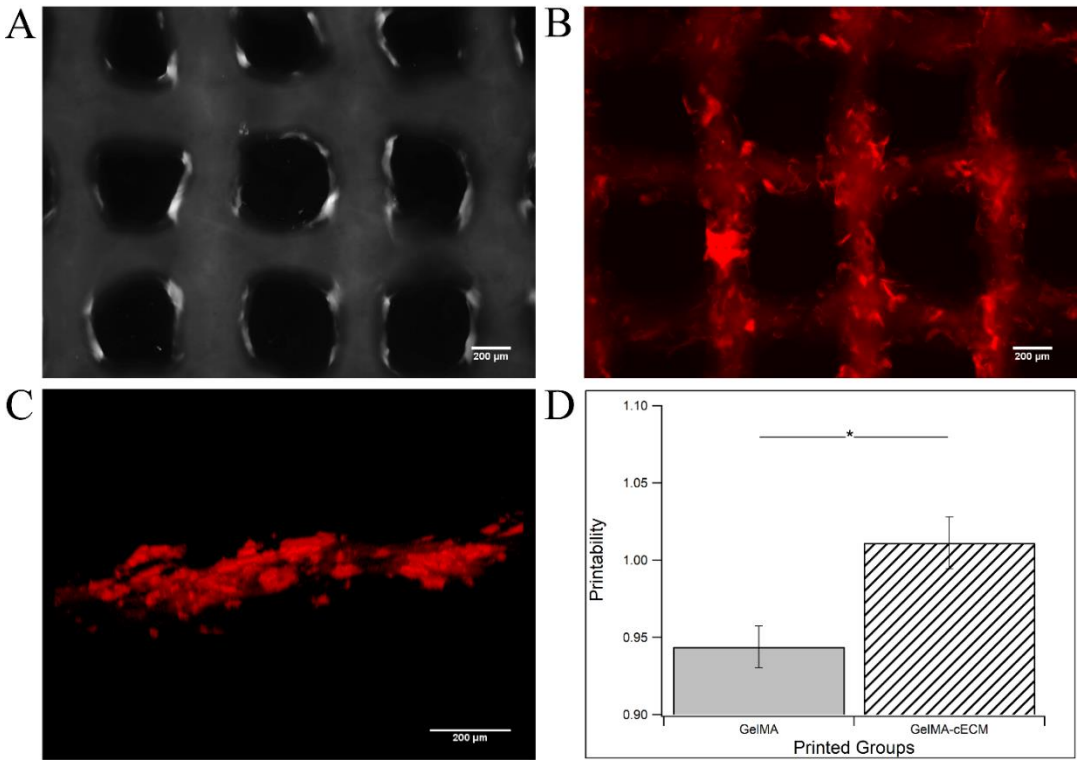

Figure 2. Printability Analysis of GelMA-cECM Bioinks. A) Bright-field image of printed test grids of GelMA. B) Fluorescence image of printed test grids of GelMA-cECM with staining for cECM by AF568. C) 3D fluorescence close-up view of a printed filament of GelMA-cECM, with staining for cECM by AF568. D) Printability comparison between GelMA and GelMA-cECM bioinks. * = p-value < 0.03, given by paired t-test, n = 5.

Following the incorporation of cECM into the printed structure, we next sought to determine if primary cells could be added to the printing mix. hCPCs were incorporated into the bioinks and evaluated for effectiveness in creating homogeneously distributed cell-laden print structures. Non-extrusion based bioprinting methods require high printing pressures that render cells non-viable or methodologies that result in the dispersion of cells towards the edges of printed constructs, rather than homogeneously distributed throughout.[209,210] Furthermore, cells can leach out of printed hydrogel constructs if the

materials are soft and not effectively polymerized, resulting in a loose network.[211] As shown in the bright-field images in **Figure 3**, we were able to add cells to the print for both GelMA alone **(Figure 3A)** and GelMA-cECM **(Figure 3B)**, where cells were retained in the gels after cross-linking. Cells were stained with a lipophilic dye (DiD) before printing to obtain a clearer image of hCPCs throughout the test grids. **Figure 3C** shows the printed grids after swelling, indicating that the cells appeared homogeneously distributed throughout the filaments. An averaged fluorescence line scan along filaments showed that the fluorescence intensity throughout the filaments was uniform and that the cells were homogeneously distributed **(Figure 3D)**. Cells were incorporated throughout the filaments, and GelMA-cECM grids once again appeared to have better printability, as indicated by the hole geometry, where the GelMA-cECM grids had more square holes then GelMA grids. Printing parameters were not modified by the incorporation of cells, maintaining a low printing pressure (0.7-0.8 bar), and thus low shear stress, on the cells. Also, cells remained firmly supported within the printed constructs, with no cells leaching out of the grids or sifting to the bottom of the filaments.

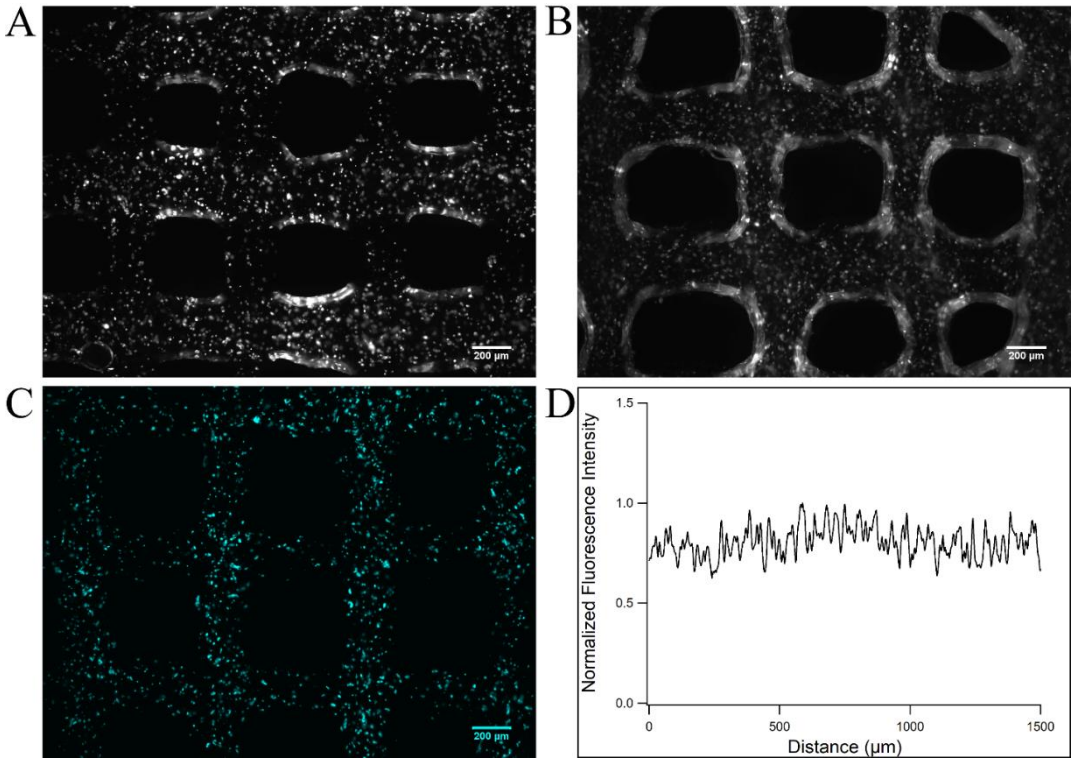

Figure 3 Printing hCPC-containing Bioinks. A) Bright-field image of printed test grids of GelMA bioinks containing hCPCs, taken 1 hour after printing. B) Bright-field image of printed test grids of GelMA-cECM bioinks containing hCPCs. C) Fluorescence image of printed test grids of GelMA-cECM with hCPCs stained with DiD. D) Normalized fluorescence intensity of line scans performed on stained hCPC test grids. Line scans were performed across several filaments.

The hCPC/cECM bioink was shown to have ideal printability with a homogeneous distribution of both cECM and hCPCs throughout the printed structures, as described in the above sections. Moving on, we were able to create cardiac patches using the cell-laden bioink, based on a cylindrical shape, as indicated in **Figure 4**. **Figure 4A** shows the printed patches before white light polymerization, while **Figure 4B** shows the CAD (computer-aided design) models using the patch design. The patches were pink due to the Eosin Y

photoinitiator and change to clear after polymerization. The printed patches maintained the same shape and structure as the CAD model, due to the high printability bioink. The infill pattern of the patches was perpendicularly aligned filaments generated through multiple print layers, indicating further degrees of printing control and structure fidelity.

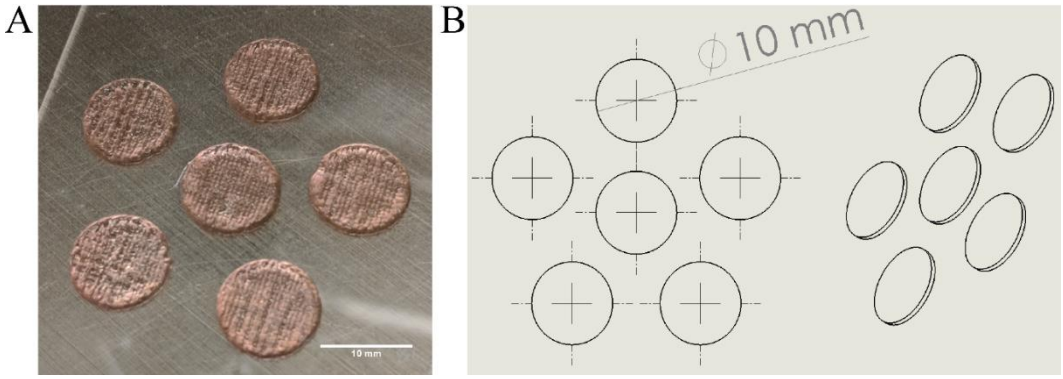

Figure 4 Printed Patches. A) Printed patches of 10 mm diameter and 0.6 mm height. Patches are printed uniformly from patch to patch, and the grid infill pattern can be seen. Patches are pink post-printing due to the inclusion of photoinitiator Eosin Y and become clear post-polymerization. B) CAD model sketch used for patch printing.

Evaluating the viability of cells within the cardiac patches is critical to ensure live cells that can participate in producing important pro-reparative paracrine factors.[12,15] Evaluation of cell viability directly is also critical within bioprinted scaffolds, particularly because bioprinting has been shown to reduce cell viability in printed constructs due to high shear stresses on the cells from small diameter needle tips, such as the tips used in this study.[209,210] Additionally, cells grown in thick 3D structures can suffer death due to lack of nutrient diffusion, particularly at the center of the structures, producing a necrotic core.[209,212] As shown in **Figure 5**, hCPCs within printed cardiac patches were stained to

determine the total number of dead (read) to live (green) cells for either GelMA **(Figure 5A)** or GelMA-cECM **(Figure 5B)**. Cell viability was quantified by measuring the number of live and dead cells at different locations and heights within the cardiac patch at days 1, 3, and 6 after formation and showed high viability, from 70-80% live cells on average seen in **Figure 5C**. There was no significant difference between groups or time-points when comparing the percent of viable cells. Throughout all structures, there was no necrotic core or reduction of cell viability, indicating that nutrient diffusion was likely not a factor. The cell viability overall was most likely not impacted significantly by the printing methodology, or if there were effects to the cells due to the printing, the degree of cell damage was mitigated by the material being an effective environment for cell growth and nutrient diffusion coupled with the printing of aligned fibers which may be beneficial to cell function.

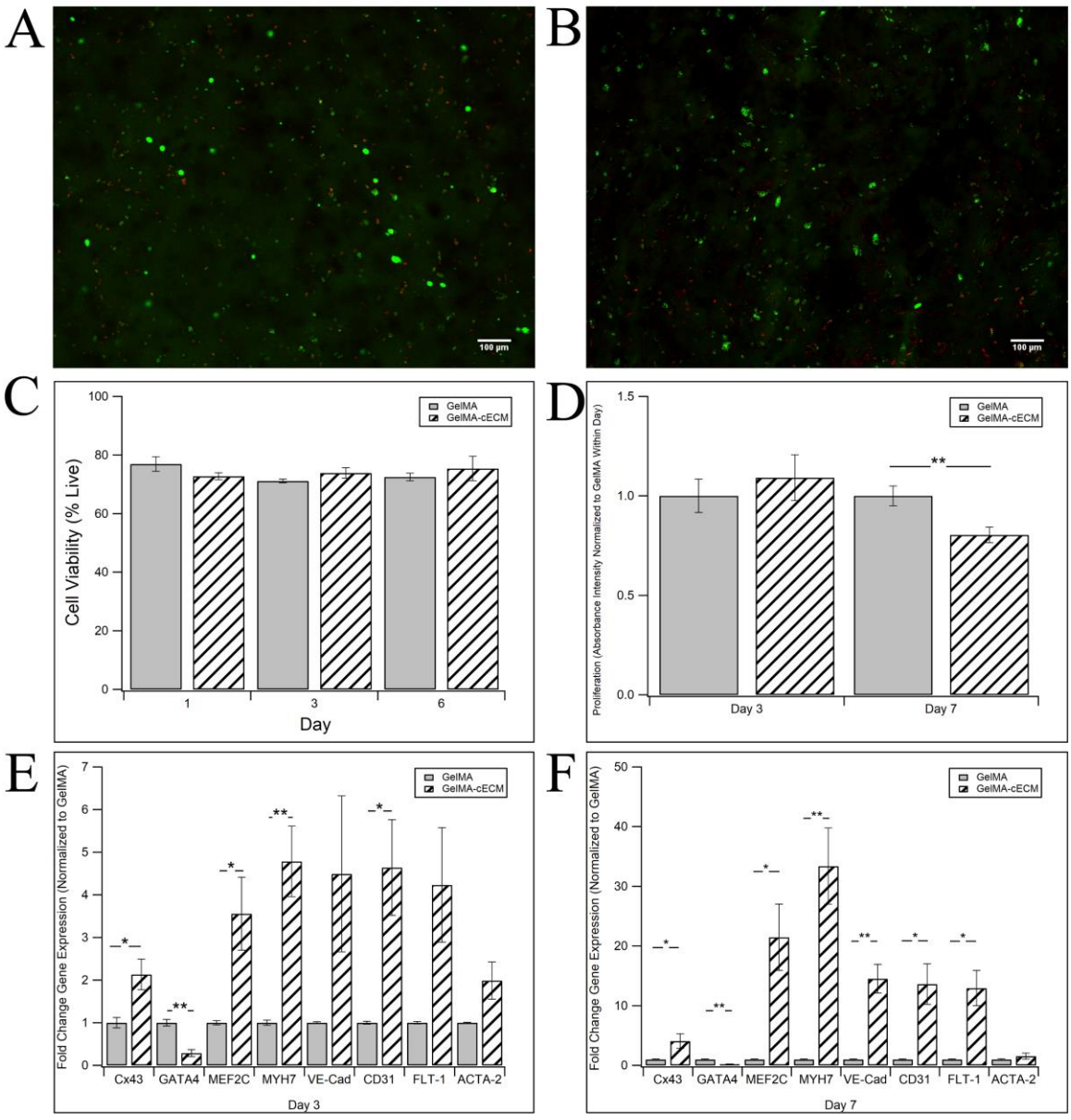

Figure 5 hCPC Functionality Within Printed Patches. A) Characteristic live/dead fluorescence image of hCPCs in GelMA patches, with live cells marked green (Calcien AM), and dead cells marked red (EtD) at one day after formation. B) Characteristic live/dead fluorescence image of hCPCs in GelMA-cECM patches at one day after formation. C) Viability of hCPCs in printed patches at 1, 3, and 6 days. D) Proliferation of hCPCs in printed patches at 3 and 7 days, where absorbance intensity is normalized to the

measured absorbance of hCPCs in GelMA patches in all experiments. E) Fold change gene expression over hCPCs in GelMA patches for Cx43, GATA4, MEF2C, MYH7, VE-Cad, CD31, FLT-1, and ACTA-2 at day 3. F) Fold change gene expression over hCPCs in GelMA patches for Cx43, GATA4, MEF2C, MYH7, VE-Cad, CD31, FLT-1, and ACTA-2 at day 7. * = p-value < 0.05, ** = p-value < 0.005, given by ANOVA with Tukey's post-test, n = 3-6 for all samples at all time-points.

Proliferation and differentiation are additional parameters that are important in characterizing the functionality of hCPCs in bioprinted patches. hCPC-laden patches were grown in culture media supplemented with EdU for 3 and 7 days, and absorbance intensity from GelMA-cECM patches was normalized to values measured from GelMA patches. While there was no difference between the proliferation of hCPCs in GelMA and GelMA-cECM patches after 3 days, as seen in **Figure 5D**, hCPCs in GelMA-cECM patches had reduced proliferation compared to GelMA patches after 7 days. Similarly, hCPC-laden patches were grown for 3 and 7 days, and the fold change in the genetic expression of key cardiac, endothelial, and smooth muscle genes from hCPCs in GelMA-cECM patches compared to hCPCs in GelMA patches was assessed through polymerase chain reaction (PCR). Analysis of gene expression of cardiac transcription factors GATA4 and MEF2C and cardiac-specific proteins connexin 43 (Cx43) and β-myosin heavy chain (MYH7), EC markers vascular endothelial cadherin (VE-Cad), platelet endothelial cell adhesion molecule (CD31), and vascular endothelial growth factor receptor 1 (FLT-1), and smooth muscle marker α-smooth muscle actin (ACTA-2) was evaluated at 3 and 7 days, as seen in **Figures 5E** and **5F**. hCPCs in GelMA-cECM patches showed enhanced cardiac differentiation through increased expression of MEF2C, Cx43, and MYH7, and decreased

expression of GATA4, an early differentiation marker, indicating that the hCPCs in GelMA-cECM patches were moving towards later differentiation then hCPCs in GelMA patches. hCPCs in GelMA-cECM patches also showed increased expression of endothelial marker CD31 at day 3, although there was no difference in expression of endothelial markers VE-Cad and FLT-1 or smooth muscle marker ACTA-2. At day 7, expression of all cardiac and endothelial markers was increased in GelMA-cECM patches, with higher fold-change values than day 3. ACTA-2 remained unchanged between groups on both days. Thus, we conclude that incorporation of cECM into patches improved both cardiac and endothelial differentiation of hCPCs, while not influencing smooth muscle differentiation. The enhanced differentiation of hCPCs in cECM incorporated patches at day 7 mirrors the proliferation trends seen in **Figure 5D**, as stem cells most often show reduced proliferation with increased commitment. These assessments also reaffirm the results measured for hCPCs in 2D culture, where cECM improved differentiation of CPCs compared to cells grown on collagen-based materials.[16] Regardless, it is clear that while hCPCs remained viable in printed patches, the inclusion of cECM improved differentiation and reduced proliferation of hCPCs, which in turn may improve the paracrine potential of hCPC-laden GelMA-cECM patches.

Many studies now attribute the true benefit of cell therapy to be the release of paracrine factors.[15,213-217] To evaluate paracrine release, we grew cell-laden patches in treatment media for up to 7 days and collected the conditioned media every two days. We then performed a tube formation assay using human umbilical vein endothelial cells (HUVECs) cultured on Matrigel with conditioned media. HUVECs grown in either non-conditioned treatment media or EC growth media with supplemented growth factors

showed similar values for total tube length formed, so non-conditioned treatment media was used as positive controls. As shown in **Figure 6**, HUVECs formed tube-like structures when cultured in conditioned media taken from both cell-laden GelMA **(Figure 6A)** and GelMA-cECM **(Figure 6B)** patches. When comparing the angiogenic potential of cell-free patches, seen in **Figure 6C**, there was no difference between GelMA and GelMA-cECM groups. In contrast, the angiogenic potential of media collected from cell-laden GelMA-cECM patches was significantly higher than media from GelMA patches alone on day 3, while both groups showed improved angiogenic potential at day 7 compared to day 3. While GelMA-cECM was superior at both time-points, both groups showed an increase in angiogenic potential over time. While there are many other parameters that conditioned media may alter, angiogenesis may be one of the most important for improving cardiac function. Additionally, we may be underestimating the effects as some growth factors released may interact with the GelMA or cECM and prevent release into the conditioned media, as studies have shown that growth factors, such as heparin binding growth factor and HGF, bind to cECM and are released gradually.[218,219]

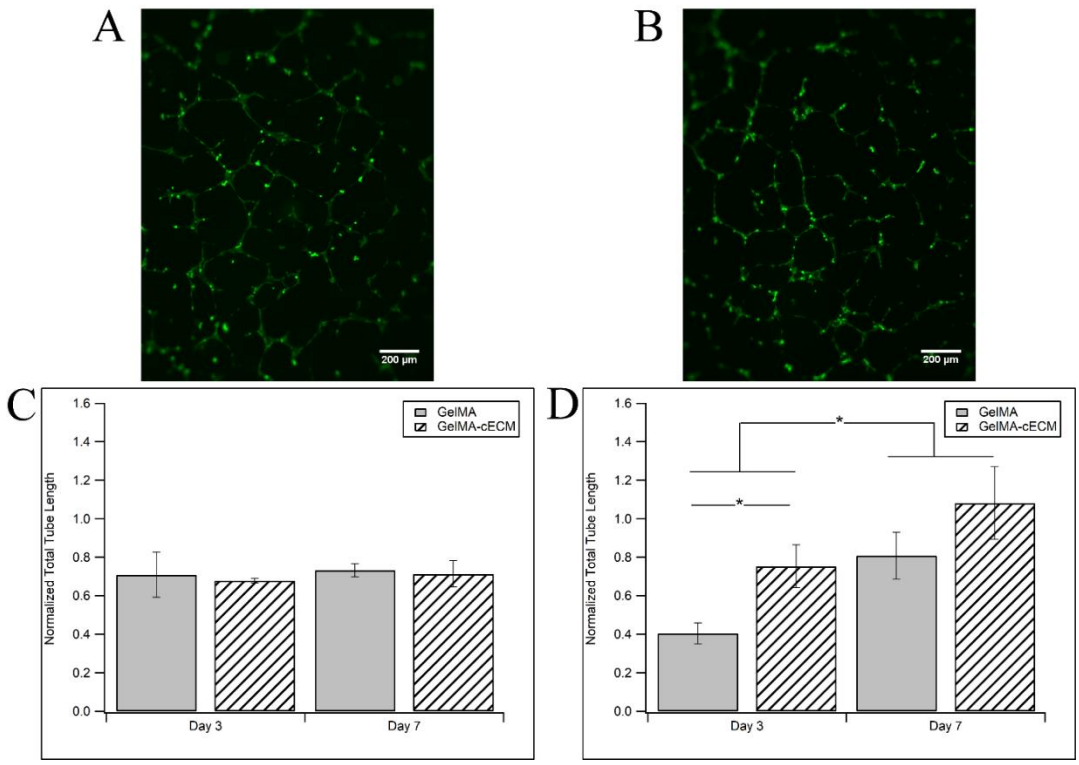

Figure 6 Angiogenic Potential of Cardiac Patches. Characteristic HUVEC tube formation after 6 hours when grown with conditioned media collected at day 7 from cell-laden A) GelMA and B) GelMA-cECM patches. Total HUVEC tube length normalized to positive controls for C) cell-free and D) cell-laden patches. * = p-value < 0.05, given by ANOVA with Tukey's post-test, n = 3-6 for all samples at all time-points.

In developing effective hydrogels for soluble factor release, it is key to generate materials that are stiff enough to allow for scaffold stability but do not have too dense a network that limits cellular functions and release of signaling factors.[211] Systems that balance these parameters have been developed around natural or synthetic materials, many of which prove effective in releasing reparative factors into damaged tissues, whether through encapsulation of regenerative cells or the factors themselves.[213-216] The hCPC-laden GelMA-cECM patches developed here also allowed for the generation of a solid

patch with enhanced factor release. These results are similar to other materials that have been developed, but with the incorporation of cardiac-specific cells and matrix that may release cardiac-specific paracrine factors. This cardiac specificity in the patch design may be most beneficial in repairing the damaged myocardium, as opposed to using non-tissue specific biomaterials such as GelMA.[19,213,217]

Mechanical properties of biomaterials play a critical role in modulating cellular function. Stem cells are more viable, proliferative, and produce more effective regenerative outcomes when grown in hydrogels that match the properties of native tissue.[12,220] This is also true as well for hCPCs, where cells perform more effectively when grown in materials that match the mechanical modulus of native myocardium from 5-15 kPa.[92-96,183] A material modulus that more closely matches the myocardium also ensures there is a limited mechanical mismatch between the hydrogel and the heart, which can otherwise cause problems such as dissection, buckling, or immune responses.[29,222] While GelMA and GelMA-cECM patches are evaluated in this study, we also evaluated the use of modifying the mechanical properties of the patches by adding acrylate groups using N-succinimidyl acrylate, as employed in previous studies.[189] While the modification increased stiffness over GelMA and GelMA-cECM groups, the patches more readily degraded compared to both groups and did not alter the hCPC viability or paracrine function over GelMA-cECM, so this direction was not pursued further, although the properties of the patch could potentially be modified through this method.

As seen in **Figure 7A**, the modulus of pure GelMA was 3000 Pa, similar to published studies, though short of the native myocardium.[183] Incorporation of cECM significantly increased the modulus to 5000 Pa, indicating that the material properties of

the GelMA-cECM patch could be tailored within physiological ranges. In addition to stiffness, we also measured the swelling ratio in **Figure 7B**. All samples were sufficiently hydrated, with a swelling ratio between 9 – 12. There was a decrease in the swelling ratio between the GelMA and GelMA-cECM groups, which was expected as increases in stiffness suggest a tighter polymer network and result in more liquid exclusion.

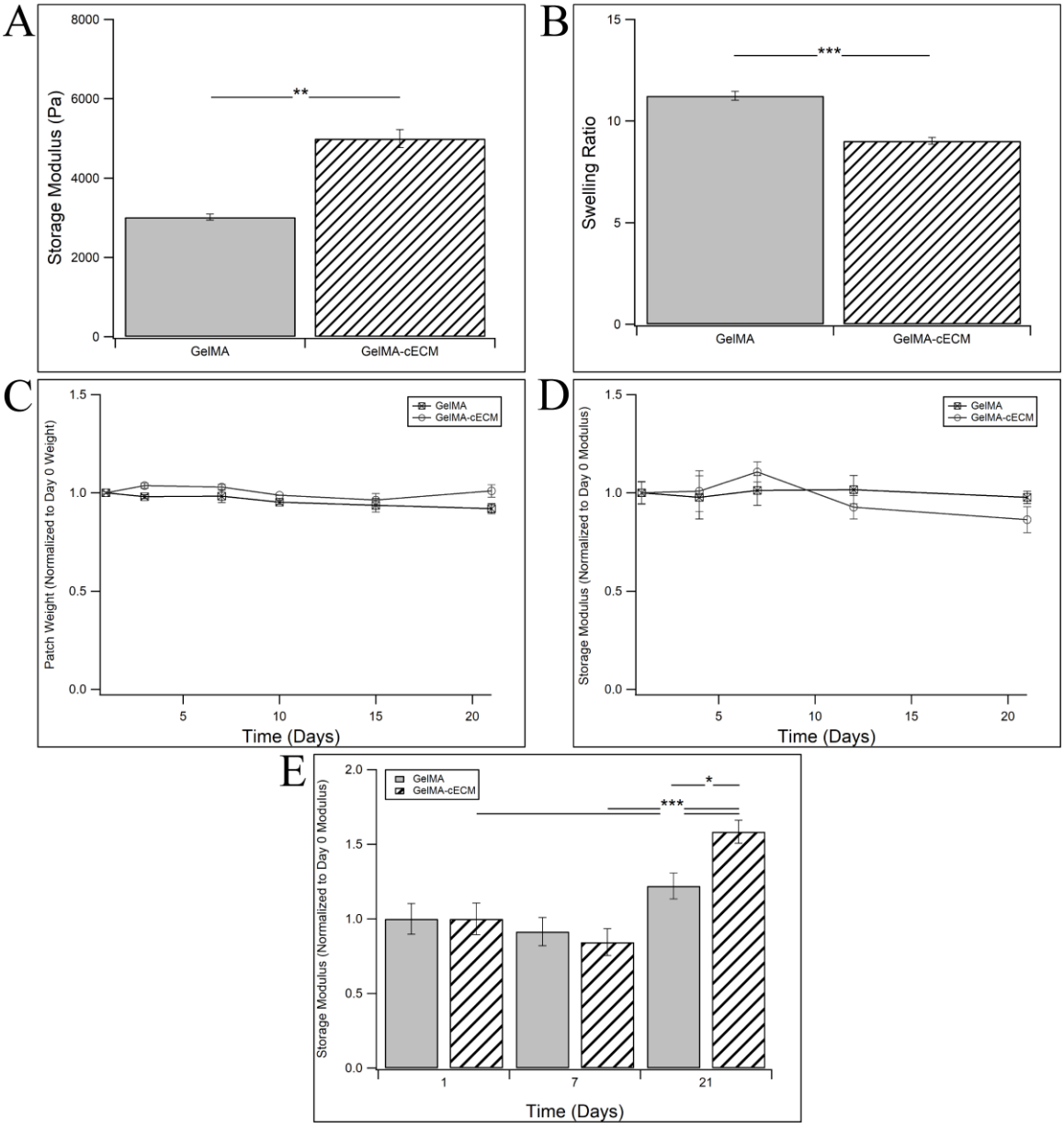

Figure 7 Material Analysis of Printed Patches. A) Viscoelastic storage moduli of GelMA and GelMA-cECM. B) Swelling ratio of GelMA and GelMA-cECM patches. C) Degradation of patches, measured as the sample weight compared to the initial weight of the patches post-swelling. D) Degradation of cell-free materials in cell culture media, measured as the sample storage modulus compared to the initial modulus of the material post-swelling. E) Remodeling of hCPC-laden materials grown in cFB conditioned media, measured as the sample storage modulus compared to the initial modulus of the material post-swelling. * = p-value < 0.05, ** = p-value < 0.01, *** = p-value < 0.005, given by ANOVA with Tukey's post-test, n = 3 for all samples in all subfigures.

As a cardiac patch must persist for the repair process, degradation time is a critical parameter to understand if patch properties are retained over time and through therapy, although ideal therapeutic timescales are unknown. We evaluated the degradation of patches and materials in cell treatment media over 21 days by examining both the change in wet weight **(Figure 7C)** and the change in stiffness **(Figure 7D)**. When comparing weight change of printed patches or the change in stiffness of the materials, both groups remained solid and did not significantly degrade over the range of 21 days. Although the data presented describes the degradation of patches without cells, patches that incorporated cells lasted the duration of testing shown in **Figures 5/6** with no observable degradation. It is important to describe this method of degradation as only evaluating hydrolysis, as opposed to exposing the patch to conditions seen *in vivo,* including proteases such as cathepsin K, cyclic strain, and shear stresses. hCPC-laden materials were cultured in conditioned media harvested from cFBs to evaluate the degradation of the patches in a more physiologically relevant environment. cFBs would be present in cases of ventricular

remodeling and hypertrophy. The cFB conditioned media more closely captures the environment of patches *in vivo* due to the incorporation of a complex mixture of remodeling components, compared to commonly employed incubation in collagenase I, which degrades the patches in a matter of hours and may not be as physiologically relevant. As seen in **Figure 7E**, hCPC-laden GelMA materials did not degrade or change mechanical modulus over 7 and 21 days in cFB conditioned media. Interestingly, while hCPC-laden GelMA-cECM materials did not degrade or change mechanical modulus over 7 days, by 21 days, the material stiffness increased compared to the stiffness at both 1 and 7 days. The change in stiffness at 21 days is also significantly greater than hCPC-laden GelMA materials at the same time and may be due to the stimulation of hCPCs in remodeling their environment. Regardless, the GelMA-cECM patches, both with and without hCPCs, do not degrade *in vitro* over an extended timeframe and may be suitable for extended retention *in vivo*.

4.4 Conclusion

In this chapter, we describe the development of a novel pediatric hCPC/cECM cardiac patch that was generated through bioprinting. The inclusion of 5% w/v GelMA allowed for printability of the hCPC/cECM bioink through GelMA polymerization via cooling to 10^0C, followed by white light radical polymerization and incubation at physiological temperatures. The inclusion of cECM allowed for improved printability over pure GelMA bioinks, and the hCPC laden GelMA-cECM bioinks showed homogeneous distribution of cells and matrix. This methodology can potentially be employed to generate cardiac patches that can be customized to the target patient tissue. hCPCs remained highly viable and proliferative within the patch up to seven days, and hCPCs in GelMA-cECM

patches had improved differentiation and angiogenic potential over pure GelMA patches, indicating their improved reparative functionality. The inclusion of cECM resulted in patches with a mechanical modulus that was similar to that of native myocardium, and all patches were sufficiently hydrated. Patches did not significantly degrade over 21 days when tested *in vitro* through weight change and rheological analysis. Also, hCPC-laden GelMA-cECM patches showed increased stiffness over 21 days when cultured in cFB conditioned media, indicating potential remodeling and retention *in vivo.*

The printing of native ECM is difficult to perform at concentrations that can be realistically used and support cell functions. The concentration of cECM used here is similar to previous studies performed in our laboratory and by others that support CPC differentiation and function. Furthermore, all materials used in this study are clinically relevant, as both cECM and hCPCs are in clinical testing alone. Thus the idea of a patient-specific, 3D printed patch is of great translational value. With printability achieved and *in vitro* cellular functionality assessed to be potentially effective for cardiac therapy, the next chapter focus on additional modifications in patch parameters, such as the incorporation of increased amounts of pro-regenerative ECM components, evaluation with child hCPCs, and growth in hypoxic environments, that may improve the paracrine factor release by inducing modulations in hCPC function for a bottom-up, modular approach to tissue engineering. In chapter 6, patch therapeutic potential will include testing the patches *in vivo* on animal models of RV failure to evaluate tissue-level changes such as angiogenesis, fibrosis, and cardiomyocyte hypertrophy, as well as cardiac functional improvements.

CHAPTER 5. EVALUATION OF MODIFIED PATCH PARAMETERS (BIOMATERIAL COMPOSITION, OXYGEN GROWTH CONDITIONS, AND CELL AGE) ON IN VITRO REPARATIVE POTENTIAL OF HCPC-CECM PATCHES

5.1 Introduction

While the hypothesis of chapter 4 is that the inclusion of cECM in hCPC-laden patches will improve cellular functionality compared to cECM-free patches, other parameters have been explored in modulating hCPC functionality, as described in sections 3.2.3 and 3.3.5.[59-81] These factors can be employed with cECM patches to further improve the functional outcomes of hCPC release profiles.[59-63] Of these factors, the inclusion of additional extracellular matrix components, growth of cells in low oxygen conditions, and modulations to cell age may be the most impactful for patch environments.[62-81] This chapter will first focus on evaluating how incorporating additional ECM components in cECM to generate a composition that resembles fetal cECM composition will affect hCPC reparative potential. Then, the chapter will focus on the effect of hypoxia and cell age (using neonatal and child hCPCs) to improve the reparative potential of GelMA-cECM patches, in singular and combinatorial systems.

5.2 Materials and Methods

Materials – Fibronectin from human plasma and recombinant mouse periostin were purchased from Sigma-Aldrich (MO, United States). Recombinant rat agrin was purchased from R&D systems. Reference materials section of chapter 4 for all additional materials.

Human Cardiac Progenitor Cell Isolation and Culture – Reference methods section of chapter 4. The difference in methods employed in this chapter in that right atrial appendage tissue was obtained from pediatric patients of various ages undergoing heart surgeries, rather than just patients aged 0-1 week. Cells were grouped into two age groups for these studies as follows: neonate (0-1 week) and child (2-5 years).

Cardiac Extracellular Matrix Isolation and Characterization – Reference methods section of chapter 4.

Biomaterial Coating and hCPC Culture – Human fibronectin, mouse periostin, rat agrin, and decellularized cECM were reconstituted by combining appropriate masses of each material in 15 mM HEPES buffer. Final solutions consisted of pure cECM at 0.5 mg/mL or combination of 0.5 mg/mL cECM, 0.1 mg/mL fibronectin, 0.01 mg/mL agrin, and 0.001 mg/mL periostin. Cell culture plates were coated with pure cECM or combination biomaterial solutions, as previously described.[16,17] Biomaterial solutions were dispensed at varying volumes to coat different well plate sizes (800 μL for 6 well plates, 50 μL for 96 well plates) and allowed to adsorb/polymerize for 1 hour at 37°C. Following adsorption, plates were washed with 1X PBS twice. Neonatal hCPCs were seeded on coated plates at $7x10^5$ cells/well for 6 well plates in serum-free media, relating to densities of 600-800 cells/mm^2 for all plate sizes. Serum-free media consisted of Hams F-12 media supplemented with 1x Pen-Strep, 1% L-glutamine, and 1x ITS. Cells were allowed to grow for 72 hours in culture before evaluation. At the endpoint of evaluation, media was harvested from cells for angiogenic potential analysis, and cells themselves were analyzed using either viability, proliferation, or genetic expression assays.

Hypoxic and Normoxic hCPC Culture (2D and 3D) – hCPCs derived from neonatal and child patients were grown in culture based on application. For 2D culture, hCPCs were seeded on treated cell culture plates at $4x10^5$ cells/plate for 6 well plates and $5x10^3$ cells/plate for 96 well plates. For 3D culture, biomaterial solutions were generated similarly to methods implemented in chapter 4. GelMA solutions of 14.432% were created by dissolving lyophilized GelMA in 15 mM HEPES buffer and allowed to dissolve under stirring at 60^0C for 1-2 hours. GelMA solutions were frozen at -20^0C until use. Stock solutions of 13 mg/mL cECM are formed by rehydrating the cECM material with HEPES buffer followed by adjusting the solution to pH 7.4 with HCl immediately before use. All formulations were prepared immediately before gel formation. GelMA formulations were prepared by mixing GelMA (final concentration 5% w/v), Eosin Y (100 µM), NVP (0.75% v/v), TEOA (0.3% v/v), and HEPES buffer (15 mM). In the case of GelMA-cECM formulations, the HEPES in the above formulation was replaced by the cECM (final concentration 8 mg/mL) solutions. Solutions were adjusted with 0.5 N HCl to achieve a final pH of 7.2-7.4. For the inclusion of cells, neonatal or child hCPCs (passage 6-10, pooled or combined across at least three donors) were removed from cell culture plates, pelleted at 1000 rpm for 5 minutes, and mixed with 1 mL of the biomaterial solution, producing a final concentration of 3 million cells/mL. Cell-laden gels were formed by depositing 50 uL of room temperature cell-biomaterial solution into cell culture plates, producing a stable pre-polymer sphere. Following deposition, gels were exposed to white light (Braintree Scientific) at 4^0C for 5 minutes to allow for radical polymerization, followed by immediate incubation at 37°C to allow for cell growth and cECM polymerization. Regardless of culture type, cells were grown in either hypoxic conditions

(1% oxygen, Billups-Rothenberg MIC-101 incubator) or normoxic conditions (13-20% oxygen) for 12 or 24 hours before evaluation (specified as "acute" growth in the initial experimental grouping). All groups were grown using serum-free media. For "preconditioned" groups, cells were removed from hypoxia or left in normoxia and grown for an additional 48 hours in normoxic conditions before evaluation. At the endpoint of evaluation, media was harvested from cells for angiogenic potential analysis, and cells themselves were analyzed using either viability, proliferation, or genetic expression assays.

Viability Analysis – Cell-laden patches or adherent cells were grown in serum-free media for 12, 24, 60, or 72 hours, based on the group. Reference methods section of chapter 4.

Proliferation – Cell-laden patches or adherent cells were grown in serum-free media for 12, 24, 60, or 72 hours, based on the group. Reference methods section of chapter 4.

RNA Isolation, Reverse Transcription, and Quantitative Real-Time PCR – Cell-laden patches or adherent cells were grown in serum-free media for 12, 24, 60, or 72 hours, based on the group. Reference methods section of chapter 4. The primer sequences used are seen in **Table 7**.

Table 7. PCR Primers for Aim 2

Name	Forward 5'-3'	Reverse 5'-3'
Connexin 43 (Cx43)	CAATCTCTCATGTGCGCTTCT	GGCAACCTTGAGTTCTTCCTC
GATA4	TAGACCGTGGGTTTTGCATTG	CATCCAGGTACATGGCAAACAG

Myocyte enhancement factor 2C (MEF2C)	TAACTTCTTTTCACTGTTGTGCTCCTT	GCCGCTTTTGGCAAATGTT
β-Myosin heavy chain (MYH7)	GGCAAGACAGTGACCGTGAAG	CGTAGCGATCCTTGAGGTTGTA
Vascular endothelial cadherin (VE-Cad)	CCGACAGTTGTAGGCCCTGTT	GGCATCTTCGGGTTGATCCT
Platelet endothelial cell adhesion molecule (CD31)	TCTATGACCTCGCCCTCCACAAA	GAACGGTGTCTTCAGGTTGGTATTTCA
Vascular endothelial growth factor receptor 1 (FLT-1)	GACTAGATAGCGTCACCAGCAG	GAAACCGTCAGAATCCTCCTC
α-Smooth muscle actin (ACTA-2)	AATACTCTGTCTGGATCGGTGGCT	ACGAGTCAGAGCTTTGGCTAGGAA
Stromal cell derived factor 1 (SDF-1)	ACTCCAAACTGTGCCCTTCA	CCACTTTAGCTTCGGGTCAAT

Tube Formation Assay – Conditioned media from adherent or hydrogel-bound hCPCs was collected at 12, 24, 60, or 72 hours of growth, depending on the group. Reference methods section of chapter 4.

Statistics – Reference methods section of chapter 4.

5.3 Results and Discussion

During development, hCPCs and other heart cells interact with fetal cardiac matrix to drive complete myocardial functional development.[46,89,90] As discussed in section 3.3.2 and **Table 1**, there is a significant difference between the composition of adult and fetal cECM, in terms of types and concentrations of matrix components.[88,89,90,99] Also, as discussed in sections 3.2.3 and 3.3.5, hCPCs and other cells have been grown on and within various natural biomaterials derived from ECM components, which has shown that ECM

derived materials may improve hCPC functionality in terms of paracrine release.[16,17,180] Specifically for hCPCs, functionality has been evaluated in the presence of traditional materials found in the adult ECM (such as collagen and laminin) and fetal ECM (such as fibronectin), and complete cECM (including the results of chapter 4).[16,17,70-80,178] Materials that are in higher concentrations in the fetal ECM, particularly fibronectin, have found the greatest impact for improving CPC paracrine release profiles and survival compared to components found in higher concentrations in the adult ECM.[17,178] Furthermore, individual fetal-specific ECM components such as agrin and periostin have been used directly as injectable therapies in treating the myocardium after ischemia or injury.[223,224] Although these individual materials may be of interest to evaluate hCPC-material interactions, the focus of this study is to employ an hCPC-cECM patch to treat the pediatric myocardium. To further improve the functionality of hCPC-cECM patches in terms of hCPC paracrine release, we hypothesize that the use of fetal instead of adult cECM may further improve hCPC paracrine release compared to the results seen in chapter 4. One limitation is the availability and sourcing of direct fetal cECM.[89,90,98,99] The cECM used in work from chapter 4 is derived from growing pigs, and the methodology of harvest and decellularization has been extensively tested and developed to provide constant batch to batch material.[16,17,152] Fetal cECM has not had this level of development in terms of harvesting and manufacturing methods, and most methods that have derived fetal cECM have resulted in poor material quality, poor reconstitution and polymerization, and high batch to batch variability.[89,90] Therefore, it may be advantageous to incorporate components within our developed cECM inks that are in higher concentration in fetal cECM compared to adult cECM. This incorporation may limit the properties of the

components compared to the structurally integrated components seen in full cECM, but with the benefit of being able to design groups and patches consistently. To achieve these, we evaluated the use of three materials that are in high concentrations in the fetal cECM compared to adult cECM and have shown effectiveness from previous studies – fibronectin, periostin, and agrin.[17,223,224] We evaluated the effect of these materials when combined with cECM compared to pure cECM in 2D systems to allow for high throughput testing and a lower total amount of costly protein required for initial testing, compared to immediate testing in 3D systems.

Cell culture plates were coated with cECM or cECM with agrin, periostin, and fibronectin at relevant concentrations (called Combo in the following data) using previously developed protocols, as described in the methods section. Neonatal hCPCs were seeded onto the biomaterial coated-plates in serum-free media, allowed to grow for 3 days in culture, and evaluated. Methods for cell evaluated include all methods used in chapter 4, specifically viability, proliferation, gene expression, and conditioned media angiogenic potential. As seen in **Figure 8A and 8C**, there was no significant difference in cECM and Combo groups in terms of cell viability and expression of cardiac, endothelial, and smooth muscle markers. The Combo group showed a decreased proliferative potential compared to cells grown on pure cECM, as seen in **Figure 8B**. Moreover, conditioned media collected from hCPCs grown on combined materials showed a significant decrease in the angiogenic potential of HUVEC tube formation compared to conditioned media from hCPCs grown on pure cECM.

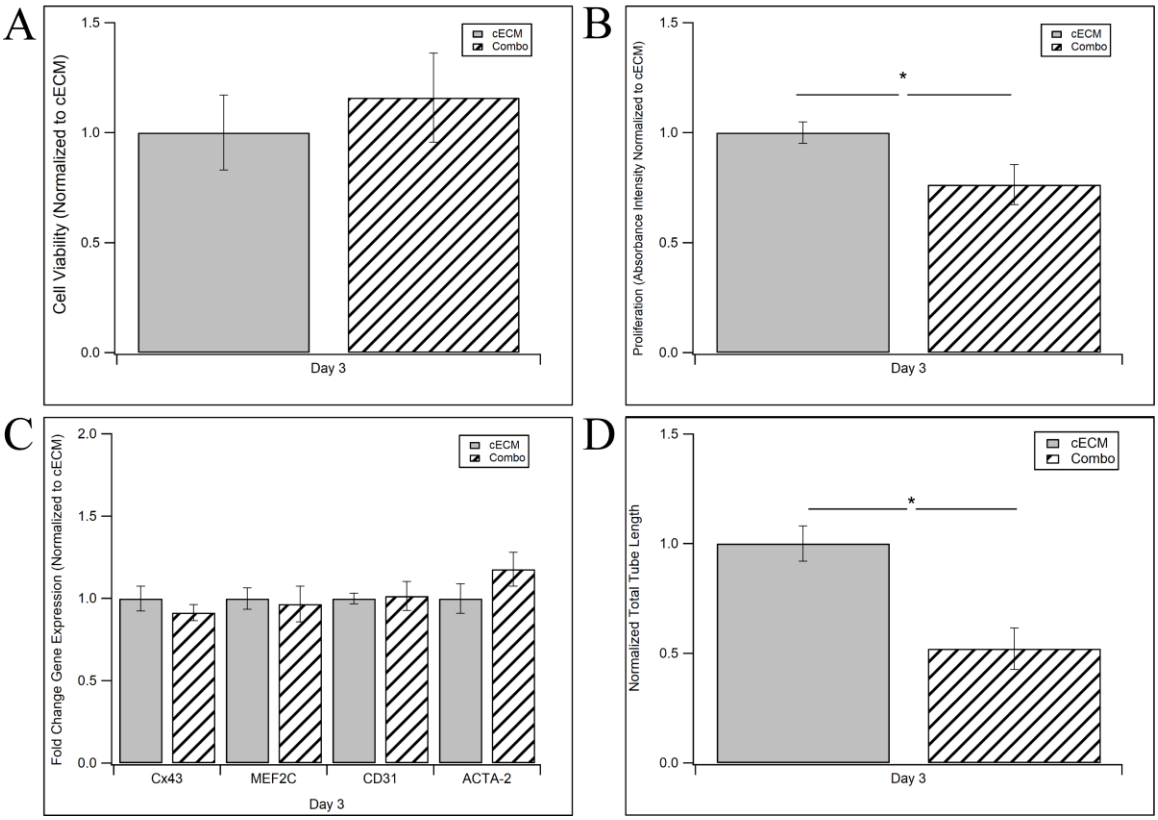

Figure 8 Fetal cECM Modulation of Neonatal hCPCs. A) Viability of hCPCs cultured on cECM or combined biomaterials at 3 days, normalized to viability of hCPCs on cECM. B) Proliferation of hCPCs in cultured on cECM or combined biomaterials at 3 days, where absorbance intensity is normalized to the measured absorbance of hCPCs on cECM in all experiments. C) Fold change gene expression over hCPCs on cECM for Cx43, MEF2C, CD31, and ACTA-2 on day 3. D) Total HUVEC tube length normalized to positive controls for cECM and Combo derived conditioned media. * = p-value < 0.05, given by ANOVA with Tukey's post-test or unpaired T-test depending on the number of groups, n = 3-5 for all samples at all time-points.

These results point towards the conclusion that the incorporation of fetal-specific ECM components with cECM materials showed no difference, and potentially even a

worsening, in hCPC functional properties. Based on the results, this direction was not pursued further in terms of incorporation of the materials into a bioink and analyzing printed patch function. There may be several reasons as to why this approach was not effective. One consideration is that the cECM itself is a complex material system and maybe the strongest modulator to hCPC phenotype and function compared to adding small amounts of secondary materials.[88,89,90,98,99] Importantly, a consideration of the physical and chemical properties of the methods and biomaterials employed in the study shows a limitation towards use in bioprinting.[23] As discussed in chapter 4, the development of a printable bioink requires the use of soluble components that polymerize post-printing to result in solid constructs. We incorporated soluble fibronectin, agrin, and periostin derived from different species, either isolated or recombinant, at varying concentrations based on previous studies and material cost.[17,223,224] In native ECM, the location, density, fiber incorporation, and active sites of each of these proteins is highly controlled. However, the soluble proteins and sources required to allow for printing may not be effective in modulating hCPC function. For fibronectin, the source is human plasma. Fibronectin is found in the body as a soluble form found in plasma, and an insoluble fibrous form found in tissue ECM.[17,225] Fibronectin polymerization within ECM is a highly complex process that involves fibronectin deposition and polymerization by specialized cells, compared to simple addition as was employed in this work.[225] Specifically, the fibronectin used in these studies may not have significant exposure of cell-interacting domains and peptides such as RGD, which are critical in driving cell-matrix mediated responses with fibronectin.[225] Therefore, the soluble fibronectin that is required for effective printability may not present the proper cues and structural formation that hCPCs would respond to for regulating

paracrine release. Modified, soluble, or cleaved fibronectin, and proteins in general, are not comparable to complete proteins and may have detrimental effects on the protein itself. While fibronectin was sourced from human tissue, the agrin and periostin used in this work were recombinant and generated in bacteria. This formulation limits the amount of material we can incorporate due to cost considerations towards a manufactural patch and domains that are incorporated into the recombinant proteins. Physiological human agrin contains an N-terminal domain that mediates cell-ECM interactions by the inclusion of a protease inhibitor domain, laminin-binding domain, laminin EGF (epidermal growth factor)-like domains, and an agrin-specific SEA domain.[223,226] Also, agrin contains a C-terminal domain with EGF-like repeats and laminin globular G domains. The recombinant agrin used in this work does not contain the C-terminal domain and laminin-binding domain of the N-terminal domain and is derived from rat agrin, which only has an 80% sequence homology to human agrin.[226] These modifications may limit the functionality of the protein in terms of cell-matrix interactions and cell signaling cascade induction. Periostin, which was incorporated at the lowest concentration of all materials, was found to play a major role in the assembly of ECM architecture, and its location within the ECM is highly conserved.[224,227] The periostin used in this work was derived from mouse protein sequence, which not fully similar to human periostin. While the protein sequence may not be as limiting compared to the agrin sequence differences, the incorporation of periostin within the ECM architecture and low concentration may limit its overall effect on hCPCs. In this work, we are limited in biomaterial formulation and concentration due to printing requirements and cost, and within these limits, the incorporation of the fetal cECM components does not improve hCPC functionality over cECM alone. For generating hCPC

patches, the strongest modulator of hCPC function may be cECM itself. It is important to state that we did not evaluate the effect of only one component (such as fibronectin) with cECM, compared to combining all components. Future experiments may include analysis of hCPC function on cECM-single protein systems, to elucidate the individual effects of these proteins. The inclusion of multiple components into a complex system may be producing a detrimental effect overall, and a combination of only one component and cECM may improve hCPC paracrine potential compared to a combination of three components and cECM. Also, optimization of relative ratios of the various biomaterials used in this work may be required to determine the optimal system. The effect of complete fetal cECM on hCPCs also remains in question and maybe more readily investigated by employing complete fetal cECM after reliable methods of generation are optimized. Finally, evaluation of different cECM types, such as RV-derived cECM instead of LV-derived cECM, may generate different outcomes towards hCPC reparative potential and maybe more effective then fetal-derived cECM itself.

Another factor that has found to modulate CPC and other stem cell phenotypes and paracrine potential is hypoxic growth.[65-69] As reviewed in section 3.2.3, hypoxia has improved the therapeutic potential of exosomes derived from hCPCs grown in 1-5% oxygen.[9,62,63] Also, hypoxia may modulate hCPC function by increasing proliferation and priming hCPCs to migrate to and repair damaged myocardial tissue.[65-69] Hypoxia-induced hCPC modulation may help improve the paracrine and therapeutic potential of hCPC-cECM patches. We studied the effect of 1% oxygen growth conditions (termed hypoxia in all data) compared to standard culture oxygen conditions (termed normoxia in all data) on hCPCs grown in cell culture plates for 12-24 hours (termed acute in all data), as methods

to optimize conditions before patch incorporation. We also incorporated groups where hypoxic or normoxic cells were returned to normoxia after initial growth (termed preconditioned in all data) to determine if the effect of hypoxia on cellular function was retained. Initially, the retention of the effects of hypoxia may be of interest if the cells are being transferred from hypoxic conditions *in vitro* to normoxic conditions *in vivo*. While cells will be entering an initial hypoxic environment *in vivo*, the initial evaluation of a preconditioned effect may help parse how hypoxia effects hCPCs.[64]

Neonatal hCPCs were first grown for 12 hours in either normoxia or hypoxia. As seen in **Figure 9A**, there was no difference in cell viability between oxygen growth conditions in the acute group. **Figures 9B** and **9C** show images of live (green) and dead (red) cells that were grown for two days in normoxia after being preconditioned in either hypoxia or normoxia, indicating there were no changes to cell viability, although not quantifiable in these groups due to high cell density. These findings indicate that neonatal hCPCs survived in hypoxic conditions for 12 hours and that viability was not an additional variable in assessing hCPC function. As seen in **Figure 9D** and **9E**, there was an increased proliferative potential of hCPCs grown for 12 hours in hypoxia compared to normoxia, although this trend was reversed in the preconditioned case. The increased proliferation mirrors the results found in previous studies, where hypoxia primed CPCs to proliferate and repair. For preconditioned groups, the hCPCs were potentially overcompensating upon return to normoxia by substantially reducing their proliferation and returning to a quiescent state, compared to cells grown in normoxia the entire timeframe of testing. **Figure 9G** shows that cells in acute hypoxia had a lower expression of cell-cell gap junction marker Cx43, potentially due to cells being primed to detach and migrate to sites of injury. This

trend if further seen in **Figure 9H** for the case of hypoxic preconditioned cells, which exhibited significant degrees of dedifferentiation in the expression of cardiac and endothelial markers compared to normoxic cells. Hypoxia may reflect the conditions of the developing heart, which induces CPC migration, proliferation, and increased potency towards cardiac and endothelial differentiation in generating new tissue, compared to CPC quiescence in healthy adult tissue. However, these results were not reflected in the angiogenic potential of hCPC angiogenic potential, as seen in **Figure 9F**. Hypoxic conditions, whether acute or preconditioned, did not improve or change the angiogenic potential of neonatal hCPCs. This finding points towards the ineffectiveness of hypoxia in improving neonatal hCPC paracrine potential, although proliferation was increased. This trend may have also been evident in previous studies, where exosomes from hypoxic cells rather than hypoxic cells themselves were found effective in therapy.[62,63]

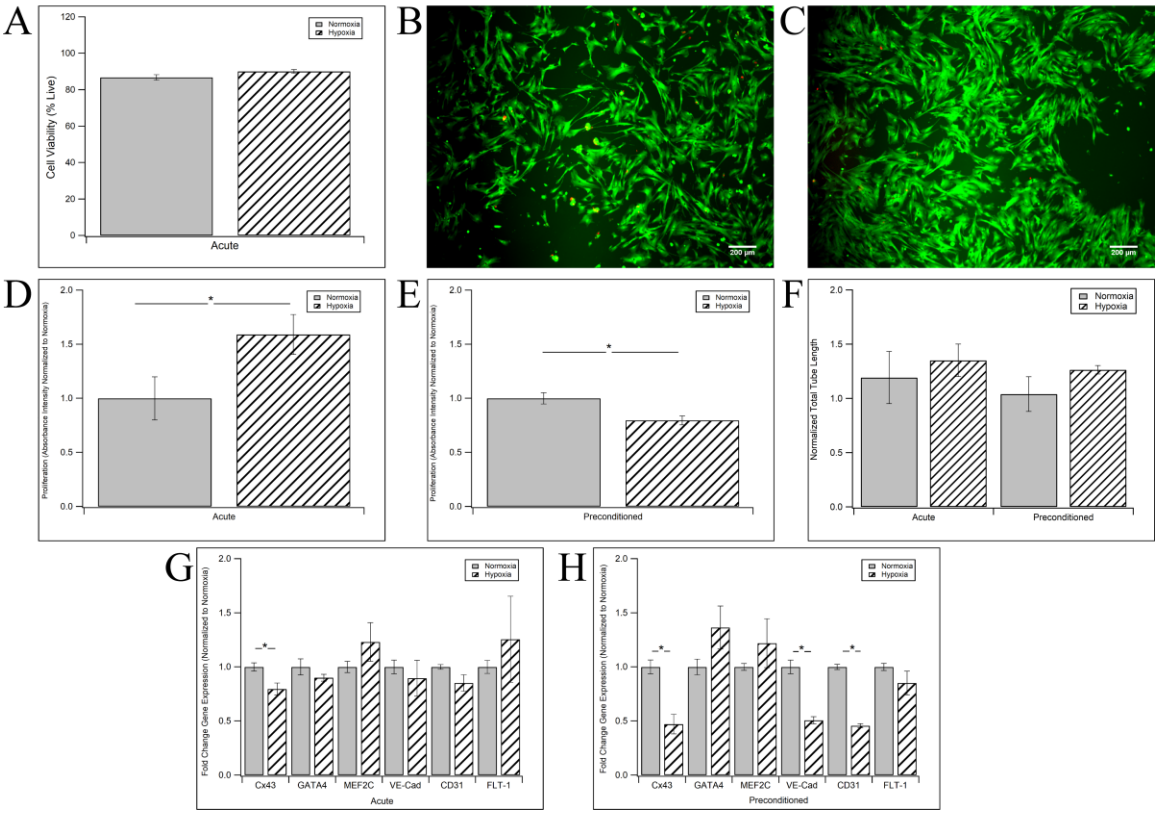

Figure 9 12 Hour Hypoxia Growth Modulation of Neonatal hCPCs. A) Viability of neonatal hCPCs cultured in hypoxic conditions for 12 hours. B) Characteristic image of hCPCs preconditioned in normoxia and grown for 48 additional hours in normoxia. Scale bar 200 µm. C) Characteristic image of hCPCs preconditioned in hypoxia and grown for 48 additional hours in normoxia. Scale bar 200 µm. D) Proliferation of hCPCs cultured in hypoxic or normoxic conditions for 12 hours, where absorbance intensity is normalized to normoxic hCPCs. E) Proliferation of hCPCs preconditioned in normoxic or hypoxic conditions for 12 hours, followed by 48 hours growth in normoxia, where absorbance intensity is normalized to normoxic hCPCs. F) Total HUVEC tube length normalized to positive controls for conditioned media derived from acute or preconditioned hypoxic or normoxic hCPCs. G) Fold change gene expression over normoxic hCPCs for cardiac and

endothelial markers of neonatal hCPCs cultured in hypoxic or normoxic conditions for 12 hours. H) Fold change gene expression over normoxic hCPCs for cardiac and endothelial markers of neonatal hCPCs cultured in hypoxic or normoxic conditions for 12 hours, followed by 48 hours growth in normoxia. * = p-value < 0.05, given by ANOVA with Tukey's post-test or unpaired T-test depending on the number of groups, n = 3-5 for all samples at all time-points.

While studies have shown that 12 hours of hypoxia is sufficient to improve the therapeutic benefits of hCPC-derived exosomes, a longer timeframe of hypoxic growth may be required to improve hCPC therapeutic potential directly.[62] We implemented the same system of growing hCPCs in normoxia or hypoxia and increased the time in hypoxia to 24 hours. Cells will encounter a hypoxic and not normoxic condition *in vivo* after patch implantation.[10,64] Further testing of the preconditioned group was not evaluated as it was not relevant to therapeutic development. As seen in **Figure 10A**, there was a trend towards dedifferentiation after 24 hours in hypoxia compared to normoxia, with decreased expression of mature cardiac marker MYH7. Once again, this trend points towards hypoxia priming CPCs for migration and repair, mirroring CPC function in heart development.[46] However, 24 hours of hypoxia significantly decreased the angiogenic potential of hypoxic hCPC conditioned media, as indicated in **Figure 10B**. One hypothesis mentioned in chapter 4 is that hCPCs derived from neonatal patients may have an improved therapeutic paracrine potential coupled with the expression of mature cardiac and endothelial markers, compared to older hCPCs. This trend was seen for neonatal hCPCs in GelMA-cECM patches, where cECM inclusion improved both differentiation and angiogenic potential. However, the reverse of this trend was seen for neonatal hCPCs grown for 24 hours in hypoxia and

indicates that long term hypoxic growth was not an effective tool in improving the therapeutic potential of hCPC patches.

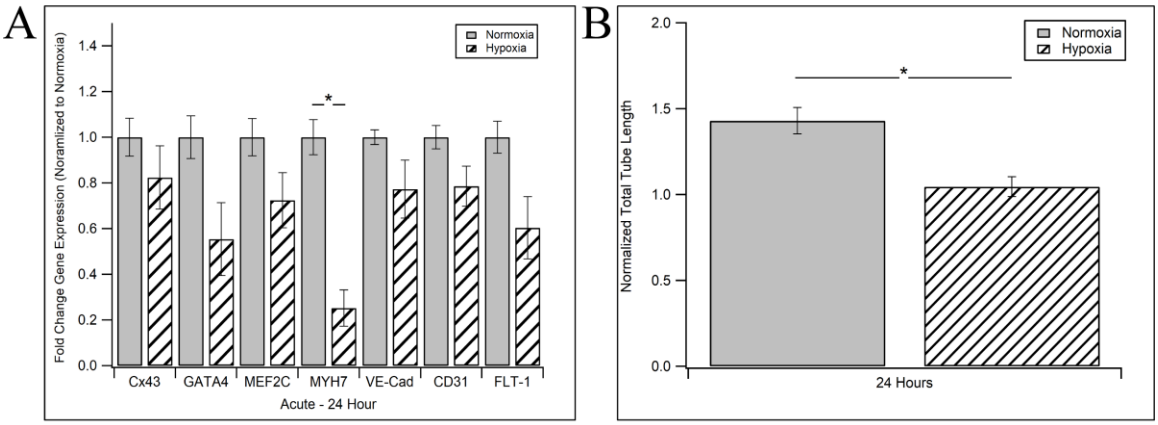

Figure 10 24 Hour Hypoxia Growth Modulation of Neonatal hCPCs. A) Fold change gene expression over normoxic hCPCs for cardiac and endothelial markers of neonatal hCPCs cultured in hypoxic or normoxic conditions for 24 hours. B) Total HUVEC tube length normalized to positive controls for conditioned media derived from hypoxic or normoxic hCPCs cultured for 24 hours. * = p-value < 0.05, given by ANOVA with Tukey's post-test or unpaired T-test depending on the number of groups, n = 3-5 for all samples at all time-points.

Although modulation of hCPCs by hypoxia resulted in unaffected or reduced *in vitro* angiogenic potential depending on hypoxic culture times, studies have shown that murine CPCs exhibited increased expression of CXCR4/7 after hypoxic growth. CXCR7 is the receptor to SDF-1, which may modulate cell migration to sites of injury in the myocardium.[65-69] The hypoxia-induced signaling cascade may also result in enhanced SDF-1 expression from hCPCs, a factor that can have potential therapeutic benefits *in vivo*. We evaluated the expression of SDF-1 in hCPCs grown for 12 hours or 24 hours in hypoxic

or normoxic conditions. As seen in **Figure 11A**, there was no change in SDF-1 expression between normoxic and hypoxic neonatal hCPCs, grown in either 12 or 24 hours, with data normalized to normoxic groups within each time group. To compare the expression of SDF-1 after 24 hour growth to 12 hour growth, Figure 11B shows the normalization of all data to 12 hour hypoxia expression. There was a significantly increased SDF-1 expression from hCPCs grown in normoxia for 24 hours compared to both hypoxia and normoxia at 12 hours, although there was no difference between any group and 24 hours of hypoxic growth. While cells that grew for a longer time expressed more SDF-1 as they replicated and interacted with each other in both oxygen conditions, this trend was not seen for 24 hours of hypoxia, indicating that long term hypoxia may be reducing the cells paracrine potential. Overall, hypoxic growth may not be improving neonatal hCPC therapeutic function and was not considered further in this study.

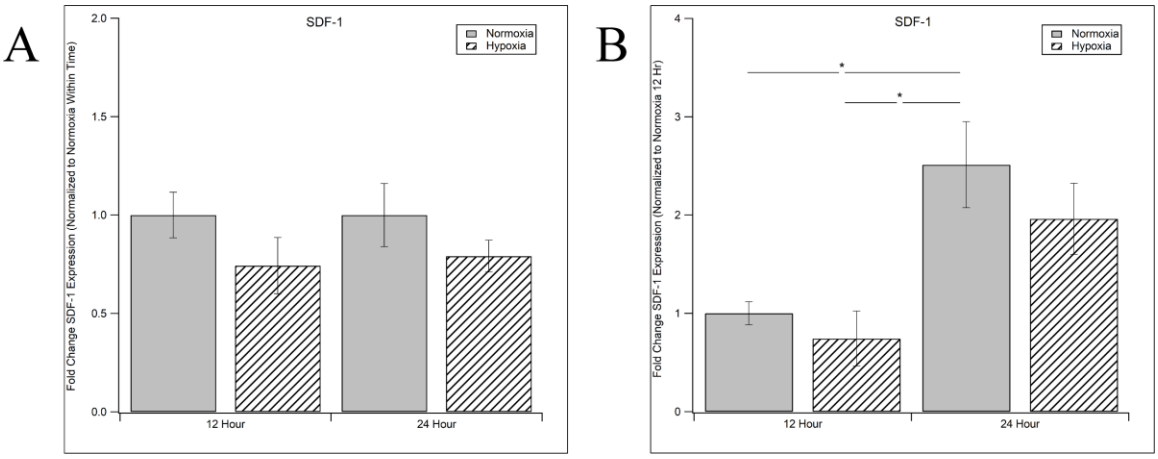

Figure 11 Hypoxia-Induced Cytokine (SDF-1) Gene Expression of Neonatal hCPCs. A) Fold change gene expression over normoxic hCPCs for SDF-1 of neonatal hCPCs cultured in hypoxic or normoxic conditions for 12 or 24 hours, normalized to the normoxic group within time group. B) Fold change gene expression over normoxic hCPCs for SDF-1 of

neonatal hCPCs cultured in hypoxic or normoxic conditions for 12 or 24 hours, normalized to normoxic 12 hour group. * = p-value < 0.05, given by ANOVA with Tukey's post-test, n = 3-5 for all samples at all time-points.

While neonatal hCPCs showed an unaffected or reduced therapeutic potential when grown in hypoxic conditions, hCPCs from older patients may respond differently to hypoxic conditions. One consideration for neonatal hCPCs is that they are harvested from patients within one week of birth.[9,62] Neonatal hCPCs are harvested from a hypoxic environment during development and immediately after birth, which may make them resistant to continuing hypoxic conditions in culture in terms of therapeutic potential. In contrast, child hCPCs are derived from patients that are 2-5 years old, and therefore have been growing in normoxic tissues.[9,46] As discussed in section 3.2.3, child hCPCs have reduced therapeutic outcomes compared to neonatal hCPCs when used in injectable therapy.[9] However, child hCPCs also have a higher propensity for *in vitro* modulation to improve therapeutic function. Child cells had seen improved therapeutic potential when electrically stimulated or clustered into spheroids, in which cases neonatal hCPCs saw minor changes to function following modulation.[60,61] Also, exosomes derived from child hCPCs grown in hypoxia showed increased therapeutic benefit compared to exosomes derived from child hCPCs grown in normoxia, the latter of which showed no changes to cardiac function or tissue structure compared to control groups.[62,63] In the same study, exosomes derived from neonatal hCPCs cultured in hypoxic conditions did not result in improved LV EF compared to exosomes derived from normoxic hCPCs.[63] Compared to neonatal hCPCs, child cells may respond more effectively to hypoxia.

We implemented the same culture system as described for hypoxic neonatal hCPCs to grow child hCPCs for 12 hours in either normoxia or hypoxia. As seen in **Figure 12A**, there was no change in proliferative potential of child hCPCs grown in acute hypoxic or normoxic conditions. This finding may be linked to the increasingly limited reparative potential of hCPCs as they age, where even child hCPCs show limited proliferation, migration, or differentiation response to physiological repair cues *in vivo*. However, there was a significant increase in the angiogenic potential of child hCPCs when grown for 12 hours in hypoxia compared to cells grown in normoxia, as seen in **Figure 12B**. Child hCPCs may respond to hypoxia by upregulating release of pro-reparative factors in an attempt to repair tissue, rather than by proliferating in preparation to replace tissue.

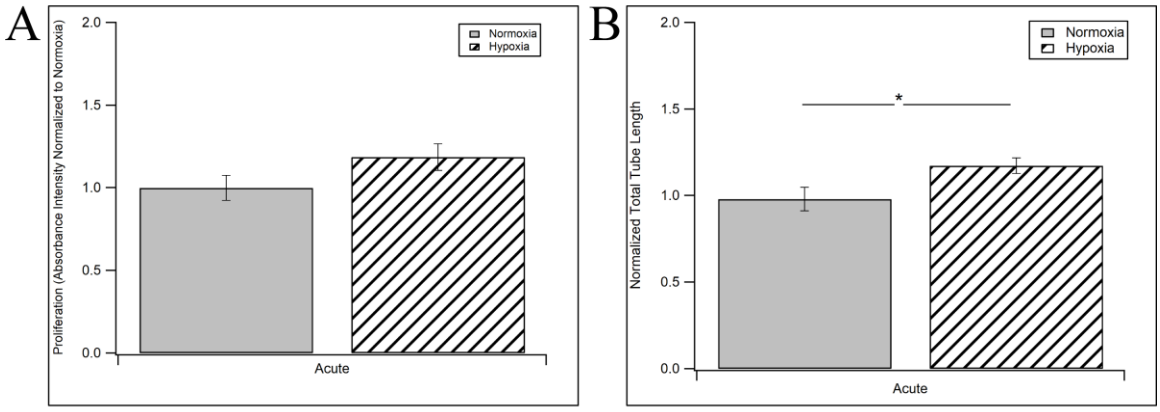

Figure 12 Hypoxia Growth Modulation of Child hCPCs. A) Proliferation of child hCPCs cultured in hypoxic or normoxic conditions for 12 hours, where absorbance intensity is normalized to the normoxic hCPCs. F) Total HUVEC tube length normalized to positive

controls for conditioned media derived from acute hypoxic or normoxic child hCPCs. * = p-value < 0.05, unpaired T-test, n = 3-5 for all samples at all time-points.

The goal of these studies was to understand if various parameters, specifically biomaterial inclusion, hypoxic growth, or cell age, can be implemented in hCPC-cECM patches to further improve therapy. The incorporation of reparative biomaterials within cECM and hypoxic growth of neonatal hCPCs did not result in any changes to neonatal hCPC therapeutic potential when evaluated on cell culture plates. However, the combined use of child hCPCs and hypoxic growth did provide a new group that can be implemented within cell-cECM patches to evaluate *in vitro* therapeutic potential. Child hCPCs also provide a necessary group of hCPCs that can be used in therapy. While autologous neonatal hCPCs can be harvested from neonatal patients, many patients suffering from CHD progression that would require the patch therapy developed here are child patients, as described in section 3.1.3.[3,7,8] Child patients would only have access to child hCPCs for implementing autologous therapy. Therefore, not only is the effect of hypoxia on the growth of hCPCs important to evaluate *in vitro*, the inclusion of child cells relates to a therapeutically necessary group that should be evaluated *in vitro* and *in vivo* concerning the effect of cECM on child hCPC paracrine potential.

Bioinks with child hCPCs were formulated in the same way as developed in chapter 4 to evaluate the duel effect of cECM inclusion within 3D GelMA gels and hypoxic growth conditions. The bioinks were deposited as large gels, polymerized under white light, and finally placed in culture for 12 hours at either normoxic or hypoxic conditions. As seen in **Figure 13A**, there was no difference in viability between child hCPCs grown in GelMA or GelMA-cECM and normoxia or hypoxia, with over 75% viability seen across groups.

Child hCPCs grown in both GelMA-cECM gels and hypoxic conditions showed a significantly increased proliferation compared to all other biomaterial and oxygen conditions, as seen in **Figure 13B**, when data is normalized within oxygen group. When normalizing all data to the GelMA-normoxia group to compare data across oxygen conditions, the inclusion of cECM significantly improved the proliferation of child hCPCs in the hypoxia group only compared to the GelMA hypoxia group. Regardless, the incorporation of cECM within hypoxic gels may be a critical factor in promoting cellular proliferation, potentially by more effectively mimicking the developing heart compared to only cECM or hypoxia. In regards to the analysis of angiogenic potential seen in **Figure 13D**, there was a significant improvement in the angiogenic potential of conditioned media derived from hypoxic child hCPC-GelMA-cECM gels compared to normoxic child hCPC-GelMA gels. The inclusion of both cECM and hypoxia may be required to improve the therapeutic potential of child hCPCs, compared to the inclusion of only cECM as was the case for neonatal hCPCs in chapter 4. Altogether, these results showed that both cECM inclusion and hypoxic conditions were important for improving child hCPC functionality within cardiac patches, compared to GelMA and normoxic conditions alone.

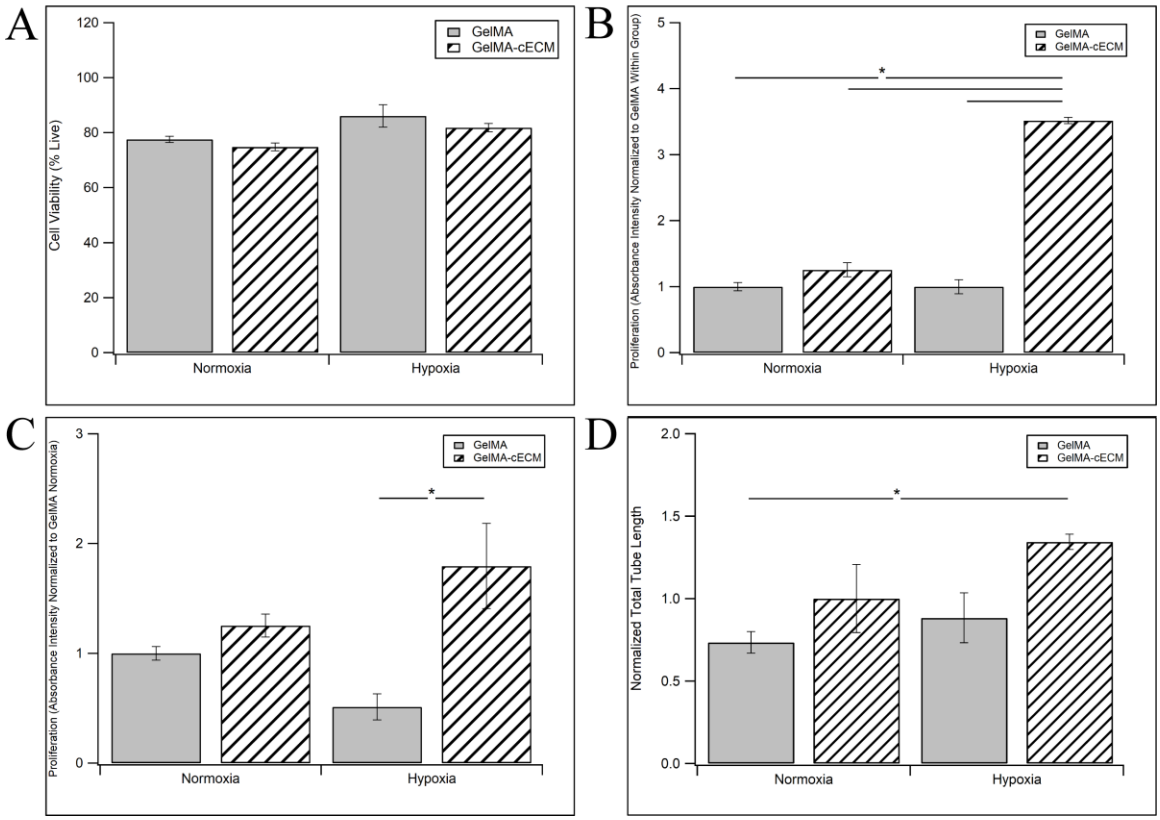

Figure 13 Hypoxia Growth and GelMA-cECM Biomaterial Interactions with Child hCPCs. A) Viability of child hCPCs cultured in GelMA or GelMA-cECM gels and normoxic or hypoxic conditions for 12 hours. B) Proliferation of child hCPCs cultured in GelMA or GelMA-cECM gels and normoxic or hypoxic conditions for 12 hours, where absorbance intensity is normalized to the GelMA group within oxygen condition. C) Proliferation of child hCPCs cultured in GelMA or GelMA-cECM gels and normoxic or hypoxic conditions for 12 hours, where absorbance intensity is normalized to the GelMA normoxia group. D) Total HUVEC tube length normalized to positive controls for conditioned media derived from child hCPCs cultured in GelMA or GelMA-cECM gels

and normoxic or hypoxic conditions for 12 hours. * = p-value < 0.05, given by ANOVA with Tukey's post-test, n = 3-5 for all samples at all time-points.

5.4 Conclusion

In this chapter, we evaluated the effects of fetal cECM components and hypoxic growth on hCPCs of varying ages by analysis of cellular viability, proliferation, genetic expression, and paracrine potential towards angiogenesis. Fetal cECM and hypoxic growth may be key modulators of hCPC functionality, particularly in the case of hCPCs derived from older patients, by recapturing the developmental niche. The effects were first investigated in 2D cell culture to evaluate the methods that would allow for enhanced hCPC therapeutic potential in 3D GelMA-cECM systems.

Pro-reparative ECM components (fibronectin, agrin, periostin) were employed to enhance cECM composition towards a more fetal cECM composition. Neonatal hCPCs grown on combined cECM systems showed no change to viability or gene expression of cardiac and endothelial markers compared to hCPCs grown on pure cECM, with decreased proliferation and angiogenic potential *in vitro*. While initially promising, the effect of cECM itself may overshadow the effect of any materials that are added to the system and maybe the strongest biomaterial modulator of hCPC function. Additionally, soluble materials were employed due to limitations placed by printability requirements. The printing requirement limited the sources and formation methods of the fetal ECM components, resulting in proteins that may not express relevant surface molecules or structural composition to promote functional hCPC-ECM interactions. Improved methods

of complete fetal cECM isolation may provide a resource in analyzing complete fetal cECM effects on hCPCs.

Hypoxic growth conditions recapture the developmental niche and have been used with hCPCs to improve the therapeutic benefit of hCPC-derived exosomes. In 2D culture for 12 and 24 hours in hypoxic conditions, neonatal hCPCs showed a mild increase in proliferation and reduced expression of cardiac and endothelial markers but showed no change in angiogenic potential. Neonatal hCPCs derived from tissue within one week of birth have been exposed to hypoxic conditions during development and immediately after birth and may not be responsive to new hypoxic conditions *in vitro*. Also, neonatal hCPCs may respond to hypoxia by preparing to proliferate and migrate to areas of damage, rather than by enhancing paracrine factor release. Child hCPCs derived from patient's age 2-5 years old have been exposed to normoxic conditions for several years post-development. Child hCPCs show reduced therapeutic potential compared to neonatal hCPCs, although child cells represent the most common autologous cell source for pediatric patients in need of RV treatment. Methods of pre-implantation modification have been required to improve child hCPC therapeutic benefit. Child hCPCs grown in hypoxia for 12 hours showed no change in proliferation and improvements in angiogenic potential, in contrast to neonatal hCPCs. The initial 2D analysis showed that child hCPCs were improved by hypoxic growth towards therapeutic potential. The combined child hCPC-hypoxia system was evaluated in 3D GelMA-cECM gels for ultimate patch implementation.

Within GelMA-cECM gels, child cells showed viability similar to neonatal hCPCs when grown in GelMA-cECM in chapter 4. Also, child cells showed increased proliferation in GelMA-cECM materials grown in hypoxia, compared to GelMA-cECM

normoxia and GelMA hypoxia groups. Importantly, child cells grown in hypoxic GelMA-cECM gels showed improved angiogenic potential compared to cells grown in normoxic GelMA gels. These results point towards the combined effect of cECM and hypoxic growth on improved therapeutic outcomes of child hCPCs.

Overall, neonatal hCPCs showed no change or a reduction in paracrine potential when cultured in hypoxia or with additional matrix components, indicating that inclusion of cECM may be the strongest modulator of neonatal hCPC function. Both 2D and 3D investigation of child hCPCs grown within GelMA-cECM materials in hypoxia point towards the use of the combined system to enhance the therapeutic potential of autologous cell therapy. While *in vitro* analysis indicated that both hypoxia and cECM conclusion were needed to improve the benefit of child hCPCs, implanted patches will experience a highly hypoxic environment due to lack of nutrients from cell culture and patch vascularization that would normally supply oxygen to tissue. Therefore, therapeutic applications of patches into the hypoxic *in vivo* environment will allow for hypoxic growth without the need for *in vitro* hypoxia before implantation. Patch vascularization may occur after several weeks of therapy, which may limit the hypoxic effect on child hCPCs. However, the *in vivo* environment is complex, and the impact of the *in vivo* environment over therapeutic timescales will have a strong impact on child hCPCs, potentially changing cellular phenotype significantly and resulting in cells that behave differently to vascularization-induced patch normoxia. Regardless, the results from this chapter pave the way for child hCPC-GelMA-cECM patches as an important group for *in vivo* evaluation. In the next chapter, we will evaluate all hCPC-GelMA-cECM patches in a murine model of pediatric heart failure to assess patch therapeutic potential.

CHAPTER 6. ASSESSMENT OF IN VIVO REPARATIVE POTENTIAL OF HCPC-CECM PATCHES DELIVERED TO FAILING RIGHT VENTRICULAR MYOCARDIUM

6.1 Introduction

RV heart failure is a prominent clinical problem in the pediatric population, as described in section 3.1.2.[37-44] This chapter will focus on investigating the therapeutic effect of hCPC-GelMA-cECM patches *in vivo* using a juvenile rat RV heart failure model. The culmination of this work is captured in this chapter, investigating the main hypothesis that pericardial application of hCPC-GelMA-cECM patches will improve cardiac function in the failing RV compared to cell-free patches, cECM-free patches, and surgical controls. First, methods of surgical attachment of patches onto the epicardium are evaluated. Following the determination of the attachment method, patches and control groups are implemented in a rat model of RV heart failure. Finally, functional cardiac outcomes and tissue-level properties are investigated four weeks after patch implantation.

6.2 Materials and Methods

Materials – Gelatin methacrylate (GelMA) was purchased from CellINK (Gothenburg, Sweden). Triethanolamine (TEOA), 1-Vinyl-2-Pyrrolidione (NVP), HEPES sodium salt, Triton X-100, sodium dodecyl sulfate, ethanol, pepsin, sucrose, bovine serum albumin (BSA), picrosirius red (direct red 80), aqueous picric acid, and neutral buffered formalin (NBF) 10% were purchased from Sigma-Aldrich (MO, United States). Hams F-12 and Penicillin Streptomycin (Pen-Strep) were purchased from Corning Cellgro (NY,

United States). Eosin Y sodium salt was purchased from TCI (MA, United States). Nordson EFD 30cc barrels, pistons, and 27-gauge plastic tips were purchased from TEK products (MN, United States). Standard fetal bovine serum (FBS) was purchased from Hyclone (PA, United States). L-glutamine was purchased from MP Biomedicals (OH, United States). Cell culture dishes were purchased from Cellstar (PA, United States). Dynal magnetic beads, 1,1-Dioctadecyl-3,3,3',3'-tetramethylindotricardbocyanine iodide (DiR), and Alexa Fluor 790 Carboxylic acid Succinimidyl Ester (AF790) were purchased from Invitrogen (CA, United States). Phosphate buffered saline (PBS), Tissue-TEK OCT compound, and isopropanol was purchased from Fisher Scientific (NH, United States). Collagenase type 2 (300 U/mL) was purchased from Worthington (NJ, United States). Anti-c-kit H300 antibodies and Ku86-AF647 antibodies were purchased from Santa Cruz (TX, United States). Bovine fibroblast growth factor (bFGF) was purchased from Stem Cell Technologies (Vancouver, Canada). Fluorescein Griffonia Simplicifolia Lectin I Isolectin B4, Wheat Germ Agglutinate Rhodamine (WGA), and Vectashield antifade mounting solution with DAPI were purchased from Vector Labs (CA, United States). Isoflurane was purchased from Piramal Healthcare (Mumbai, India). Prolene was purchased from Ethicon (NJ, United States). Sprague Dawley Rats and male adolescent (6-8 week old) athymic rats (Crl:NIH-*Fox1*$_{rnu}$) were obtained from Charles River Laboratories (Wilmington, MA). Cytoseal mounting medium was purchased from VWR International (Radnor, PA). Histoclear II was purchased from National Diagnostics (Atlanta, GA).

Human Cardiac Progenitor Cell Isolation and Culture – The Institutional Review Board at Children's Healthcare of Atlanta and Emory University approved the harvesting of human neonatal c-kit expressing CPCs from the atrial appendage, as previously

described.[17,62] In short, right atrial appendage tissue was obtained from pediatric patients of various ages undergoing heart surgeries due to congenital heart diseases. The atrial appendage tissue was transported using Krebs-Ringer solution, washed with HBSS, and broken down into small sections. The tissue was then enzymatically degraded using 1 mg/mL of collagenase type II at 37^0C, 5% CO_2 for 30 minutes and passed through a 70 μm filter. The mixture was centrifuged at 1000g for 5 minutes to pellet the cells. The cells were combined with magnetic beads conjugated with anti-c-kit antibody, allowed to incubate for 2 hours at 37^0C, followed by magnetic sorting and successive washes with cell culture media. Separated c-kit+ cells were expanded, and the expression of c-kit in the cell population was measured by flow cytometry to ensure they were at least 90% positive. Cells were grouped into two age groups for these studies as follows: neonate (0-1 week) and child (2-5 years). Cells from three donors within the same group were either pooled at the first passage or cultured separately and combined before printing, for all experiments described in this research. hCPCs were grown in T-75 cell culture treated dishes with culture media for expansion. The media was changed every 2-3 days until cells were used in further experiments. Cell culture media consisted of Ham's F-12 media supplemented with 1x Pen-Strep, 1% L-glutamine, 10% FBS, and 10 ng/mL bFGF.

Cardiac Extracellular Matrix Isolation and Characterization – Decellularized porcine ventricular extracellular matrix (cECM) was generated and processed as previously described.[17,16,18] Briefly, porcine ventricular tissue was separated, sectioned into small pieces, rinsed in PBS, and decellularized using a 1% solution of SDS for 4-5 days. The decellularized cECM was rinsed with water, frozen at -80^0C overnight, lyophilized, and milled into a fine powder. Then, the cECM was processed into liquid form by partial

digestion with pepsin (1 mg/mL) in 0.1 M HCl for two days, at a ratio of 10:1 of cECM to pepsin. The cECM was then raised to basic pH by adding 1 M NaOH and salt concentration of 1x PBS, followed by adjustment to pH of 7.4 using HCl and NaOH and diluted to a solution concentration of 8 mg/mL. The solution was aliquoted, immediately frozen at -80^{0}C overnight, lyophilized for 24 hours, and stored at -80^{0}C before use.

Bioink Preparation – GelMA solutions of 14.432% were created by dissolving lyophilized GelMA in 15 mM HEPES buffer and allowed to dissolve under stirring at 60^{0}C for 1-2 hours. GelMA solutions were frozen at -20^{0}C until use. Stock solutions of 13 mg/mL cECM are formed by rehydrating the cECM material with HEPES buffer. All bioinks were prepared immediately before printing. GelMA bioinks were prepared by mixing GelMA (final concentration 5% w/v), Eosin Y (100 µM), NVP (0.75% v/v), TEOA (0.3% v/v), and HEPES buffer (15 mM). In the case of GelMA-cECM bioinks, the HEPES in the above formulation was replaced by the cECM (final concentration 8 mg/mL) solutions. Bioink pH was adjusted to pH 7.4 using HCl. For the inclusion of cells, neonatal or child hCPCs (passage 6-10, pooled or combined across at least three donors) were removed from cell culture plates, pelleted at 1000 rpm for 5 minutes, and labeled with DiR following manufacturer instructions.[60,61] After labeling, cells were mixed with 1 mL solution of the bioink solution, producing a final concentration of 3 million cells/mL.

Bioprinting and Patch Formation – All bioink solutions, with or without cells, underwent similar printing protocols. 1 mL of bioink was deposited into sterilized 30 cc printer barrels and pushed towards the barrel head with a sterile loose fit plunger, removing any air bubbles that formed. A sterile 27-gauge plastic needle tip was added to the barrel, and a cap connecting the print head to the barrel as added. The barrels were put in the low-

temperature head of the bioprinter (EnvisionTEC 3D-bioplotter Developer Series), which was set to 10^0C, and the bioink was allowed to polymerize for 10 minutes. After initial gelation, the printer head was calibrated and purged at 1.2 bar for 1-3 seconds to ensure free-flowing and uniform filaments. Patches and grids were printed onto a glass slide platform at room temperature, using a pressure 0.7-1 bar and speed of 10 mm/s. Patches were 10 mm in diameter and 0.6 um thick, which printed in 3 layers, with an infill pattern of 90^0 grids with 0.5 mm spacing. Eight patches were printed at once. CAD models of the patches printed were generated using SOLIDWORKS and imported to the printing control system through the Bioplotter RP program. Following printing, patches were exposed to white light (Braintree Scientific) at 4^0C for 5 minutes to allow for radical polymerization. The patches were removed from glass slides and put in 2 mL solutions of cell culture media in 24-well plates. All patches were kept in cell culture incubators for several hours before surgery to allow for cECM polymerization after GelMA radical polymerization.

Rat-Patch Attachment Surgery and Imaging – All animal experiments were performed with the approval of the Institutional Animal Care and Use Committee of Emory University. GelMA-cECM patches used for *in vivo* attachment experiments were created in the same way as described in the bioprinting section, with the difference being that the cECM pre-polymer solution was incubated with AF790-carboxylic acid succinimidyl ester before bioink formation. Sprague-Dawley Rats (~250g in weight) were anesthetized with 2% isoflurane, intubated, and placed on a ventilator (Hallowell Emc Microvent 1). Following thoracotomy, the pericardial sac was then very carefully exposed and pulled back. The patch was then gently placed over the RV of the heart, ensuring that there was no folding of the patch. Patches were left without further attachment, tucked underneath

the pericardium, or attached the ventricle using a single suture. After 7 and 14 days, rats were sacrificed, and hearts were excised. Hearts were imaged using an Odyssey CLx (Li-Cor) for both patch fluorescence and heart background fluorescence, with an acquisition area of 20.07 mm x 20.07 mm.

Rat RV Failure Induction, Patch Surgery, and Echocardiogram Follow-up – RV heart failure was induced in male juvenile immunocompromised (nude, athymic) rats by placing a pulmonary artery band (PAB) to increase RV afterload.[60,61] This model was created with the assistance of the Emory and Children's Animal Physiology Core and has been used by our group and others.[60,61] Briefly, an 18-gauge needle was placed alongside the PA, and a suture was tied around the PA and needle. Pulmonary trunk growth leads to a gradual development of clinically relevant RV heart failure. Serial echocardiography was employed to follow the development of RV failure. RV failure was established by two weeks post-banding and is characterized by significantly reduced tricuspid annular plane systolic excursion (TAPSE).[37,60,61] Following RV failure, surgical treatment patch groups (bare GelMA, bare GelMA-cECM, neonatal hCPC-GelMA, neonatal hCPC-GelMA-cECM, child hCPC-GelMA, and child hCPC-GelMA-cECM) were attached to the right ventricular epicardium. Animals were randomized to treatment groups. Briefly, rats were anesthetized with 2% isoflurane, intubated, and placed on a ventilator (Hallowell Emc Microvent 1). Following thoracotomy, the pericardial sac was very carefully exposed and pulled back. Patches were attached to the RV using sutures. Sham rats were not given full PAB surgery or any patch surgery. PAB control rats where given PAB surgery and thoracotomy after RV failure development, but received no patch. Rats were followed longitudinally with echocardiographic exams performed at 2 and 4 weeks post attachment

to monitor cardiac function as previously described.[61] Briefly, transthoracic echocardiography was evaluated using a Vevo 2100 digital high-frequency ultrasound system (Fujifilm VisualSonics) equipped with an MS250 probe. TAPSE was measured in the apical four-chamber view in M-mode, RV end systolic and diastolic areas and RA-area were measured in the apical four-chamber view in B-mode. Echocardiographic measurements were used to determine changes in TAPSE, end diastolic dimensions, end systolic dimensions, and right aria area. TAPSE data was normalized to pre-PAB TAPSE values within individual rats. A total of 78 rats were originally provided by Charles River Laboratories, of which 52 survived for PAB surgery. Following PAB surgery, 22 rats exhibited no change in TAPSE post-PAB or died just before implantation, and were excluded from data analysis and subsequent surgeries. All patch surgeries, data acquisition, and raw data analysis were blinded prior to final grouping and analysis.

In Vivo Cell Retention Imaging and Analysis – Rats were imaged for cell retention *in vivo* by evaluating the fluorescence signal from DiR loaded within cells as previously described.[60,61] Rats were imaged at 0, 14, and 28 days after patch implantation using an IVIS Spectrum *in vivo* imager (Perkin Elmer). DiR fluorescence from the hearts was measured as radiant efficiency and normalized within individual rats as percentage retention (given as 100% on day 0) over time.

Animal Sacrifice and Heart Tissue Fixation/Freezing – Rats were sacrificed on day 28 after patch implantation via carbon dioxide. Hearts were removed en bloc, washed with sterile 1X PBS, and fixed with 10% NBF for 4-5 hours. Following fixation, hearts were washed with 1X PBS to remove excess NBF, then submerged in 30% sucrose overnight to ensure cryoprotection.[60,61] Following cryoprotection, hearts were washed with 1X PBS to

remove excess sucrose and immediately frozen in OCT within tissue blocks using liquid nitrogen chilled isopropanol. Hearts were retained at -80°C before tissue sectioning and analysis.

Immunohistochemistry Methods and Analysis – Cryopreserved heart tissues were sectioned into 10 μm thick sections and mounted on charged slides. Tissue sections are allowed to air dry for 10 minutes, followed by fixation with 10% NBF for 5 minutes. Sections were then washed with a wash buffer composed of 1X PBS and 0.1% Triton X-100 3 times for 5 minutes each. Sections were blocked in blocking buffer composed of 1X PBS, 0.1% Triton X-100, and 5% BSA for 30 minutes in a dark, humidified chamber. Following blocking, sections were incubated with a dye/antibody cocktail overnight at 4°C or for 90 minutes at room temperature.[60,61] The dye/antibody cocktail was composed of isolectin-fluorescein (1:100 dilution, Griffonia simplicifolia lectin I isolectin B4, fluorescein), WGA-rhodamine (1:300 dilution, wheat germ agglutinin, rhodamine), and monoclonal Ku86-AF647 (1:500 dilution) suspended in blocking buffer.[60,61] Sections were then washed with wash buffer three times for 5 minutes each. Vectashield antifade mounting medium with DAPI was added to each slide, and a coverslip was placed over the section, followed by a 10-minute incubation to allow DAPI to interact with cell nuclei. Slides were imaged on an Olympus IX81 FluoView FV1000 confocal microscope. Each tissue section was imaged at multiple locations within the RV for all groups, and adjacent to the implanted patch for patch groups. Sequential imaging of different fluorescence channels was employed to reduce nonspecific dye bleed-through. Vessel density was analyzed by isolectin staining of EC tubule formation. The number of vessels per 0.2 mm^2 area was counted for each tissue section across multiple replicates and averaged within

patch or control groups. For patch-adjacent vessel analysis, the number of vessels in the area adjacent to patches was counted, divided by the evaluated area (in cm^2), and averaged within groups. Cardiomyocyte hypertrophy was analyzed by WGA staining of cardiomyocyte cell walls. Cardiomyocyte cross-sectional areas were evaluated for each tissue section across multiple replicates and averaged within patch or control groups. Cell retention was analyzed by co-expression of human marker Ku86 and DAPI within cardiac patches.

Fibrosis Staining and Analysis – Cryopreserved heart tissues were sectioned into 10 μm thick sections and mounted on charged slides. Tissue sections are allowed to air dry for 10 minutes, followed by fixation with 10% NBF for 5 minutes. Sections were rinsed with deionized water for 3 minutes, rehydrated with 1X PBS for 5 minutes, and stained with a 1 mg/mL solution of Picrosirius red in aqueous picric acid for 90 minutes. Following staining, slides were rinsed with acidified water for 1 minute, rinsed with deionized water for 3 minutes, and dehydrated with 70% ethanol for 30 seconds. Finally, slides were cleared with Histoclear for 1 minute and mounted with Cytoseal. Slides were imaged on a Hamamatsu NanoZoomer S210 slide scanner (Hamamatsu Photonics). The fibrotic area was quantified using color thresholding on ImagJ (G. Landini software), and % fibrosis was calculated as the fibrotic area/total area of the RV free wall for each slide across replicates and groups.

Statistics – Numerical data are the mean ± SEM. All data was analyzed using one-way ANOVAs with Tukey's multiple comparison post-test. Sample size (n) was 3-6 for all samples. In cases where both days and groups were involved, data were compared across groups within the same day and across days within the same group to determine significant

differences. Control time group error for normalized measurements is presented either as SEM of replicates across experiments or SEM of normalized values across n. All animal-group randomization, patch surgical implantation, raw data acquisition, and raw data analysis were performed blinded, prior to final grouping and data analysis.

6.3 Results and Discussion

Both hCPCs and cECM have found success in clinical trials for treating adult patients post-MI or pediatric patients with CHD.[6,7,8,152] Phase II and III clinical trials are either underway or will be undertaken, with hopeful success for RV repair. However, and as discussed in section 3.4.1 and chapter 4, there are significant limitations to injectable therapy that may reduce the therapeutic effect overall and for pediatric patients suffering from CHD and RV dysfunction.[10,11] This study evaluates hCPC-cECM patches in effecting functional and tissue-level improvements in an animal model of RV failure.

Before moving forward to the evaluation of patch therapeutic benefits in an animal model, the attachment method of GelMA-cECM patches onto the epicardial surface must be assessed to ensure that devices can be deployed with minimal manipulation. We evaluated the potential of GelMA-cECM patches to remain attached to rat hearts after placement on the epicardium. Surgical attachment of the patches was achieved on healthy rat hearts via placement on top of the epicardial surface of the RV after opening the chest cavity and exposing the heart. Three methods of attachment were evaluated – simple placement on the epicardium without secondary support, placement on the epicardium followed by covering with the pericardium, and placement on the epicardium with a single suture. All three methods allowed for patch placement on beating rat hearts, without

buckling or patch damage. Before patch generation, cECM incorporated into patches was incubated with a fluorescent dye for post-implantation imaging. The simple placement without secondary support resulted in patch movement during and after surgery, indicating that some support was needed for patch retention. Following the pericardial and suturing methods, hearts were excised from rats and fluorescently imaged to determine if the patch remained on the heart. Of 8 patches implanted, all were retained up to 7 and 14 days, regardless of pericardial or suturing attachment method. As seen in **Figure 14**, patches were retained at day 7 **(Figure 14A suture)**, and day 14 **(Figure 14B pericardial, Figure 14C suture)** with clear and stable fluorescent signal up to 14 days. Both methods did not require the use of a surgical adhesive such as fibrin, which may impose a barrier layer for paracrine release.[228] However, the pericardial method required cutting of the patches into smaller than 10 mm sizes before placement in two out of the three animals evaluated with this method, as the full patch tended to fold upon covering with the pericardium, indicating that the suturing method may be ideal for implementing a large device. In either case, the patches were retained throughout 14 days without change to patch shape, fluorescence expression of the cECM-bound dye, or buckling. The rat heart beats approximately 400-500 times per minute, significantly more than the human heart, and thus these results are quite promising.[229] In these healthy rat models, interactions between the patches and myocardium were evaluated using staining for host vessel formation. As seen in **Figure 14D**, vessels were formed in the patches after 14 days *in vivo*, indicating that the patches integrate with the native myocardium and may allow for nutrient delivery to the implanted cells. Overall, the patches were retained on the myocardium and became vascularized over

14 days in healthy rats. The method of suturing the patch to the heart was implemented for all assessment surgeries moving forward.

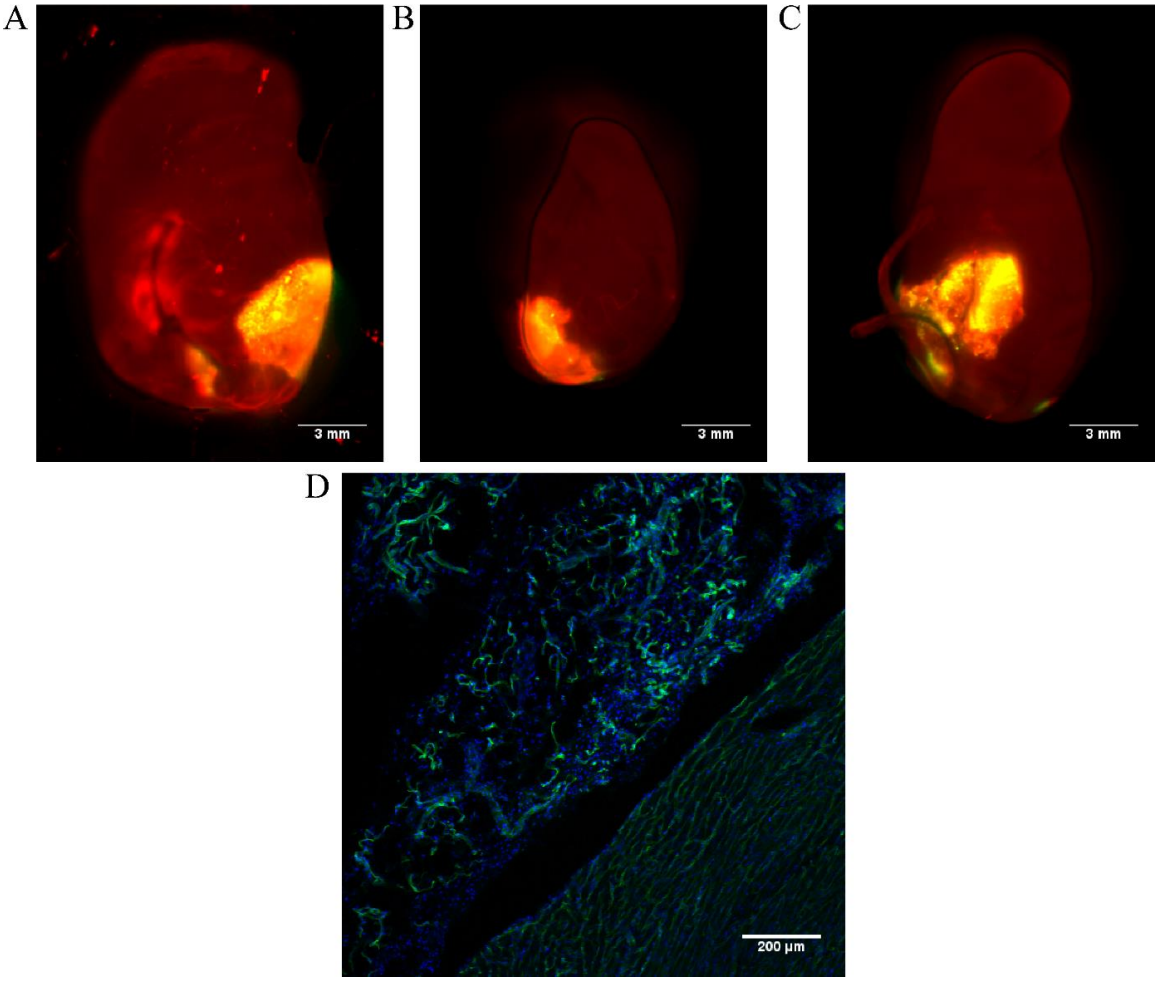

Figure 14 *In Vivo* Patch Retention – Attachment Studies. hCPC-GelMA-cECM patches (yellow) are retained after 7 (A, suture method) and 14 (B, pericardial tucking method and C, suture method) days following implantation. D) Immunohistological analysis of vasculature formation (green) and cells (blue) after 14 days *in vivo*.

The true assessment of patch therapeutic function is in a model of RV failure. Our lab and others have employed a pediatric murine model of RV failure using a PAB method

to increase RV afterload.[60,61] As discussed in the methods section, juvenile immunocompromised rats (nude, athymic) had a band placed on their pulmonary arteries. This method reduced blood flow into the pulmonary artery, resulting in pulmonary trunk growth and gradual development of RV failure due to the poor ability of the RV to respond to changes in afterload (as discussed in section 3.1.2), mimicking the development of RV failure in CHD.[37,38,60,61] After PAB surgery, rats were followed for two weeks and assessed for the development of heart failure by a significant reduction in TAPSE, a measure of global RV function which describes apex to base shortening.[37,60,61] After the development of RV failure using the PAB method, patches across different groups were attached to hearts using the suturing method determined above. Groups included Sham controls, PAB controls that did not receive patches, bare GelMA patches, bare GelMA-cECM patches, neonatal hCPC-GelMA patches, neonatal hCPC-GelMA-cECM patches, child hCPC-GelMA patches, and child hCPC-GelMA-cECM patches. In **figures 16-21** in this chapter, patch groups are split into three groups – bare, neonatal, and child – which contain both GelMA and GelMA-cECM patches within the groups. Rats were followed throughout the 4-week therapy timeline with echocardiographic and *in vivo* fluorescent imaging methods. After four weeks, animals were sacrificed, the hearts were explanted and fixed/frozen en bloc, and the tissue was further analyzed.

A key hypothesis of this work is that the incorporation of hCPCs within cardiac patches will improve cellular retention over therapeutic timescales compared to cell injection alone. Previous studies from our lab and others have shown that injected hCPCs, both fresh from culture or post-modulation, are quickly cleared from the tissue, and only 0-30% of hCPCs are retained after 28 days of therapy depending on the method of

modulation.[9,10,60,61] All cells laden within patches were labeled with a dye that can produce a fluorescent signal *in vivo*, allowing for tracking of cell retention during therapy in similar ways as was employed in previous studies.[60,61] This methodology has previously shown no detrimental effects on the cells themselves.[60,61] The rats were tracked over 28 days (4 weeks) of therapy for fluorescence signal, and the radiant efficiency of the fluorescent signal at day 0 after patch implantation was used to normalize signals from days 14 and 28, as seen in **Figure 15**. Rats across all four cell-laden patch groups exhibited a clear, strong fluorescent signal that was specifically derived from the heart location, as seen by **Figure 15A**. Quantification of cell retention, seen in **Figure 15B**, shows that fluorescent signal remained consistent throughout 28 days of therapy without any significant differences between days or patch groups. An initial increase in fluorescent signal was seen between days 0 and 14, mirroring results in other studies, which may be attributed to reduced fluorescent signal at day 0 due to location inflammation in the chest from patch implantation surgery, other chest cavity responses with surgery, or thick tissue layer post-surgery.[60,61] Regardless, these results show that cells were being retained without significant loss to the circulation or tissue environment throughout therapy. The cell retention was consistent even after 28 days, while studies using injected hCPCs have shown only a 0-30% retention after this timescale.[9,10,60,61] Another key finding is that there was no difference in retention across all material types and cell types, indicating that the effectiveness in retention was not an additional confounding variable in assessment of patch therapeutic benefit across study groups. While these results show that cells were retained during therapy, the *in vivo* signal must be complemented by tissue analysis to support retention. Explanted tissue sections were analyzed using a human-specific Ku86

marker and nucleus staining with DAPI.[60,61] As seen in **Figure 15C**, fluorescent images focused on patches attached to tissue sections showed clear expression of Ku86 (magenta) and nuclei (blue) across patch groups. Regardless of patch type or cell type, cells were retained within patches after 28 days of therapy, supporting the *in vivo* imaging results. Overall, these studies support the idea that patch therapy retains cells during surgery without loss compared to injectable therapies and that there were no differences in retention across material type and cell type employed across patch groups.

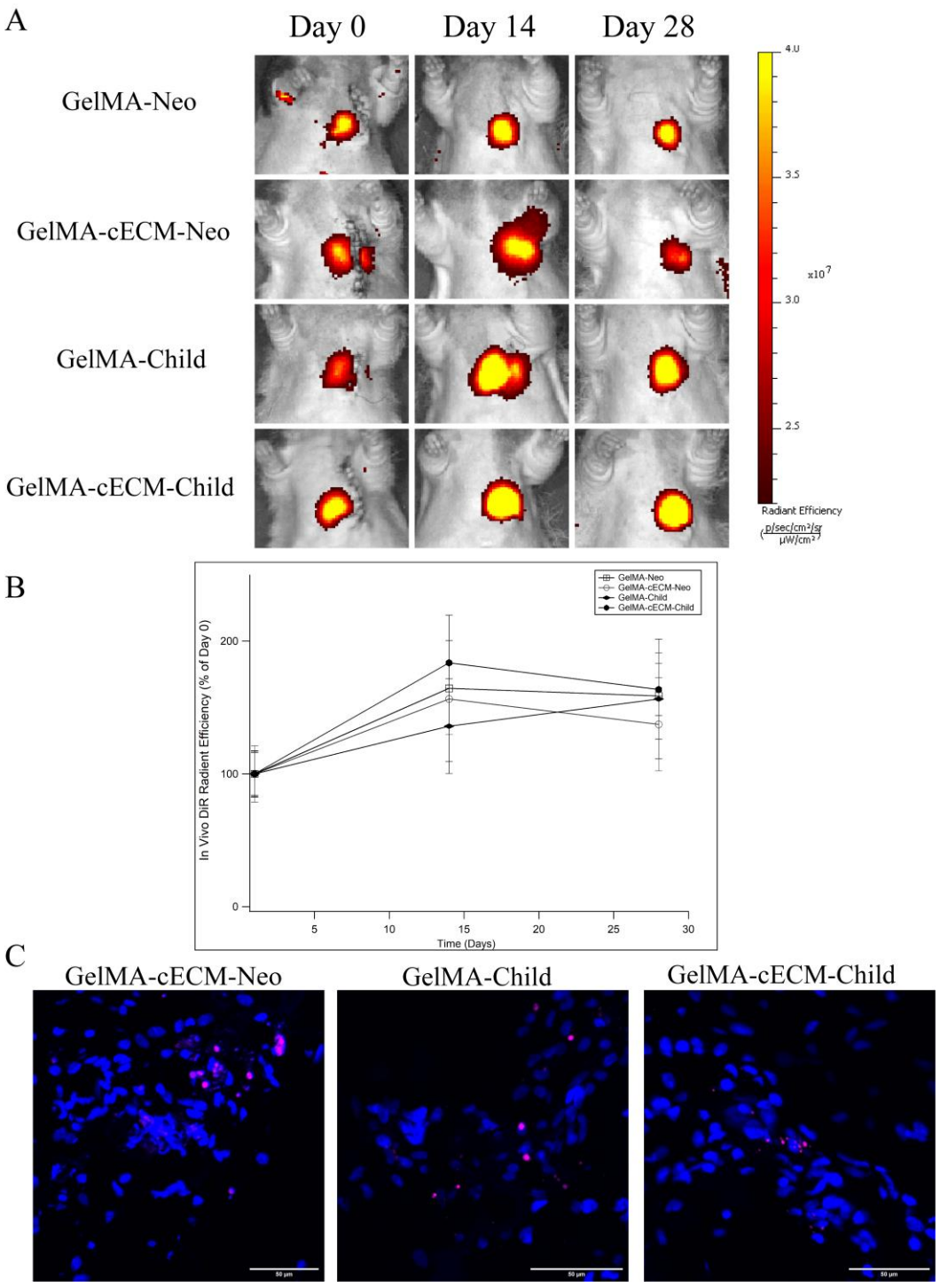

Figure 15 *In Vivo* Cell Retention. A) Radiant efficiency signal of rats across different cell-patch groups over 28 days of therapy. B) Quantified fluorescent signal across all cell-patch groups over 28 days of therapy, presented as radiant efficiency (% of Day 0) normalized

to day 0 measurements within rats. n = 3-4 for all time-points C) Immunohistological staining of patches within tissue sections across several cell-patch groups, where human marker Ku86 (magenta) and nuclei marker DAPI (blue) is co-localized. Scale bar for stained images is 50 μm.

Rats were tracked throughout therapy by echocardiographic measurements for TAPSE, end diastolic dimension (EDD), end systolic dimensions (ESD), and right atrium area (RA-Area). As previously discussed, TAPSE is a critical indicator of RV global function and has been employed in previous studies as a key metric to assess therapeutic effects.[37,38] In **Figure 16A**, TAPSE is presented for all groups across 0, 2, and 4 weeks post-patch implantation, while **Figure 16B** shows a close up of only the week 4 TAPSE values for clarity. There was a consistent difference between Sham and PAB groups at all time-points, indicating that Sham and PAB controls were effective tools for the analysis of therapeutic function. While statistical differences were displayed in **Figure 16A** between Sham and PAB values between weeks 0-4 for reinforcement of control animal results, all other groups showed a significantly lower TAPSE compared to Sham controls unless otherwise noted by the # symbol. Immediately before patch implantation (week 0 values), all groups showed a significantly lower TAPSE value then Sham controls, indicating that all rats evaluated had developed RV failure post-PAB surgery. Two weeks post-implantation, neonatal hCPC-GelMA, neonatal hCPC-GelMA-cECM, and child hCPC-GelMA-cECM groups showed no significant differences in TAPSE values compared to Sham groups, indicating that these patch groups may be improving RV function. Specifically, child hCPC-GelMA-cECM patches also showed a significant improvement in TAPSE compared to PAB controls, indicating that the child hCPC-GelMA-cECM patch

had short term beneficial therapeutic benefits in treating RV failure. **Figure 16B** shows week 4 results only, for clarity. Four weeks post-implantation, GelMA-cECM, neonatal hCPC-GelMA, neonatal hCPC-GelMA-cECM, and child hCPC-GelMA-cECM groups all showed no significant TAPSE difference compared to Sham controls, with the neonatal hCPC-GelMA-cECM group showing significant improvements in TAPSE compared to PAB controls as well. These findings point towards the effectiveness of ECM-laden patches in improving RV function across all groups compared to controls, with a combined inclusion of cECM and neonatal hCPCs showing the best improvements after four weeks. Additionally, neonatal hCPC-GelMA-cECM patches were the only patches to show significant improvements in TAPSE within the patch group, where TAPSE significantly improved in neonatal hCPC-GelMA-cECM treated rats between week 0 and week 4. Within cell type, child hCPC-GelMA-cECM groups showed a significant improvement in TAPSE compared to child hCPC-GelMA groups, indicating that the inclusion of cECM is a critical factor in enhancing the therapeutic potential of child cells.

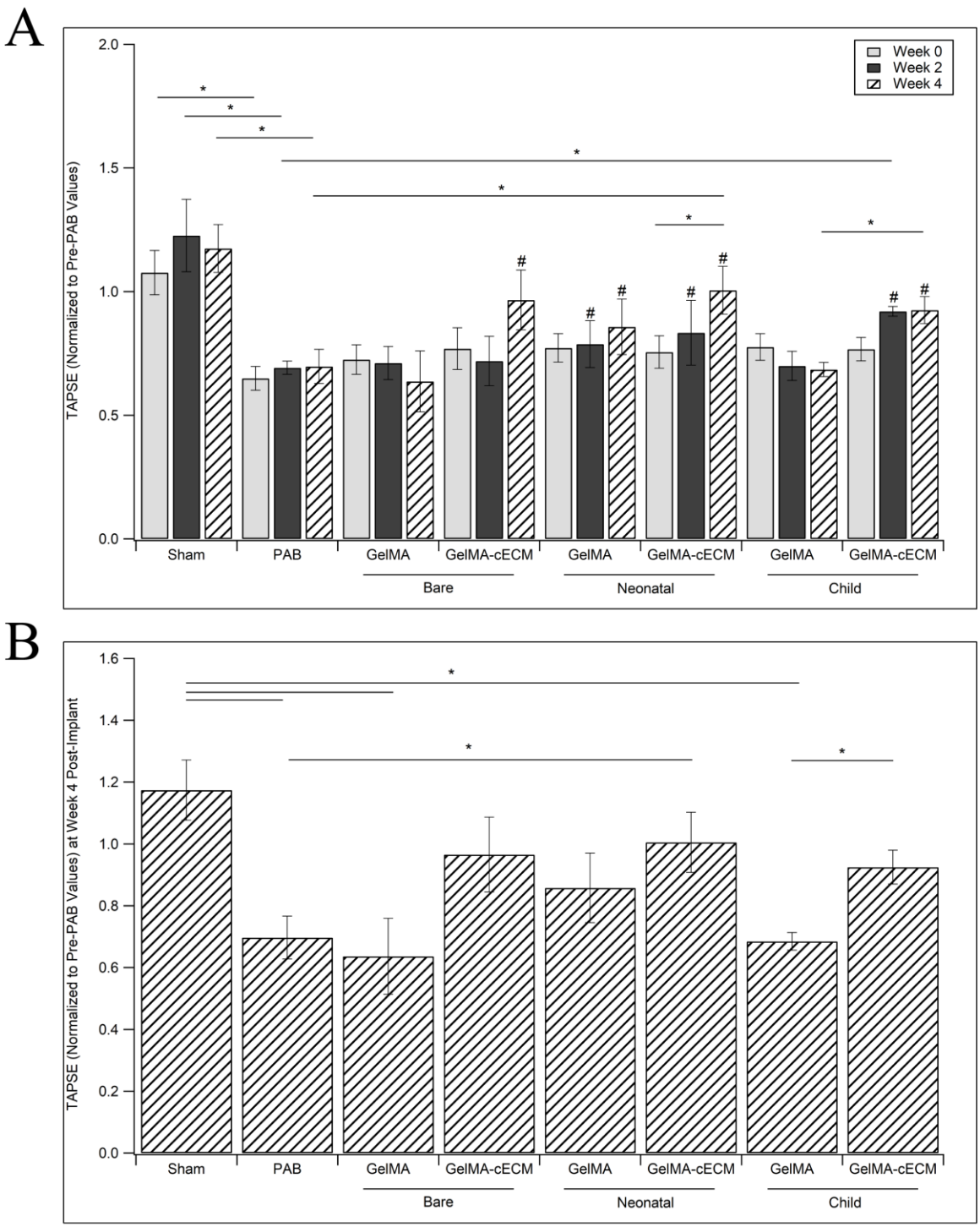

Figure 16 Echocardiographic Measurements – TAPSE. A) TAPSE measurements for all groups across 0-4 weeks of treatment. TAPSE value is normalized to TAPSE at two weeks

prior to patch implantation (immediately before PAB surgery) within rat. * = p-value < 0.05, # = no significant difference from Sham group values within week grouping. B) TAPSE measurements at week 4 post-patch implantation only. TAPSE value is normalized to TAPSE at week 2 prior to patch implantation (immediately before PAB surgery) within rat. * = p-value < 0.05. Statistical values are given by ANOVA with Tukey's post-test, n = 3-6 for all groups at all time-points.

Evaluation of EDD, ESD, and RA-Area produce less definitive results, where comparisons are evident only when compared to Sham controls at four weeks post-implantation. **Figure 17** shows EDD, ESD, and RA-Area values, where all figures show data from the control (Sham and PAB) and bare patch (GelMA and GelMA-cECM) groups. Additionally, **Figures 17A, 17C,** and **17E** show data from neonatal patch groups (GelMA and GelMA-cECM) and **Figures 17B, 17D,** and **17F** show data from child patch groups (GelMA and GelMA-cECM). As seen in **Figures 17A-D**, EDD and ESD values for PAB groups compared to Sham groups are significantly different and provide effective controls. While no groups showed differences from PAB controls, GelMA, GelMA-cECM, and neonatal hCPC-GelMA-cECM groups showed no differences in EDD and ESD compared to Sham controls, and the child hCPC-GelMA-cECM group showed no differences from Sham for ESD values only. While not significant over PAB controls, these results show that the inclusion of cECM, regardless of cell inclusion or cell type, improved the RV dimensions during therapy while GelMA-cell groups were no different than PAB controls compared to Sham values. This trend is further seen in RA-Area measurements **(Figure 17E and 17F)**. In addition to RV changes, the RA is significantly affected by the PAB method through the enlargement of the RA area.[37,60,61] While PAB controls showed

continued significant enlargement of the RA compared to Sham controls after four weeks post-implantation, the only groups that showed no difference from Sham controls were neonatal hCPC-GelMA, neonatal hCPC-GelMA-cECM, and child hCPC-GelMA, although the effect may be minor for the latter case. These results point towards the effectiveness of cell-laden materials in improving RA function in addition to RV function, although no groups were different from PAB values.

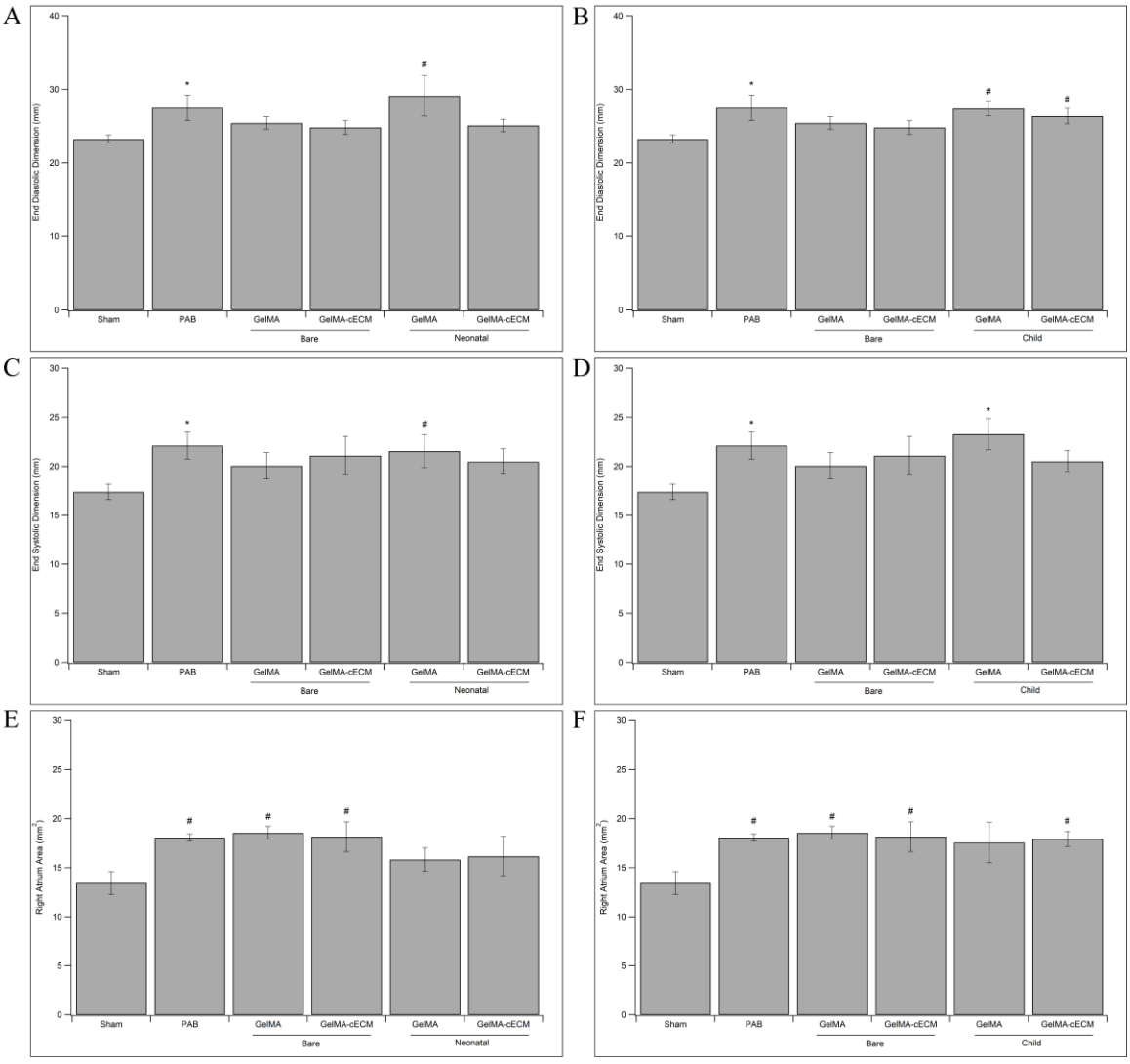

Figure 17 Echocardiographic Measurements – EDD, ESD, RA-Area. A) End diastolic dimension (EDD) measurements for control groups, bare patch groups, and neonatal patch groups at week 4 post-patch implantation. B) EDD measurements for control groups, bare patch groups, and child patch groups at week 4 post-patch implantation. C) End systolic dimension (ESD) measurements for control groups, bare patch groups, and neonatal patch groups at week 4 post-patch implantation. D) ESD measurements for control groups, bare patch groups, and child patch groups at week 4 post-patch implantation. E) Right Atrium Area (RA-Area) measurements for control groups, bare patch groups, and neonatal patch groups at week 4 post-patch implantation. F) RA-Area measurements for control groups, bare patch groups, and child patch groups at week 4 post-patch implantation. * = p-value < 0.01 compared to Sham group, # = p-value < 0.05 compared to Sham group for all subfigures. Statistical values are given by ANOVA with Tukey's post-test, n = 3-6 for all groups at all time-points.

Overall, cardiac function (TAPSE, EDD, ESD, RA Area) was improved with implantation of neonatal hCPC-GelMA-cECM and child hCPC-GelMA-cECM patches after 4 or 2 weeks post-implantation. Trends towards functional improvement were seen with bare GelMA-cECM and neonatal hCPC-GelMA groups as well in terms of TAPSE. All cECM groups showed repair or improvements in TAPSE, while only the only GelMA group that showed improvements during therapy was neonatal hCPC-GelMA, pointing towards the effectiveness of cECM in treatment. This trend is reinforced by EDD and EDD improvements of GelMA vs. cECM groups, where cECM groups improved ESD and EDD regardless of cell incorporation, while GelMA-cell groups saw non-consistent improvements. Within cell type, the inclusion of cECM was necessary for improvements

in EDD and ESD function over Sham compared to GelMA alone. When comparing cell types within biomaterial groups for TAPSE and RA-Area measurements, GelMA required incorporation of neonatal cells to improve cardiac function compared to bare GelMA or child hCPC-GelMA groups, while cECM groups did not require cellular incorporation for functional improvements, although the incorporation of neonatal or child hCPCs may have boosted this effect for cECM groups. Regardless, neonatal hCPC-GelMA-cECM patches were the only patches that showed improvements in cardiac function across all functional measurements, although bare GelMA-cECM patches showed equivalent improvements in most analysis methods. Another important hypothesis of this work is that incorporation of cECM within patches will improve cellular functionality when comparing the GelMA vs. cECM groups laden with the same cell type (neonatal or child). While the neonatal hCPC-GelMA-cECM patch group showed the highest degree of cardiac repair across all cell groups, there were fewer significant differences between neonatal hCPC-GelMA-cECM and neonatal hCPC-GelMA groups directly. Also, functional cardiac measurements showed that cECM inclusion for neonatal patches was needed to improve RV dimensions closer to Sham values, compared to neonatal hCPC-GelMA groups. For child cells, there was a clear improvement in cardiac outcomes in terms of RV function and dimensions in the child hCPC-GelMA-cECM group compared to controls, while the child hCPC-GelMA group saw no improvements in cardiac function across many analysis methods. These results could indicate that cECM may be the strongest modulator of patch therapeutic potential. For cases when child patients require therapy and only child hCPCs are available as autologous cell sources, the inclusion of cECM within patches is important to facilitate functional improvements compared to child hCPC-GelMA patches alone.

While cardiac functional measurements are critical parameters in evaluating the therapeutic effect of bioprinted patches, tissue-level effects must also be evaluated to understand how therapies affect cardiac remodeling and function.[60-63] As mentioned in section 3.1.2, pediatric RV failure is characterized by progressively increased cardiomyocyte hypertrophy, decreased vascular density, and increased tissue fibrosis.[37-40] Quantification of these variables allows for a clear understanding of tissue-level changes due to therapy. As described in the methods section, the hearts explanted from rats after four weeks of therapy were analyzed using histological methods. The first of these assess the vascularization of the RV, as seen in **Figure 18**, where **Figure 18A** shows characteristic images of vessel staining, and **Figure 18B** shows quantified vessel density across all groups. PAB, neonatal hCPC-GelMA, child hCPC-GelMA, and child hCPC-GelMA-cECM groups showed significantly lower tissue vascularization compared to Sham groups, indicating limitations in patch therapy towards tissue remodeling when using pure GelMA or child hCPC patches. On the other hand, both GelMA-cECM and neonatal hCPC-GelMA-cECM groups showed improvements in vascularization over PAB controls. These results reinforce the cardiac functional results since only cECM laden groups showed improvements in tissue remodeling and vasculature formation. Also, both GelMA-cECM and neonatal hCPC-GelMA-cECM groups showed improved vascularization compared to neonatal hCPC-GelMA and child hCPC-GelMA-cECM groups. These results directly reinforce the *in vitro* findings in chapter 4, where cECM inclusion improved the angiogenic potential of neonatal hCPC-GelMA-cECM patches compared to neonatal hCPC-GelMA patches, although this trend was not seen when comparing child hCPC-GelMA and child hCPC-GelMA-cECM groups. The effect of cECM on neonatal cell reparative potential

may be primarily improving angiogenic effects, such as by releasing pro-vascularization cytokines over other cytokines, which is supported by both *in vitro* and *in vivo* results in this study.[180] Additionally, within the cECM groups, only GelMA-cECM and neonatal hCPC-GelMA-cECM groups saw improvements while child hCPC-GelMA-cECM groups did not, reinforcing previous studies that showed the limited therapeutic potential of child cells compared to neonatal cells.

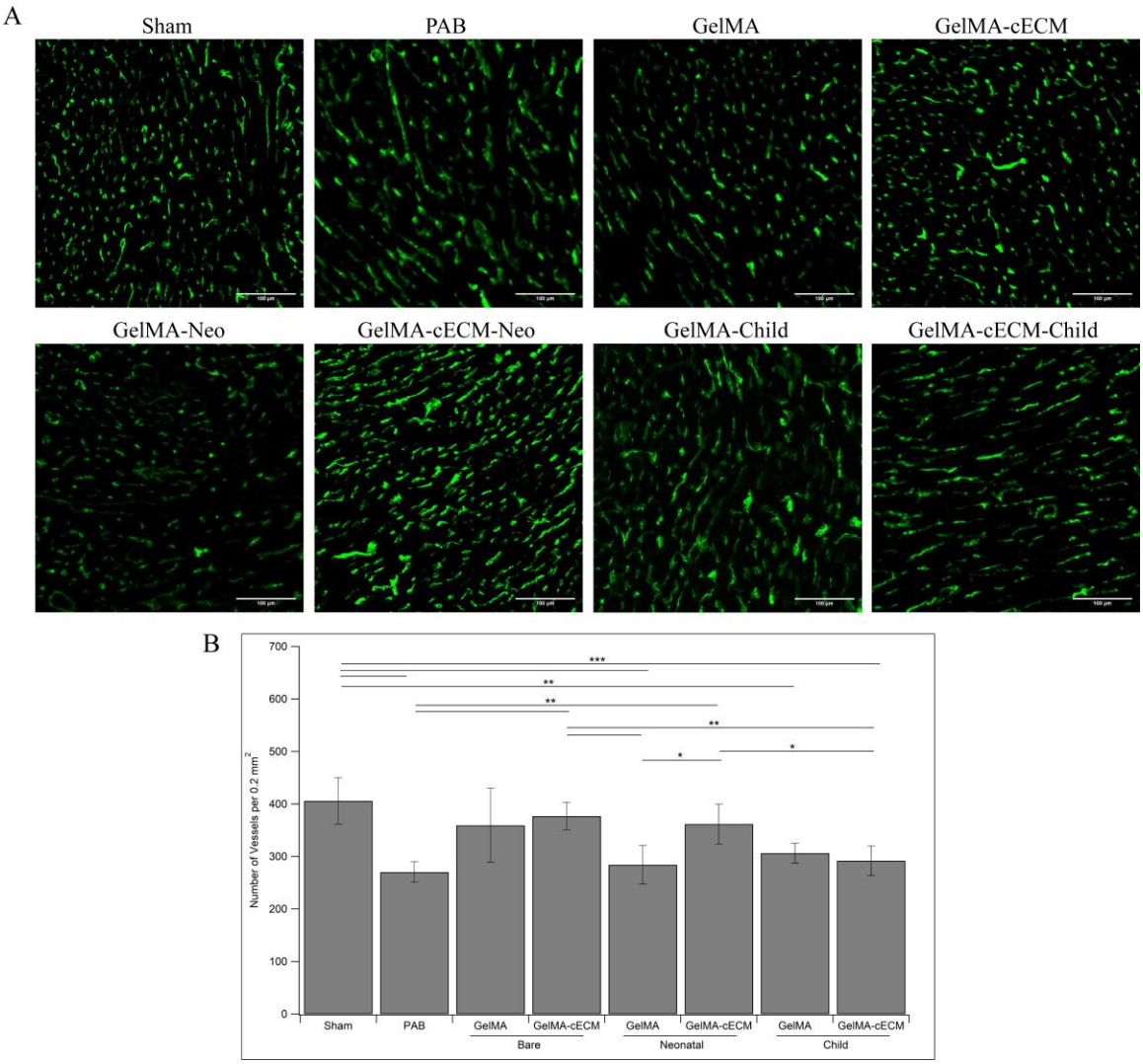

Figure 18 Tissue Vascularization. A) Characteristic images of fluorescent signals from tissue sections stained with vessel-specific dye. Scale bar for all images is 200 μm. B)

Quantified vessel density given as number of vessels per 0.2 mm^2 area of the RV. * = p-value < 0.05, ** = p-value < 0.01, *** = p-value < 0.005, given by ANOVA with Tukey's post-test, n = 3 for all groups at all time-points.

The analysis in **Figure 18** described the vascularization across groups evaluated at multiple sections within the RV. During implantation, patches are placed on the epicardial wall of the RV, rather than inside the RV tissue itself, which may mean that there are local changes to tissue vascularization close to the patch implantation site compared to the RV in general. Also, reparative factors such as growth factors are quickly bound to cell surface receptors by endogenous cells within the myocardium close to the patch and by hCPCs within the patch itself, which may drive local changes.[230] Vessel density analysis for RV tissue adjacent to patches is presented in **Figure 19**, where only patch groups are considered. As can be seen, only GelMA-cECM and neonatal hCPC-GelMA-cECM patches show an improved vessel density adjacent to patches, compared to GelMA patches. This trend mirrors the vascularization data seen in **Figure 18**, where only GelMA-cECM and neonatal hCPC-GelMA-cECM patches show an improved vessel density compared to controls. Unlike RV vascularization overall, there were no significant differences between GelMA-cECM/neonatal hCPC-GelMA-cECM patches and neonatal hCPC-GelMA/child hCPC-GelMA-cECM patches when considering only patch-adjacent tissue. These results may indicate that neonatal cell inclusion in GelMA or child cell inclusion within GelMA-cECM may be producing a local improvement in tissue angiogenesis, although the effects were not sufficiently stronger than the effect of bare GelMA patches. Additionally, child hCPC-GelMA-cECM patches did not show improvements in vessel density compared to GelMA patches, even though the child hCPC-GelMA-cECM patches included what may

be the strongest factor towards therapy – cECM inclusion. The child hCPCs were maybe remodeling the ECM within the patch and reducing the pro-reparative tissue effect of the cECM seen in the bare and neonatal hCPC-laden GelMA-cECM patches. Overall, these results indicate that there may be a local response related to material, of which cell-inclusion does not significantly modulate.

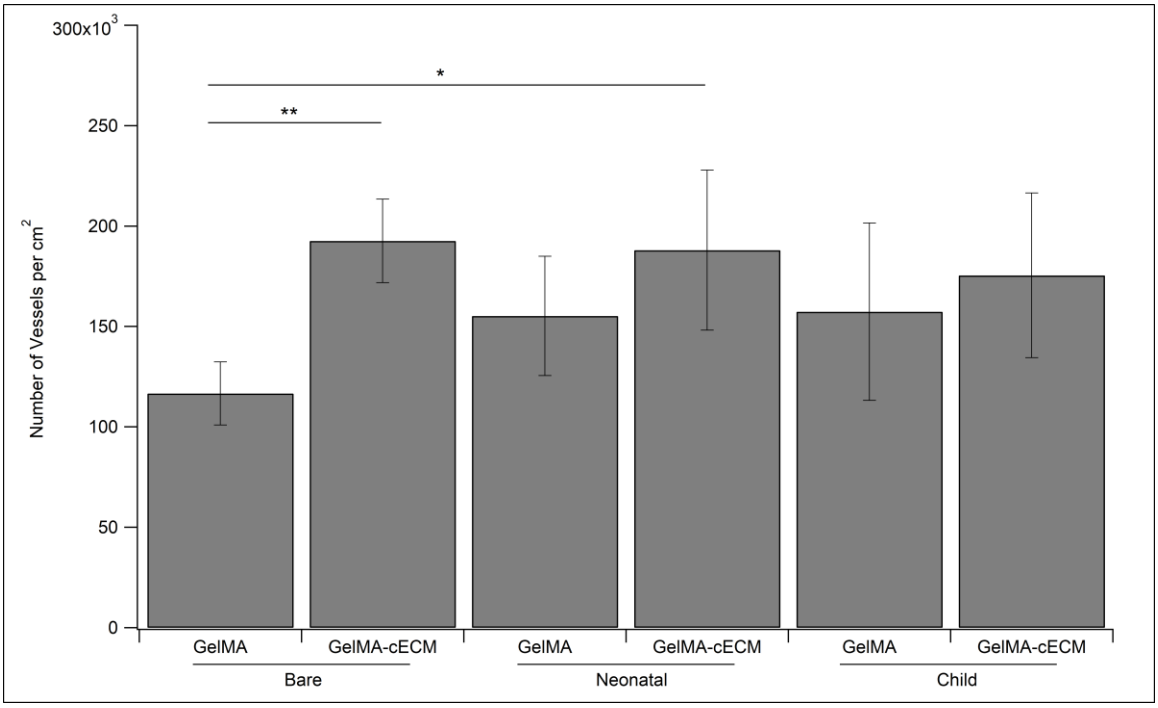

Figure 19 Patch-Adjacent Vascularization. Quantified vessel density given as number of vessels per cm^2 area of the RV adjacent to location of implanted patch. * = p-value < 0.05, ** = p-value < 0.01, given by ANOVA with Tukey's post-test, n = 3 for all groups at all time-points.

Cardiomyocyte hypertrophy is a driving factor of RV failure and the development of non-contractile tissue.[37-40] Analysis of cardiomyocyte hypertrophy for all groups is seen in **Figure 20**, where **Figure 20A** shows characteristic images of cardiomyocyte outlines,

and **Figure 20B** shows quantified cardiomyocyte area across all groups. PAB, GelMA, neonatal hCPC-GelMA, child hCPC-GelMA, and child hCPC-GelMA-cECM groups showed significantly higher cardiomyocyte area compared to Sham groups, indicating limitations in patch therapy towards tissue remodeling that goes hand in hand with the vascularization results, although it is notable that neonatal hCPC-GelMA and child hCPC-GelMA-cECM groups were closer to values of Sham then GelMA and child hCPC-GelMA groups. Both GelMA-cECM and neonatal hCPC-GelMA-cECM groups showed reductions in cardiomyocyte hypertrophy over PAB controls. These results reinforce the cardiac functional measurements and vessel density analysis, where only cECM laden groups showed improvements in tissue remodeling and vasculature formation. Also, there was a significant difference between GelMA-cECM and neonatal hCPC-GelMA-cECM groups with cardiomyocyte area of child hCPC-GelMA groups, along with differences between GelMA-cECM and GelMA groups. These findings point once again towards cECM laden patches outperforming pure GelMA patches, regardless of cell inclusion or type, in terms of improving tissue remodeling towards tissue repair. Although there was no significant difference between biomaterial types within cell groups in comparing cardiomyocyte area, there was a trend towards reduced cardiomyocyte hypertrophy in the child/neonatal GelMA-cECM groups compared to the child/neonatal GelMA groups.

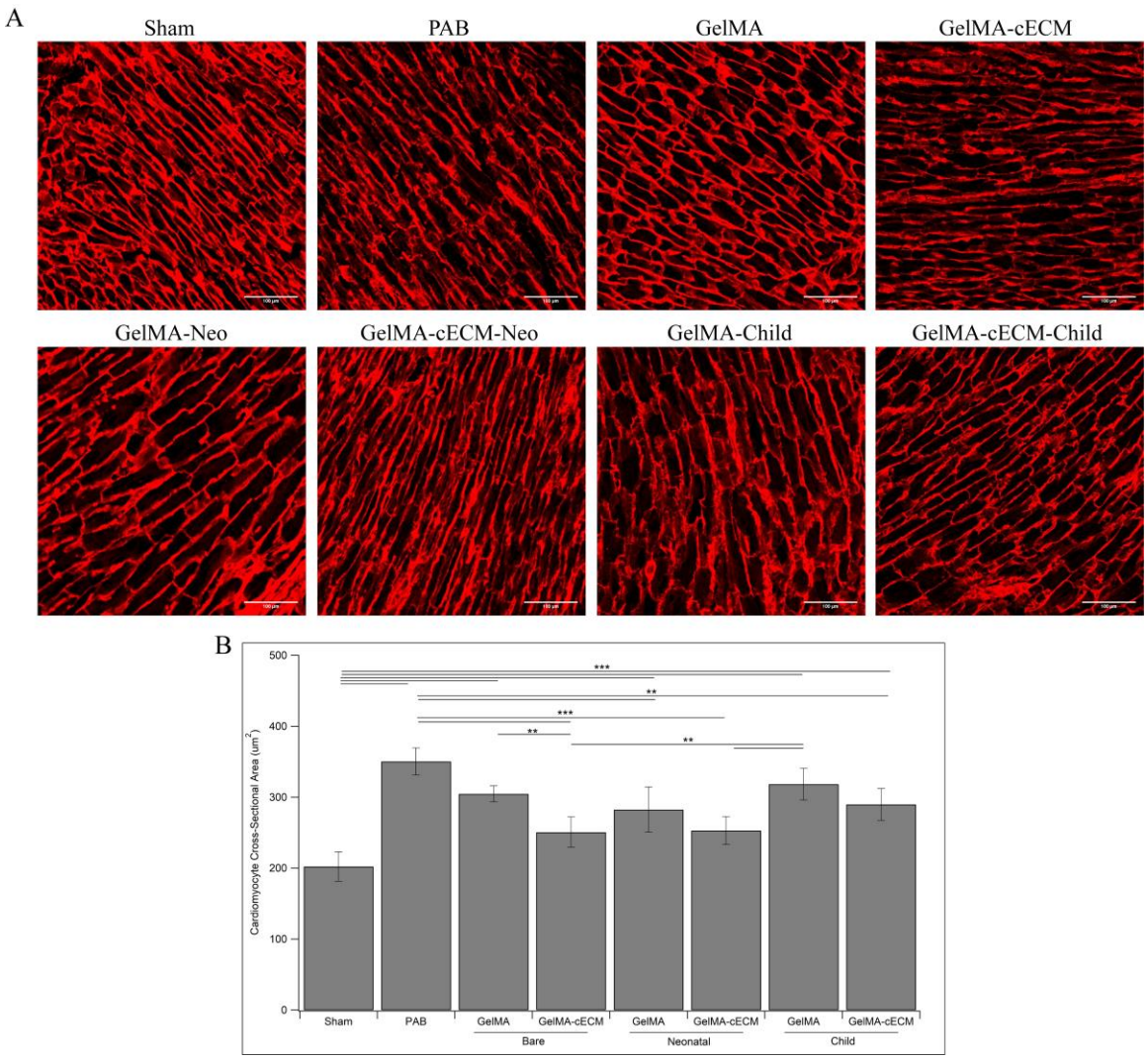

Figure 20 Cardiomyocyte Hypertrophy. A) Characteristic images of fluorescent signals from tissue sections stained with cardiomyocyte cell membrane-specific dye. Scale bar for all images is 200 μm. B) Quantified cardiomyocyte hypertrophy given as average cardiomyocyte cross-sectional area (um^2) in the RV. ** = p-value < 0.01, *** = p-value < 0.005, given by ANOVA with Tukey's post-test, n = 3 for all groups at all time-points.

Finally, RV free wall total fibrosis was evaluated across all groups to understand the therapeutic impact of patches towards tissue remodeling.[60,61] Fibrosis in RV dysfunction can result in contractile limitations and myofibroblast recruitment,

perpetuating a cycle of tissue damage leading to RV failure.[37-40] Analysis of fibrosis for all groups is seen in **Figure 21**, where **Figure 21A** shows characteristic images of hearts where fibrotic areas are indicated by darker sections, and **Figure 21B** shows quantified % fibrosis of the RV free wall across all groups. Similar to results seen in vessel density and cardiomyocyte hypertrophy across groups, PAB, neonatal hCPC-GelMA, and child hCPC-GelMA groups showed significantly higher fibrosis compared to Sham groups, reinforcing the ineffectiveness of GelMA patches in repairing the myocardium. However, these were no groups that showed improvements over PAB values, unlike vascularization and hypertrophy analysis, which showed that GelMA-cECM and neonatal hCPC-GelMA-cECM patches improved tissue remodeling. Also, GelMA-cECM patches decreased fibrosis compared to GelMA patches, and child hCPC-GelMA-cECM patches decreased fibrosis compared to child hCPC-GelMA patches. These combined results reinforce the findings that inclusion of cECM is a critical factor in developing improved therapy for treating heart failure, compared to pure GelMA patches. The improvement in fibrosis for child hCPC-GelMA-cECM groups over child hCPC-GelMA groups reinforces the results seen in TAPSE improvements for child hCPC-GelMA-cECM patches, where there were functional improvements over child hCPC-GelMA patches. This trend in terms of fibrosis was not seen for neonatal hCPC-GelMA-cECM and neonatal hCPC-GelMA patches. The effect of cECM on child cells was strongest in terms of cardiac TAPSE repair, which was mirrored only in fibrosis reduction at the tissue level. Additionally, the local vessel density data indicated that the child hCPCs maybe remodeling cECM within patches. These combined results indicate that the inclusion of cECM may be required to improve cardiac

functionality when implanting child cell-laden patches, where the effect of cECM inclusion on child hCPCs may be targeting hCPC remodeling factor release.

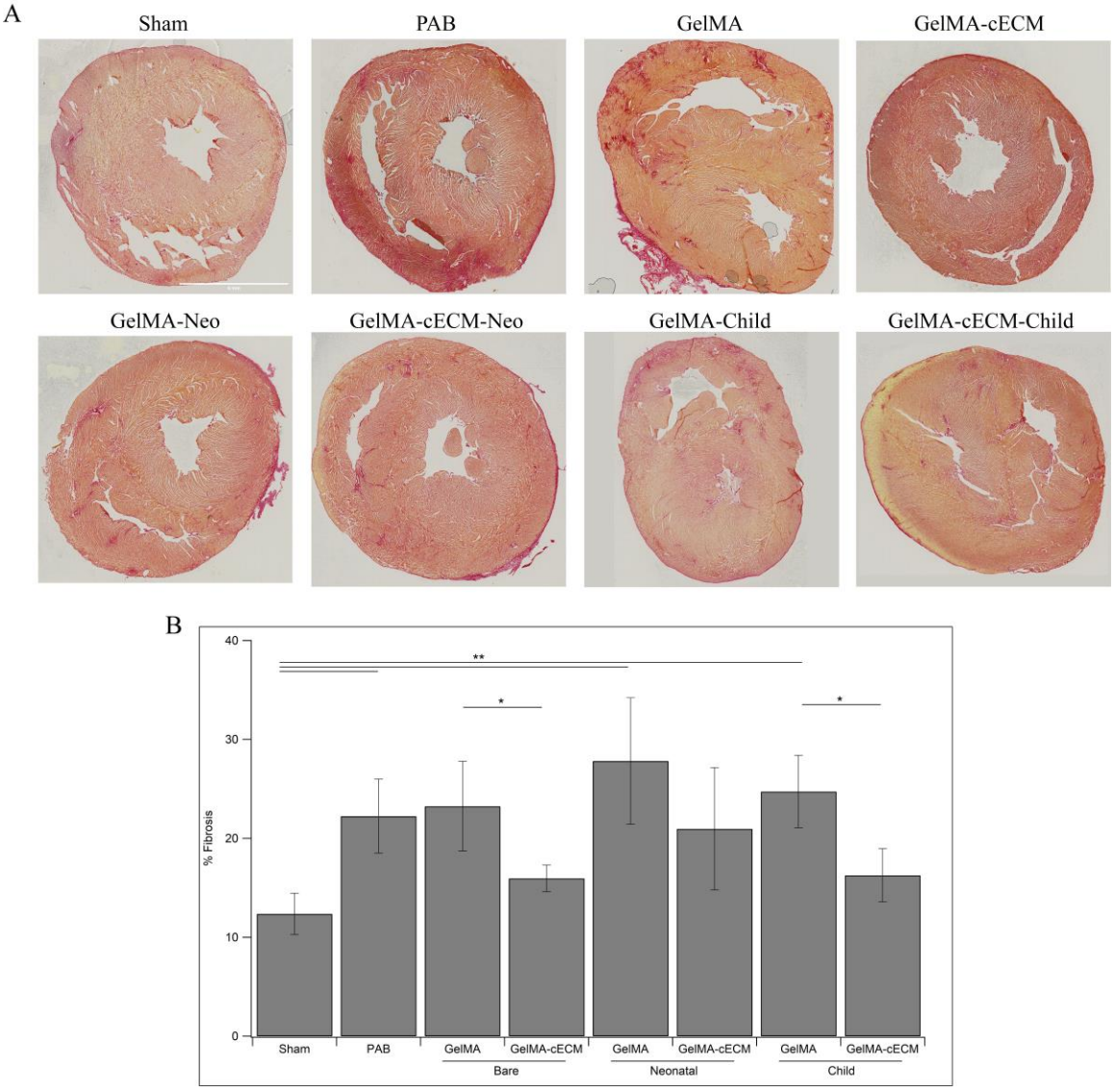

Figure 21 Tissue Fibrosis. A) Characteristic images of tissue sections stained with collagen density/fibrosis-specific dye. Scale bar for all images is set in the Sham image. Scale bar is 4 mm. B) Quantified tissue fibrosis given as % fibrosis of the RV free wall. * = p-value

< 0.05, ** = p-value < 0.01, given by ANOVA with Tukey's post-test, n = 3 for all groups at all time-points.

Overall, tissue analysis of rat hearts after four weeks of therapy showed differences between test groups and controls in improvements to vasculature formation, reduction in cardiomyocyte hypertrophy, and reduction in cardiac fibrosis. Of all groups, only bare GelMA-cECM and neonatal hCPC-GelMA-cECM patches showed increased vasculature formation and decreased cardiomyocyte hypertrophy over PAB values, with no significant differences compared to Sham values. Both bare GelMA-cECM and neonatal hCPC-GelMA-cECM patches showed tissue-level improvements over GelMA groups, such as significance over neonatal hCPC-GelMA in regards to improved vascularization, bare GelMA and child hCPC-GelMA in regards to reduced myocyte hypertrophy, and bare GelMA in regards to reduced cardiac fibrosis. Additionally, cECM-laden patches overall were the only patches that showed tissue level improvements over controls compared to the GelMA groups (which showed no improvements), showing significant repair across all assessment methods (vasculature, cardiomyocyte hypertrophy, and fibrosis). These results point towards cECM inclusion being a critical factor for tissue level remodeling in the developed biomaterial-cellular patches. There were no significant differences between bare or cell-incorporated patches across vascularization, hypertrophy, or fibrosis analysis for within either GelMA or cECM groups, although child cells trended towards having less reparative potential then neonatal cells within patches. One consideration for the tissue level differences between child hCPC-GelMA-cECM and neonatal hCPC-GelMA-cECM patches, although both included cECM, could be that child cells reduce the reparative impact of cECM components by more readily modifying and interacting with the cECM

than neonatal cells. Child cells may also be less secretory and focused on survival compared to neonatal cells, reducing their therapeutic potential. This is indicated by a reduction in fibrosis through secretion of pro-remodeling factors, which may be linked to a drive for proliferation and transition through the tissue. In contrast, the only comparisons between the neonatal patches in terms of tissue-level remodeling was an improvement in vessel density with the inclusion of cECM, indicating that the neonatal and child hCPCs are either responding differently to cECM or have inherent differences in therapeutic potential. Similar to results seen in chapter 5, initial hypoxic conditions in patches pre-vascularization may explain the initial improvements in TAPSE in child hCPC-GelMA-cECM patches, without longer-term tissue improvements at four weeks post-implantation. Regardless, the inclusion of cECM was required to show improved cardiac functionality in child cell-laden patches specifically.

6.4 Conclusion

The *in vivo* assessment of bioprinted hCPC-GelMA-cECM patches in a clinically relevant model of pediatric heart failure was investigated in terms of cardiac functional and tissue-level remodeling effects. First, the surgical attachment method of cardiac patches was assessed in healthy rats. Printed GelMA-cECM patches were effectively attached to rat hearts epicardially through suturing methods, remained on the hearts for 14 days, and showed patch vascularization in healthy animals. For analysis of patch therapeutic potential, a juvenile rat model of RV failure generated through PAB banding was used to establish a clinically relevant heart failure condition. RV failure is characterized by decreased RV function, given by echocardiographic measurements (TAPSE, EDD, ESD, RA-Area), and tissue level effects such as decreased vessel density, increased

cardiomyocyte hypertrophy, and increased fibrosis. Patches across different biomaterial and cell types were implanted onto the failing RV of PAB rats. Test groups included Sham controls, PAB controls that did not receive patches, bare GelMA patches, bare GelMA-cECM patches, neonatal hCPC-GelMA patches, neonatal hCPC-GelMA-cECM patches, child hCPC-GelMA patches, and child hCPC-GelMA-cECM patches. Rats were followed by echocardiographic measurement and *in vivo* fluorescent imaging over four weeks of therapy post-implantation, followed by heart explanation and tissue analysis.

Several key questions must be evaluated in the context of patch therapy. Do bioprinted cardiac patches show effective cell retention compared to studies using injectable hCPCs? Do any patch groups results in RV repair, characterized as significant differences compared to PAB control results without significant differences compared to Sham control results across analysis methods? Does the inclusion of cECM within GelMA patches improve cardiac outcomes compared to GelMA patches alone, across cell groups? Does the inclusion of cells improve cardiac outcomes compared to bare patches, across material types? Finally, does the inclusion of cECM result in different cardiac outcomes when comparing GelMA and GelMA-cECM patches within patches employing cells of the same cell age classification?

The findings of this work provide answers to these questions that can be summarized in several key results. First, patches across all cell ages and biomaterial types showed consistent and complete retention of cells during the timeframe of therapy, compared to 0-30% retention seen in studies that employ cell injection. There were no significant differences in retention across cell types and biomaterial groups, showing that

cell retention was not an additional variable required to analyze patch-related cardiac functional outcomes.

Both cardiac function and tissue-level remodeling were repaired with implantation of neonatal hCPC-GelMA-cECM patches compared to all other groups relative to controls. Additionally, bare GelMA-cECM patches showed effectiveness in repairing tissue properties (improved vascularization, reduced cardiomyocyte hypertrophy, and reduced cardiac fibrosis) and some cardiac functional changes (EDD and ESD). These results point towards both neonatal hCPC-GelMA-cECM and GelMA-cECM patches being effective for cardiac repair, although bare GelMA-cECM patches may be more valuable in terms of translation without the need for inclusion of primary human cells.

Incorporation of cECM into patches was necessary to facilitate cardiac functional and tissue-level repair across all analysis methods and patch types (bare or cell-laden), compared to GelMA groups that saw very few changes compared to PAB controls. Also, bare and cell-laden GelMA-cECM patches showed directly significant tissue-level improvements over GelMA groups. These results point to cECM as the critical component in producing the therapeutic benefit of bioprinted hCPC-GelMA-cECM patches.

Inclusion of cells may not be required for cardiac functional improvements compared to bare patches in the case of cECM groups. While RV functional evaluation during therapy indicated that neonatal hCPC-GelMA-cECM and child hCPC-GelMA-cECM groups were the only patches to show TAPSE differences from PAB controls, bare GelMA-cECM patches showed improvements in many other analysis methods. While complete results point towards neonatal hCPC-GelMA-cECM patches being most effective

for cardiac repair, this effect may be minor compared to bare GelMA-cECM results and bare GelMA-cECM patches may be just as effective without the need for inclusion of primary human cells. In the case of GelMA groups, very little improvements over controls or within groups were seen with the inclusion of cells or bare patches. However, given that neonatal cell inclusion was needed to facilitate improvements for GelMA groups in regards to cardiac functional measurements, the inclusion of cells may improve therapy for pure GelMA patches, although this trend was not observed at the tissue–level.

Finally, cECM inclusion may induce substantial changes in child hCPCs compared to GelMA-cell groups. While the neonatal hCPC-GelMA-cECM patch group showed the highest degree of cardiac repair across all groups, there were fewer significant differences between neonatal hCPC-GelMA-cECM and neonatal hCPC-GelMA groups directly. Importantly, there was a significant improvement in vascularization at the tissue level for neonatal hCPC-GelMA-cECM patches compared to neonatal hCPC-GelMA patches. The effect of cECM on neonatal cell reparative potential may be primarily improving angiogenic effects, such as by releasing angiogenic cytokines over other cytokines, which is supported by both *in vitro* and *in vivo* results. For child cells, there was a clear improvement in cardiac function outcomes in terms of RV function and dimensions in the child hCPC-GelMA-cECM group, while the child hCPC-GelMA group saw few improvements in cardiac function across analysis methods. In regards to tissue level effects, child hCPC-GelMA-cECM patches significantly reduced cardiac fibrosis compared to child hCPC-GelMA patches, indicating that the effect of cECM inclusion on child hCPCs may be targeting remodeling factors. Although there were no significant differences in child hCPC-GelMA-cECM and child hCPC-GelMA groups in terms of

vascularization or hypertrophy, there was a trend towards reduced cardiomyocyte hypertrophy in the child hCPC-GelMA-cECM group compared to the child hCPC-GelMA group. The effect of cECM on child cells was strongest in terms of cardiac functional repair, which was mirrored only in fibrosis reduction at the tissue level. These combined results indicate that the inclusion of cECM may be required to improve cardiac functionality when implanting child cell-laden patches. Both child and neonatal hCPC-GelMA-cECM patches saw improved TAPSE over PAB values during therapy, but at different times (week 2 vs. week 4). While the reparative improvements of neonatal hCPC-GelMA-cECM patches were carried through tissue analysis, the effect of child hCPC-GelMA-cECM patches was only evident in cardiac functional measurements and fibrosis reduction. However, when comparing child or neonatal hCPC tissue-level effects of cECM-laden vs. pure GelMA patches, there is a clear difference in therapeutic direction. Neonatal cells showed an enhanced angiogenic effect, both *in vitro* and *in vivo*, when cECM was included in patches compared to neonatal hCPC-GelMA. Alternatively, child hCPCs showed an enhanced ability to reduce fibrosis *in vivo* when cECM was included in patches compared to child hCPC-GelMA, with potential cECM remodeling within patches themselves. These differences may elucidate the effects of cECM in addition to intrinsic differences in therapeutic benefit between cells of different ages, with neonatal cells enhancing angiogenesis and child cells reducing fibrotic remodeling. These differences may be elucidated with additional studies.

Altogether, the *in vivo* analysis of bioprinted hCPC-GelMA-cECM patches provides two key conclusions. The first is that acellular GelMA-cECM patches and neonatal hCPC-GelMA-cECM patches are equally effective in treating RV failure, both in

terms of functional and tissue improvements over PAB controls, and in comparison to cECM-free GelMA patches, regardless of cell type. The second is that for child hCPCs specifically, the inclusion of cECM within patches results in enhanced child cell therapeutic potential, compared to child hCPC-GelMA patches alone. The overlap between these findings is that cECM is the strongest modulator of patch therapeutic improvements. These findings point towards the use of GelMA-cECM patches as effective therapies in treating pediatric RV failure. Potentially, loading the patches with pro-reparative factors, such as exosomes or growth factor cocktails, will provide an even more effective treatment of RV failure towards reaching functional improvements that closely match Sham values. Also, autologous hCPC therapy using hCPCs derived from child patients may be further improved by the incorporation of cECM, either in patch form or in combined cECM-hCPC injectable therapy. It is important to note that while there were several methods of analysis employed in this work, additional tissue-level effects that were not measured could provide differing conclusions. These methods include analyzing cardiomyocyte proliferation, myofibroblast activation, macrophage phenotype and activation, and endogenous progenitor recruitment, and provide interesting future experiments to understand the *in vivo* effect of bare and cell-laden GelMA-cECM patches.[231,232] Future directions on patch improvements towards therapy will be discussed further in chapter 7.

CHAPTER 7. CONCLUSIONS AND FUTURE DIRECTIONS

This project involves the development and therapeutic assessment of bioprinted hCPC-GelMA-cECM cardiac patches for the treatment of pediatric RV failure. In chapter 4, a bioprinting methodology was developed to manufacture cardiac patches. The inclusion of 5% w/v GelMA allowed for printability of the hCPC/cECM bioink through GelMA polymerization via cooling to 10^0C, followed by white light radical polymerization and incubation at physiological temperatures. The inclusion of cECM allowed for improved printability over pure GelMA bioinks, and the hCPC laden GelMA-cECM bioinks showed homogeneous distribution of cells and matrix. hCPCs remained highly viable and proliferative within the patch up to seven days, and hCPCs in GelMA-cECM patches had improved differentiation and angiogenic potential over pure GelMA patches, indicating their improved reparative functionality. The inclusion of cECM resulted in patches with a mechanical modulus that was similar to that of native myocardium, and all patches were sufficiently hydrated. Patches did not significantly degrade over 21 days when tested *in vitro* through weight change and rheological analysis. Also, hCPC-laden GelMA-cECM patches showed increased stiffness over 21 days when cultured in cFB conditioned media, indicating potential remodeling and retention *in vivo.* The printing of native ECM is difficult to perform at concentrations that can be realistically used and support cell functions. The concentration of cECM used here is similar to previous studies performed in our laboratory and by others that support CPC differentiation and function. Additionally, all materials used in this study are clinically relevant, as both cECM and hCPCs are in clinical testing alone. Thus the idea of a patient-specific, 3D printed patch is of great

translational value. Altogether, printability was achieved, and *in vitro* cellular functionality was assessed to be potentially effective for cardiac therapy for the following studies.

In chapter 5, we evaluated additional modifications in patch parameters, including the incorporation of increased amounts of pro-regenerative ECM components, evaluation with child hCPCs, and growth in hypoxic environments, to improve the paracrine factor release by inducing modulations in hCPC function for a bottom-up, modular approach to tissue engineering. Neonatal hCPCs did not see significant changes in cellular function towards improved therapeutic improvements, related to proliferation, differentiation, and angiogenic paracrine potential, when cultured on fetal modified cECM or hypoxic growth conditions. While there were limitations on types and sources of ECM proteins that could be added to the fetal cECM formulation due to bioprinting requirements, results showed that pure cECM might be the strongest modulator for improving hCPC therapeutic potential. Child hCPCs, which represent an important cell population to allow for autologous cell therapy in child patients, showed significant improvements in angiogenic paracrine potential when grown in hypoxic growth conditions compared to normoxic conditions. While neonatal hCPCs are derived from hypoxic tissue immediately after birth, child hCPCs are derived from patients of ages 2-5, representing a normoxic tissue environment before isolation. These differences in tissue condition may explain the improved function of child hCPCs in a new hypoxic environment compared to neonatal hCPCs. Within hypoxic GelMA-cECM gels, child hCPCs showed increased proliferation and angiogenic paracrine potential in GelMA-cECM materials grown in hypoxia, compared to growth in GelMA and normoxia. These results point towards the combined effect of cECM and hypoxic growth on improved therapeutic outcomes of child hCPCs.

Both 2D and 3D investigation of child hCPCs grown within GelMA-cECM materials in hypoxia pointed towards the use of combined methods to enhance the therapeutic potential of autologous cell therapy. While *in vitro* analysis indicated that both hypoxia and cECM conclusion were needed to improve the benefit of child hCPCs, implanted patches experience a highly hypoxic environment due to lack of nutrients from cell culture and vascularization that would normally supply oxygen to tissue. Therefore, therapeutic applications of patches into the hypoxic *in vivo* environment allow for hypoxic growth without the need for *in vitro* hypoxia before implantation.

Finally, the *in vivo* assessment of bioprinted hCPC-GelMA-cECM patches in a clinically relevant model of pediatric heart failure was investigated in terms of cardiac functional and tissue-level remodeling effects. Printed GelMA-cECM patches were effectively attached to rat hearts epicardially through suturing methods, remained on the hearts for 14 days, and showed patch vascularization in healthy animals. For analysis of patch therapeutic potential, a juvenile rat model of RV failure generated through PAB banding was used to establish a clinically relevant heart failure condition, characterized by decreased RV function, decreased vessel density, increased cardiomyocyte hypertrophy, and increased fibrosis. Patches across different biomaterial and cell types were implanted onto the failing RV of PAB rats. Test groups included Sham controls, PAB controls that did not receive patches, bare GelMA patches, bare GelMA-cECM patches, neonatal hCPC-GelMA patches, neonatal hCPC-GelMA-cECM patches, child hCPC-GelMA patches, and child hCPC-GelMA-cECM patches. Patches across all cell ages and biomaterial types showed consistent and complete retention of cells during the timeframe of therapy, indicated by both *in vivo* imaging and excised heart tissue analysis, compared to 0-30%

retention seen in studies that employ cell injection. Both cardiac function and tissue-level remodeling were improved with the implantation of neonatal hCPC-GelMA-cECM patches compared to controls. Additionally, bare GelMA-cECM patches showed effectiveness in repairing tissue properties and cardiac functional changes. While both neonatal hCPC-GelMA-cECM and bare GelMA-cECM patches may be effective for cardiac repair, bare GelMA-cECM patches do not include primary human cells, making the use of bare GelMA-cECM patches a powerful and reproducible therapeutic technology. Incorporation of cECM into patches was necessary to facilitate cardiac functional and tissue-level repair across all analysis methods and patch types (bare or cell-laden), compared to GelMA groups and PAB controls. cECM inclusion may be the most critical component in producing therapeutic benefit in bioprinted hCPC-GelMA-cECM patches. Also, a comparison of cell-laden and bare patches showed that the inclusion of cells might not be required for cardiac functional improvements compared to bare patches in the case of GelMA-cECM groups. However, given that neonatal cell inclusion was needed to facilitate improvements for GelMA groups in regards to cardiac functional measurements, the inclusion of cells may improve therapeutic outcomes with pure GelMA patches. Finally, cECM inclusion may induce substantial changes in child hCPCs compared to child hCPCs in pure GelMA groups. Comparisons between neonatal hCPC laden patches, both with and without cECM incorporation, showed an improved RV vessel density from neonatal hCPC-GelMA-cECM patches compared to neonatal hCPC-GelMA patches, with no other significant comparative results across analysis methods. In contrast, child hCPC laden patches showed cardiac functional improvements and reduction in tissue fibrosis when cECM was incorporated into patches, compared to child hCPC-GelMA patches,

indicating that cECM may be a key modulator of child hCPCs. Altogether, the *in vivo* analysis of bioprinted hCPC-GelMA-cECM patches provides two key conclusions. The first is that acellular GelMA-cECM patches and neonatal hCPC-GelMA-cECM patches are equally effective in treating RV failure, both in terms of functional and tissue improvements over PAB controls, and in comparison to cECM-free GelMA patches, regardless of cell type. The second is that for child hCPCs specifically, the inclusion of cECM within patches results in enhanced child cell therapeutic potential, compared to child hCPC-GelMA patches alone. The overlap between these findings is that cECM is the strongest modulator of patch therapeutic improvements in a model of RV failure. These findings point towards the use of bioprinted GelMA-cECM patches as effective and reproducible therapies in treating pediatric RV failure, paving the way for larger-scale animal models and human clinical trials using the technology. Additional tissue level analysis (such as cardiomyocyte proliferation, myofibroblast activation, and macrophage phenotype and activation) may provide interesting future experiments to understand the *in vivo* effect of bare and cell-laden GelMA-cECM patches.

Future directions include improving allogeneic and autologous hCPC-GelMA-cECM patch therapy, improving patch therapeutic potential through the incorporation of non-cellular components, and clinical investigations of patch therapy overall.

Primary cells, and even established cell lines, are highly heterogonous living organisms that can be difficult to develop into reliable and reproducible tools for therapy.[232] Investigations into effective cell manufacturing methods for reproducible lots and devices are ongoing and present a powerful method of generating consistent devices when coupled with bioprinting methods.[232,233] Additionally, methods of computational

and genomic analysis are being developed to understand which patient-derived cell lines are most effective for therapeutic applications.[59,60,62] Identification of optimal cell lines, efficient cellular manufacturing, and reproducible device production through bioprinting can help create reproducible and reliable allogeneic cell therapy, which can be applied to a wide range of patients. Many studies on cell therapy show the benefit of autologous cell transplantation, providing patient-specific cellular support towards RV repair.[6-9,11,60-64] While neonatal hCPCs may only require cellular injection within biomaterials, the results of this study show that non-reparative child hCPCs can be modulated by cECM materials to improve therapeutic potential. Further modulation of child hCPC function within patches, such as by employing previously designed methods of hCPC spheroid formation or electrical stimulation, can allow for even more effective enhancements in patch function, improving the aspects of child hCPC-patch function that were lacking in this work (cardiac functional, angiogenic, and hypertrophic improvements).[60,61] In another direction, studies are also showing that allogeneic cells maybe even more effective in repairing the myocardium compared to autologous sources, when cell lines and sourcing from patients are not optimized.[234,235] While this debate is ongoing, GelMA-cECM patches can be easily modified to employ allogeneic cells or incorporate different cell types such as MSCs. MSCs are powerful cells that rely on paracrine factor release to drive therapeutic outcomes.[169,171,173-177] MSCs are moving towards more robust cellular manufacturing then primary stem cells like hCPCs, while also potentially being more secretory.[232,233] The use of MSCs and other paracrine factor releasing allogeneic cell sources may provide an even more powerful tool in improving the therapeutic potential of GelMA-cECM patches, along with additional modulation such as cell clustering or electrical stimulation.

A critical finding of this work is that acellular GelMA-cECM patches are just as effective as cell-laden GelMA-cECM patches in treating RV failure. While alternate cellular modulation and sourcing may produce more effective cardiac patches, acellular patches may be just as effective, or more effective, with the inclusion of both cECM and bioactive soluble factors. hCPCs were laden in GelMA-cECM patches in this work to employ the therapeutic ability of hCPCs, driven by the release of reparative cytokines, chemokines, growth factors, and exosomes, rather than direct differentiation and integration of implanted hCPCs within the myocardium.[11,15] A key reason why hCPCs were chosen over simply loading patches with GFs such as VEGF is that healthy cells produce a wide variety of GFs, exosomes, MMPs, and additional paracrine signals that would be difficult and expensive to recapitulate with purified paracrine components alone.[11,15] These factors induce tissue remodeling, reduce inflammation, enhance angiogenesis *in vivo*, and modulate stem cell response based on multiple GF concentrations.[11,15,236] However, several recent studies have pointed to one specific paracrine factor, exosomes, as a powerful therapeutic tool for repairing the myocardium.[62,63,170,237] Exosomes are extracellular vesicles generated by cells in small quantities, containing a variety of pro-reparative and cell-modulating factors such as miRNAs. Exosomes may be more beneficial then GF treatment, as exosomes show cardiac-specific induction of repair through direct cellular phenotypic modification.[170,237] Studies in our lab and others have shown that hCPC exosomes, rather than cells themselves, maybe a more effective and reproducible tool in cardiac therapy.[62,63] Also, there are problems with sourcing and conditioning of hCPCs that may be difficult to optimize for therapy, as discussed in the previous paragraph. Other studies have shown that acellular cECM is a

powerful tool in cardiac therapies for adults, which is reinforced in our current work by showing that inclusion of cECM, not cells, is the key factor that induced the therapeutic benefit of GelMA-cECM patches.[81,152,180] Loading GelMA-cECM patches with exosomes would replace the function of hCPCs within patches, by generating a patch that allows for the sustained and controllable release of exosomes at higher concentrations than would be produced by cells, in addition to therapeutic benefits of GelMA-cECM patches themselves. A bioprinting methodology can be easily employed to tailor loading extent and device properties. Additionally, dECM scaffold components contain high degrees of functional sites that bind GFs to sequester factors and modulate release rates, which would otherwise need to be tailored through functionalization in synthetic or non-ECM based materials. Specifically, cECM hydrogels have been shown to retain and gradually release growth factors when injected *in vivo*, promoting heart repair in models for adult cardiac dysfunction.[218,219] A combined exosome-GelMA-cECM patch may significantly improve patch therapeutic potential by using reproducible exosomes rather than heterogeneous primary stem cells, where exosomes at high concentrations may have a stronger impact then cellular paracrine release.

Improved cell sourcing, manufacturing, and optimization, additional cellular modulation, and exosome loading of GelMA-cECM patches may produce substantial improvements to the therapeutic potential of hCPC-GelMA-cECM patches compared to the results seen in this work. However, the improvements to RV function and tissue-level properties seen in chapter 6 pave the way for the translation of patches towards the clinic. The next steps in device evaluation can include the treatment of large animal models of RV failure as preclinical assessments of bare and cell-laden GelMA-cECM patches towards

pediatric heart repair. If successful, clinical trials of safety, efficacy, and ultimate implementation of patches in treating pediatric patients can be undertaken. GelMA-cECM patches may provide effective therapy for decreasing the mortality rate and improving the quality of life for the many pediatric patients suffering from RV dysfunction and failure.

REFERENCES

[1] J. W. Rossano, J. J. Kim, J. A. Decker, J. F. Price, F. Zafar, D. E. Graves, D. L. Morales, J. S. Heinle, B. Bozkurt, S. W. Denfield, *Circulation*. **2010**, *122*, A1374.

[2] J.M. Robbins, T.M. Bird, J.M. Tilford, M.A. Cleves, C.A. Hobbs, S.D. Grosse, A. Correa, *MMWR*. **2007**, *56*, 25.

[3] E. L. Bove, *Pediatr. Cardiol.* **1998**, *19*, 308.

[4] V. F. Segers, R. T. Lee, *Nature* **2008**, *451*, 937.

[5] R. Bolli, A. R. Chugh, D. D'Amario, J. H. Loughran, M. F. Stoddard, S. Ikram, G. M. Beache, S. G. Wagner, A. Leri, T. Hosoda, *The Lancet* **2011**, *378*, 1847.

[6] R. R. Makkar, R. R. Smith, K. Cheng, K. Malliaras, L. E. Thomson, D. Berman, L. S. Czer, L. Marbán, A. Mendizabal, P. V. Johnston, *The Lancet* **2012**, *379*, 895.

[7] S. Ishigami, S. Ohtsuki, S. Tarui, D. Ousaka, T. Eitoku, M. Kondo, M. Okuyama, J. Kobayashi, K. Baba, S. Arai, *Circ. Res.* **2014**, *116*, 653.

[8] H. M. Burkhart, M. Y. Qureshi, S. C. Peral, P. W. O'leary, T. M. Olson, F. Cetta, T. J. Nelson, *J. Thorac. Cardiov. Sur.* **2015**, *149*, e35.

[9] U. Agarwal, A. W. Smith, K. M. French, A. V. Boopathy, A. George, D. Trac, M. E. Brown, M. Shen, R. Jiang, J. D. Fernandez, *Stem Cell Transl. Med.* **2016**, *5*, 883.

[10] L. Ye, W.-H. Zimmermann, D. J. Garry, J. Zhang, *Circ. Res.* **2013**, 113, 922.

[11] D. A. Feyen, R. Gaetani, P. A. Doevendans, J. P. Sluijter, *Adv. Drug Deliver. Rev.* **2016**, *106*, 104.

[12] E. Dawson, G. Mapili, K. Erickson, S. Taqvi, K. Roy, *Adv. Drug Deliver. Rev.* **2008**, *60*, 215.

[13] M. Lutolf, J. Hubbell, *Nat. Biotechnol.* **2005**, *23*, 47.

[14] E. T. Pashuck, M. M. Stevens, *Sci. Transl. Med.* **2012**, *4*, 160sr4.

[15] M. Gnecchi, Z. Zhang, A. Ni, V. J. Dzau, *Circ. Res.* **2008**, *103*, 1204.

[16] K. M. French, A. V. Boopathy, J. A. DeQuach, L. Chingozha, H. Lu, K. L. Christman, M. E. Davis, *Acta Biomater.* **2012**, *8*, 4357.

[17] K. M. French, J. T. Maxwell, S. Bhutani, S. Ghosh-Choudhary, M. J. Fierro, T. D. Johnson, K. L. Christman, W. R. Taylor, M. E. Davis, *Stem Cell Transl. Med.* **2016**.

[18] J. M. Singelyn, J. A. DeQuach, S. B. Seif-Naraghi, R. B. Littlefield, P. J. Schup-Magoffin, K. L. Christman, *Biomaterials* **2009**, *30*, 5409.

[19] J. W. Wassenaar, R. Gaetani, J. J. Garcia, R. L. Braden, C. G. Luo, D. Huang, A. N. DeMaria, J. H. Omens, K. L. Christman, *J. Am. Coll. Cardiol.* **2016**, *67*, 1074.

[20] R. Gaetani, C. Yin, N. Srikumar, R. Braden, P. A. Doevendans, J. P. Sluijter, K. L. Christman, *Cell Transplant.* **2016**, *25*, 1653.

[21] G. Agmon, K. L. Christman, *Curr. Opin. Solid St. M.* **2016**, *20*, 193.

[22] L. Yu, J. Ding, *Chem. Soc. Rev.* **2008**, *37*, 1473.

[23] B. Duan, *Ann. Biomed. Eng.* **2017**, *45*, 195.

[24] S. Kyle, Z. M. Jessop, A. Al-Sabah, I. S. Whitaker, *Adv. Healthc. Mater.* **2017**, *16*.

[25] S. V. Murphy, A. Skardal, A. Atala, *J. Biomed. Mater. Res. A* **2013**, *101*, 272.

[26] F. Pati, J. Jang, D.-H. Ha, S. W. Kim, J.-W. Rhie, J.-H. Shim, D.-H. Kim, D.-W. Cho, *Nat. Commun.* **2014**, *5*, 3935.

[27] J. Jang, T. G. Kim, B. S. Kim, S.-W. Kim, S.-M. Kwon, D.-W. Cho, *Acta Biomater.* **2016**, *33*, 88.

[28] S. Huang, B. Yao, J. Xie, X. Fu, *Acta Biomater.* **2016**, *32*, 170.

[29] B. Xu, Y. Li, X. Fang, G. A. Thouas, W. D. Cook, D. F. Newgreen, Q. Chen, *J. Mech. Behav. Biomed.* **2013**, *28*, 354.

[30] Y. Efraim, H. Sarig, N. C. Anavy, U. Sarig, E. de Berardinis, S.-Y. Chaw, M. Krishnamoorthi, J. Kalifa, H. Bogireddi, T. V. Duc, *Acta Biomater.* **2017**, *50*, 220.

[31] S. Pok, O. M. Benavides, P. Hallal, J. G. Jacot, *Tissue Eng. Pt. A* **2014**, *20*, 1877.

[32] T. van der Bom, B. J. Bouma, F. J. Meijboom, A. H. Zwinderman, B. J. Mulder, *American heart journal* **2012**, 164, 568.

[33] D. van der Linde, E. E. Konings, M. A. Slager, M. Witsenburg, W. A. Helbing, J. J. Takkenberg, J. W. Roos-Hesselink, *Journal of the American College of Cardiology* **2011**, 58, 2241.

[34] A. Green, *Pediatric nursing* **2004**, 30.

[35] A. U. Tikkanen, A. R. Oyaga, O. A. Riano, E. M. Alvaro, J. Rhodes, *Cardiology in the young* **2012**, 22, 241.

[36] B. S. Marino, P. H. Lipkin, J. W. Newburger, G. Peacock, M. Gerdes, J. W. Gaynor, K. A. Mussatto, K. Uzark, C. S. Goldberg, W. H. Johnson Jr, *Circulation* **2012**, 126, 1143.

[37] S. A. Mandras, S. Desai, in *StatPearls [Internet]*, StatPearls Publishing **2019**.

[38] S. Reddy, D. Bernstein, *Circulation* **2015**, 132, 1734.

[39] C. R. Greyson, *Critical care medicine* **2008**, 36, S57.

[40] M. Ma, K. Gauvreau, C. K. Allan, J. E. Mayer Jr, K. J. Jenkins, *The Annals of thoracic surgery* **2007**, 83, 1438.

[41] S. P. Marathe, S. Talwar, *Annals of pediatric cardiology* **2015**, 8, 122.

[42] K. K. Stout, C. J. Daniels, J. A. Aboulhosn, B. Bozkurt, C. S. Broberg, J. M. Colman, S. R. Crumb, J. A. Dearani, S. Fuller, M. Gurvitz, *Journal of the American*

College of Cardiology **2018**.

[43] R. Kirk, A. I. Dipchand, L. B. Edwards, A. Y. Kucheryavaya, C. Benden, J. D. Christie, F. Dobbles, A. O. Rahmel, J. Stehlik, M. I. Hertz, *Journal of Heart and Lung Transplantation* **2012**, 31, 1065.

[44] B. Alsoufi, S. Deshpande, C. McCracken, B. Kogon, R. Vincent, W. Mahle, K. Kanter, *The Journal of thoracic and cardiovascular surgery* **2015**, 150, 1455.

[45] J. W. Cheng, M. Nayar, *The American journal of geriatric pharmacotherapy* **2009**, 7, 233.

[46] S. M. Wu, K. R. Chien, C. Mummery, *Cell* **2008**, 132, 537.

[47] T. Le, J. Chong, *Cell death discovery* **2016**, 2, 16052.

[48] C.-L. Cai, J. D. Molkentin, *Circulation research* **2017**, 120, 400.

[49] M. Valente, D. S. Nascimento, A. Cumano, P. Pinto-Do-Ó, *Stem cells and development* **2014**, 23, 2263.

[50] J. H. Van Berlo, O. Kanisicak, M. Maillet, R. J. Vagnozzi, J. Karch, S.-C. J. Lin, R. C. Middleton, E. Marbán, J. D. Molkentin, *Nature* **2014**, 509, 337.

[51] X.-L. Tang, Q. Li, G. Rokosh, S. K. Sanganalmath, N. Chen, Q. Ou, H. Stowers, G. Hunt, R. Bolli, *Circulation research* **2016**, 118, 1091.

[52] V. Bianconi, A. Sahebkar, P. Kovanen, F. Bagaglia, B. Ricciuti, P. Calabrò, G. Patti, M. Pirro, *Pharmacology & therapeutics* **2018**, 181, 156.

[53] J. Ye, Y. Yeghiazarians, *Journal of cardiovascular pharmacology* **2014**, 63, 85.

[54] R. E. Ahmed, T. Anzai, N. Chanthra, H. Uosaki, *Frontiers in Cell and Developmental Biology* **2020**, 8, 178.

[55] H. Hashimoto, E. N. Olson, R. Bassel-Duby, *Nature Reviews Cardiology* **2018**, 15, 585.

[56] P. K. Nguyen, J.-W. Rhee, J. C. Wu, *JAMA cardiology* **2016**, 1, 831.

[57] S. Ishigami, S. Ohtsuki, T. Eitoku, D. Ousaka, M. Kondo, Y. Kurita, K. Hirai, Y. Fukushima, K. Baba, T. Goto, *Circulation research* **2017**, 120, 1162.

[58] B. Özlek, E. Özlek, O. Çelik, C. Çil, V. Doğan, Ö. Başaran, M. Biteker, *American Journal of Cardiology* **2018**, 121, e60.

[59] V. N. S. Garikipati, F. Shoja-Taheri, M. E. Davis, R. Kishore, *Circulation research* **2018**, 123, 188.

[60] D. Trac, J. T. Maxwell, M. E. Brown, C. Xu, M. E. Davis, *Circulation research* **2019**, 124, 526.

[61] J. T. Maxwell, D. Trac, M. Shen, M. E. Brown, M. E. Davis, M. S. Chao, K. J. Supapannachart, C. A. Zaladonis, E. Baker, M. L. Li, *STEM CELLS* **2019**, 37, 1528.

[62] W. D. Gray, K. M. French, S. Ghosh-Choudhary, J. T. Maxwell, M. E. Brown, M. O. Platt, C. D. Searles, M. E. Davis, *Circulation research* **2015**, 116, 255.

[63] U. Agarwal, A. George, S. Bhutani, S. Ghosh-Choudhary, J. T. Maxwell, M. E. Brown, Y. Mehta, M. O. Platt, Y. Liang, S. Sahoo, *Circulation research* **2017**, 120, 701.

[64] M. Douglas-Escobar, M. D. Weiss, *JAMA pediatrics* **2015**, 169, 397.

[65] A. Mauretti, S. Spaans, N. A. Bax, C. Sahlgren, C. V. Bouten, *Stem cells international* **2017**, 2017.

[66] D. J. Ceradini, A. R. Kulkarni, M. J. Callaghan, O. M. Tepper, N. Bastidas, M. E. Kleinman, J. M. Capla, R. D. Galiano, J. P. Levine, G. C. Gurtner, *Nature medicine* **2004**, 10, 858.

[67] Y. L. Tang, W. Zhu, M. Cheng, L. Chen, J. Zhang, T. Sun, R. Kishore, M. I. Phillips, D. W. Losordo, G. Qin, *Circulation research* **2009**, 104, 1209.

[68] A. A. van Oorschot, A. M. Smits, E. Pardali, P. A. Doevendans, M. J. Goumans, *Journal of cellular and molecular medicine* **2011**, 15, 2723.

[69] D. Chen, Y. Xia, K. Zuo, Y. Wang, S. Zhang, D. Kuang, Y. Duan, X. Zhao, G. Wang, *Scientific reports* **2015**, 5, 1.

[70] S. Bhutani, A. L. Nachlas, M. E. Brown, T. Pete, C. T. Johnson, A. J. García, M. E. Davis, *ACS biomaterials science & engineering* **2018**, 4, 200.

[71] C. D. Waring, C. Vicinanza, A. Papalamprou, A. J. Smith, S. Purushothaman, D. F. Goldspink, B. Nadal-Ginard, D. Torella, G. M. Ellison, *European heart journal* **2014**, 35, 2722.

[72] M. Mochizuki, V. Lorenz, R. Ivanek, G. Della Verde, E. Gaudiello, A. Marsano, O. Pfister, G. M. Kuster, *Journal of the American Heart Association* **2017**, 6, e005920.

[73] C. Williams, E. Budina, W. L. Stoppel, K. E. Sullivan, S. Emani, S. M. Emani, L. D. Black III, *Acta biomaterialia* **2015**, 14, 84.

[74] M. H. Konstandin, H. Toko, G. M. Gastelum, P. Quijada, A. De La Torre, M. Quintana, B. Collins, S. Din, D. Avitabile, M. Völkers, *Circulation research* **2013**, 113, 115.

[75] A. Mauretti, N. A. Bax, M. H. van Marion, M. J. Goumans, C. Sahlgren, C. V. Bouten, *Integrative Biology* **2016**, 8, 991.

[76] R. Gaetani, D. A. Feyen, V. Verhage, R. Slaats, E. Messina, K. L. Christman, A. Giacomello, P. A. Doevendans, J. P. Sluijter, *Biomaterials* **2015**, 61, 339.

[77] K. Cheng, A. Blusztajn, D. Shen, T.-S. Li, B. Sun, G. Galang, T. I. Zarembinski, G. D. Prestwich, E. Marbán, R. R. Smith, *Biomaterials* **2012**, 33, 5317.

[78] A. K. Jha, K. M. Tharp, S. Browne, J. Ye, A. Stahl, Y. Yeghiazarians, K. E. Healy, *Biomaterials* **2016**, 89, 136.

[79] A. E. Mayfield, E. L. Tilokee, N. Latham, B. McNeill, B.-K. Lam, M. Ruel, E. J. Suuronen, D. W. Courtman, D. J. Stewart, D. R. Davis, *Biomaterials* **2014**, 35, 133.

[80] M. H. van Marion, N. A. Bax, M. C. van Turnhout, A. Mauretti, D. W. van der Schaft, M. J. T. Goumans, C. V. Bouten, *Journal of molecular and cellular*

cardiology **2015**, 87, 79.

[81] D. Bejleri, M. E. Davis, *Advanced healthcare materials* **2019**, 8, 1801217.

[82] L. Gaffney, E. A. Wrona, D. O. Freytes, *ACS Biomater. Sci. Eng.* **2017**, *4*, 1208-1222.

[83] R. Mecham, *The extracellular matrix: an overview*, Springer Science & Business Media, **2011**.

[84] I. Valiente-Alandi, A. E. Schafer, B. C. Blaxall, *J. Mol. Cell. Cardiol.* **2016**, *91*, 228-237.

[85] B. S. Kim, H. Kim, G. Gao, J. Jang, D.-W. Cho, *Biofabrication* **2017**, *9*, 034104.

[86] T. D. Johnson, R. C. Hill, M. Dzieciatkowska, V. Nigam, A. Behfar, K. L. Christman, K. C. Hansen, *Proteomics: Clin. Appl.* **2016**, *10*, 75-83.

[87] M. Rienks, A.-P. Papageorgiou, N. G. Frangogiannis, S. Heymans, *Circ. Res.* **2014**, *114*, 872-888.

[88] C. Williams, L. D. Black, in *Biomaterials for Cardiac Regeneration*, Springer, **2015**, pp. 1-35.

[89] C. Williams, K. P. Quinn, I. Georgakoudi, L. D. Black III, *Acta Biomater.* **2014**, *10*, 194-204.

[90] A. Silva, S. Rodrigues, J. Caldeira, A. Nunes, V. Sampaio-Pinto, T. Resende, M. Oliveira, M. Barbosa, S. Thorsteinsdóttir, D. Nascimento, *Biomaterials* **2016**, *104*, 52-64.

[91] P. K. Mishra, S. Givvimani, V. Chavali, S. C. Tyagi, *Biochim. Biophys. Acta, Mol. Basis Dis.* **2013**, *1832*, 2271-2276.

[92] T. Bronshtein, G. C. T. Au-Yeung, U. Sarig, E. B.-V. Nguyen, P. S. Mhaisalkar, F. Y. C. Boey, S. S. Venkatraman, M. Machluf, *Tissue Eng., Part C* **2013**, *19*, 620-630.

[93] H. Wen, E. Bennett, N. Epstein, J. Plehn, *Magn. Reson. Med.* **2005**, *54*, 538-548.

[94] C. Pislaru, M. W. Urban, S. V. Pislaru, R. R. Kinnick, J. F. Greenleaf, *Ultrasound Med. Biol.* **2014**, *40*, 1785-1795.

[95] W. Hiesinger, M. J. Brukman, R. C. McCormick, J. R. Fitzpatrick III, J. R. Frederick, E. C. Yang, J. R. Muenzer, N. A. Marotta, M. F. Berry, P. Atluri, *J. Thorac. Cardiovasc. Surg.* **2012**, *143*, 962-966.

[96] D. N. Ghista, W. H. Vayo, H. Sandler, *Med. Biol. Eng.* **1975**, *13*, 151-161.

[97] M. R. Zile, C. F. Baicu, J. S. Ikonomidis, R. E. Stroud, P. J. Nietert, A. D. Bradshaw, R. Slater, B. M. Palmer, P. Van Buren, M. Meyer, *Circulation* **2015**, *131*, 1247-1259.

[98] K. E. Sullivan, K. P. Quinn, K. M. Tang, I. Georgakoudi, L. D. Black, *Stem Cell. Res. Ther.* **2014**, *5*, 14.

[99] J. R. Gershlak, J. I. Resnikoff, K. E. Sullivan, C. Williams, R. M. Wang, L. D. Black, *Biochem. Biophys. Res. Commun.* **2013**, *439*, 161-166.

[100] J. P. Cleutjens, E. E. Creemers, *J. Card. Fail.* **2002**, *8*, S344-S348.

[101] C. Bonnans, J. Chou, Z. Werb, *Nat. Rev. Mol. Cell Biol.***2014**, *15*, 786.

[102] H.-B. Kwak, *J. Exerc. Rehabil.* **2013**, *9*, 338.

[103] D. Fan, A. Takawale, J. Lee, Z. Kassiri, *Fibrog. Tissue Repair* **2012**, *5*, 15.

[104] F. G. Spinale, *Physiol. Rev.* **2007**, *87*, 1285-1342.

[105] Z. Kassiri, R. Khokha, *Thromb. Haemost.* **2005**, *94*, 212-219.

[106] C. M. Howard, T. A. Baudino, *J. Mol. Cell. Cardiol.* **2014**, *70*, 19-26.

[107] K. P. Quinn, K. E. Sullivan, Z. Liu, Z. Ballard, C. Siokatas, I. Georgakoudi, L. D.

Black, *Sci. Rep.* **2016**, *6*, 35823.

[108] M. T. Spang, K. L. Christman, *Acta Biomater.* **2017**.

[109] L. Ye, W.-H. Zimmermann, D. J. Garry, J. Zhang, *Circ. Res.* **2013**, *113*, 922-932.

[110] T. Ota, T. W. Gilbert, D. Schwartzman, C. F. McTiernan, T. Kitajima, Y. Ito, Y. Sawa, S. F. Badylak, M. A. Zenati, *J. Thorac. Cardiovasc. Surg.* **2008**, *136*, 1309-1317.

[111] B. Wang, A. Borazjani, M. Tahai, A. L. de Jongh Curry, D. T. Simionescu, J. Guan, F. To, S. H. Elder, J. Liao, *J. Biomed. Mater. Res., Part A* **2010**, *94*, 1100-1110.

[112] Z.-Q. Zhao, J. D. Puskas, D. Xu, N.-P. Wang, M. Mosunjac, R. A. Guyton, J. Vinten-Johansen, R. Matheny, *J. Am. Coll. Cardiol.* **2010**, *55*, 1250-1261.

[113] D. O. Freytes, J. Martin, S. S. Velankar, A. S. Lee, S. F. Badylak, *Biomaterials* **2008**, *29*, 1630-1637.

[114] H. C. Ott, T. S. Matthiesen, S.-K. Goh, L. D. Black, S. M. Kren, T. I. Netoff, D. A. Taylor, *Nat. Med.* **2008**, *14*, 213.

[115] S. F. Badylak, D. O. Freytes, T. W. Gilbert, *Acta Biomater.* **2009**, *5*, 1-13.

[116] S. B. Seif-Naraghi, D. Horn, P. A. Schup-Magoffin, M. M. Madani, K. L. Christman, *J. Cardiovasc. Transl. Res.* **2011**, *4*, 545.

[117] X. Hong, Y. Yuan, X. Sun, M. Zhou, G. Guo, Q. Zhang, J. Hescheler, J. Xi, *Cell. Physiol. Biochem.* **2018**, *45*, 319-331.

[118] S. Higuchi, Q. Lin, J. Wang, T. K. Lim, S. B. Joshi, G. S. Anand, M. C. Chung, M. P. Sheetz, H. Fujita, *J. Biosci. Bioeng.* **2013**, *115*, 320-325.

[119] I. Perea-Gil, C. Gálvez-Montón, C. Prat-Vidal, I. Jorba, C. Segú-Vergés, S. Roura, C. Soler-Botija, O. Iborra-Egea, E. Revuelta-López, M. A. Fernández, *Sci. Rep.* **2018**, *8*.

[120] J. A. DeQuach, V. Mezzano, A. Miglani, S. Lange, G. M. Keller, F. Sheikh, K. L. Christman, *PLoS One* **2010**, *5*, e13039.

[121] J. Ungerleider, T. Johnson, N. Rao, K. Christman, *Methods* **2015**, *84*, 53-59.

[122] M. Tabuchi, J. Negishi, A. Yamashita, T. Higami, A. Kishida, S. Funamoto, *Mater. Sci. Eng., C* **2015**, *56*, 494-500.

[123] N. Merna, K. M. Fung, J. J. Wang, C. R. King, K. C. Hansen, K. L. Christman, S. C. George, *Tissue Eng., Part A* **2015**, *21*, 2195-2205.

[124] T. D. Johnson, J. A. DeQuach, R. Gaetani, J. Ungerleider, D. Elhag, V. Nigam, A. Behfar, K. L. Christman, *Biomater. Sci.* **2014**, *2*, 735-744.

[125] D. A. Taylor, L. C. Sampaio, Z. Ferdous, A. S. Gobin, L. J. Taite, *Acta Biomater.* **2018**.

[126] N. Momtahan, S. Sukavaneshvar, B. L. Roeder, A. D. Cook, *Tissue Eng., Part B* **2014**, *21*, 115-132.

[127] C. Fidalgo, L. Iop, M. Sciro, M. Harder, D. Mavrilas, S. Korossis, A. Bagno, G. Palù, P. Aguiari, G. Gerosa, *Acta Biomater.* **2018**, *67*, 282-294.

[128] B. Crawford, S. T. Koshy, G. Jhamb, C. Woodford, C. M. Thompson, A. S. Levy, J. W. Rush, J. G. Guillemette, D. Lillicrap, E. Jervis, *Can. J. Chem. Eng.* **2012**, *90*, 1457-1464.

[129] Y. Eitan, U. Sarig, N. Dahan, M. Machluf, *Tissue Eng., Part C* **2009**, *16*, 671-683.

[130] S. Rajabi, S. Pahlavan, M. K. Ashtiani, H. Ansari, S. Abbasalizadeh, F. A. Sayahpour, F. Varzideh, S. Kostin, N. Aghdami, T. Braun, *Biomaterials* **2018**, *154*, 99-112.

[131] H. Yasui, J.-K. Lee, A. Yoshida, T. Yokoyama, H. Nakanishi, K. Miwa, A. T. Naito, T. Oka, H. Akazawa, J. Nakai, *Biomaterials* **2014**, *35*, 7839-7850.

[132] P. L. Sánchez, M. E. Fernández-Santos, S. Costanza, A. M. Climent, I. Moscoso, M. A. Gonzalez-Nicolas, R. Sanz-Ruiz, H. Rodríguez, S. M. Kren, G. Garrido,

Biomaterials **2015**, *61*, 279-289.

[133] E. Garreta, L. De Oñate, M. E. Fernández-Santos, R. Oria, C. Tarantino, A. M. Climent, A. Marco, M. Samitier, E. Martínez, M. Valls-Margarit, *Biomaterials* **2016**, *98*, 64-78.

[134] J. P. Guyette, J. M. Charest, R. W. Mills, B. J. Jank, P. T. Moser, S. E. Gilpin, J. R. Gershlak, T. Okamoto, G. Gonzalez, D. J. Milan, *Circ. Res.* **2016**, *118*, 56-72.

[135] B. Oberwallner, A. Brodarac, P. Anić, T. Šarić, K. Wassilew, K. Neef, Y.-H. Choi, C. Stamm, *Eur. J. Cardiothorac. Surg.* **2014**, *47*, 416-425.

[136] A. F. Godier-Furnémont, T. P. Martens, M. S. Koeckert, L. Wan, J. Parks, K. Arai, G. Zhang, B. Hudson, S. Homma, G. Vunjak-Novakovic, *Proc. Natl. Acad. Sci.* **2011**, *108*, 7974-7979.

[137] U. Sarig, E. B.-V. Nguyen, Y. Wang, S. Ting, T. Bronshtein, H. Sarig, N. Dahan, M. Gvirtz, S. Reuveny, S. K. Oh, *Tissue Eng., Part A* **2015**, *21*, 1507-1519.

[138] C. W. Chang, T. Petrie, A. Clark, X. Lin, C. S. Sondergaard, L. G. Griffiths, *PLoS One* **2016**, *11*, e0153412.

[139] Q. Wang, H. Yang, A. Bai, W. Jiang, X. Li, X. Wang, Y. Mao, C. Lu, R. Qian, F. Guo, *Biomaterials* **2016**, *105*, 52-65.

[140] U. Sarig, H. Sarig, A. Gora, M. K. Krishnamoorthi, G. C. T. Au-Yeung, E. de-Berardinis, S. Y. Chaw, P. Mhaisalkar, H. Bogireddi, S. Ramakrishna, *Sci. Rep.* **2018**, *8*, 3937.

[141] K. Sullivan, L. Black, *Tissue Eng., Part A* **2015**, *21*, S69-S70.

[142] J. R. Gershlak, L. D. Black, *Exp. Cell Res.* **2015**, *330*, 311-324.

[143] K. M. French, J. T. Maxwell, S. Bhutani, S. Ghosh-Choudhary, M. J. Fierro, T. D. Johnson, K. L. Christman, W. R. Taylor, M. E. Davis, *Stem Cells Int.* **2016**, *2016*.

[144] M. Baghalishahi, S. hasan Efthekhar-vaghefi, A. Piryaei, S. Nematolahi-Mahani, H. R. Mollaei, Y. Sadeghi, *Biochem. Biophys. Res. Commun.* **2018**.

[145] S. Rajabi-Zeleti, S. Jalili-Firoozinezhad, M. Azarnia, F. Khayyatan, S. Vahdat, S. Nikeghbalian, A. Khademhosseini, H. Baharvand, N. Aghdami, *Biomaterials* **2014**, *35*, 970-982.

[146] A. H. Fong, M. Romero-López, C. M. Heylman, M. Keating, D. Tran, A. Sobrino, A. Q. Tran, H. H. Pham, C. Fimbres, P. D. Gershon, *Tissue Eng., Part A* **2016**, *22*, 1016-1025.

[147] T. D. Johnson, S. Y. Lin, K. L. Christman, *Nanotechnology* **2011**, *22*, 494015.

[148] M. Parmaksiz, A. Dogan, S. Odabas, A. E. Elçin, Y. M. Elçin, *Biomed. Mater.* **2016**, *11*, 022003.

[149] W. M. Neethling, G. Strange, L. Firth, F. E. Smit, *Interact. Cardiovasc. Thorac. Surg.* **2013**, *17*, 698-702.

[150] R. M. Wang, K. L. Christman, *Adv. Drug Delivery Rev.* **2016**, *96*, 77-82.

[151] J. M. Singelyn, P. Sundaramurthy, T. D. Johnson, P. J. Schup-Magoffin, D. P. Hu, D. M. Faulk, J. Wang, K. M. Mayle, K. Bartels, M. Salvatore, *J. Am. Coll. Cardiol.* **2012**, *59*, 751-763.

[152] J. W. Wassenaar, R. Gaetani, J. J. Garcia, R. L. Braden, C. G. Luo, D. Huang, A. N. DeMaria, J. H. Omens, K. L. Christman, *J. Am. Coll. Cardiol.* **2016**, *67*, 1074-1086.

[153] S. B. Seif-Naraghi, J. M. Singelyn, M. A. Salvatore, K. G. Osborn, J. J. Wang, U. Sampat, O. L. Kwan, G. M. Strachan, J. Wong, P. J. Schup-Magoffin, *Sci. Transl. Med.* **2013**, *5*, 173ra125-173ra125.

[154] H. E. Mewhort, J. D. Turnbull, H. C. Meijndert, J. M. Ngu, P. W. Fedak, *J. Thorac. Cardiovasc. Surg.* **2014**, *147*, 1650-1659.

[155] H. E. Mewhort, D. A. Svystonyuk, J. D. Turnbull, G. Teng, D. D. Belke, D. G. Guzzardi, D. S. Park, S. Kang, M. D. Hollenberg, P. W. Fedak, *JACC Basic Transl. Sci.***2017**, *2*, 450-464.

[156] H. E. Mewhort, J. D. Turnbull, A. Satriano, K. Chow, J. A. Flewitt, A.-C. Andrei,

D. G. Guzzardi, D. A. Svystonyuk, J. A. White, P. W. Fedak, *J. Heart Lung Transplant.* **2016**, *35*, 661-670.

[157] R. J. Avery, S. Yu, G. Cherukuri, R. B. Runyan, J. Konhilas, Z. I. Khalpey, *ASAIO J.* **2017**.

[158] A. Ferng, A. Connell, M. Nunez, K. Johnson, B. Braunhut, S. Lick, A. Desai, T. Kazui, R. Runyan, Z. Khalpey, *Ann. Thorac. Surg.* **2017**, *104*, e239-e241.

[159] S. Barreto, L. Hamel, T. Schiatti, Y. Yang, V. George, *Cells* **2019**, 8, 1536.

[160] J. Zhang, W. Zhu, M. Radisic, G. Vunjak-Novakovic, *Circulation research* **2018**, 123, 244.

[161] E. Tzahor, K. D. Poss, *Science* **2017**, 356, 1035.

[162] J. Riegler, M. Tiburcy, A. Ebert, E. Tzatzalos, U. Raaz, O. J. Abilez, Q. Shen, N. G. Kooreman, E. Neofytou, V. C. Chen, *Circulation research* **2015**, 117, 720.

[163] X. Qin, J. Riegler, M. Tiburcy, X. Zhao, T. Chour, B. Ndoye, M. Nguyen, J. Adams, M. Ameen, T. S. Denney Jr, *Circulation: Cardiovascular Imaging* **2016**, 9, e004731.

[164] P. Menasché, V. Vanneaux, A. Hagège, A. Bel, B. Cholley, I. Cacciapuoti, A. Parouchev, N. Benhamouda, G. Tachdjian, L. Tosca, *European heart journal* **2015**, 36, 2011.

[165] L. Ye, Y.-H. Chang, Q. Xiong, P. Zhang, L. Zhang, P. Somasundaram, M. Lepley, C. Swingen, L. Su, J. S. Wendel, *Cell stem cell* **2014**, 15, 750.

[166] F. Weinberger, K. Breckwoldt, S. Pecha, A. Kelly, B. Geertz, J. Starbatty, T. Yorgan, K.-H. Cheng, K. Lessmann, T. Stolen, *Science translational medicine* **2016**, 8, 363ra148.

[167] A.-M. Yousefi, P. F. James, R. Akbarzadeh, A. Subramanian, C. Flavin, H. Oudadesse, *Stem cells international* **2016**, 2016.

[168] J. H. van Weerd, V. M. Christoffels, *Development* **2016**, 143, 197.

[169] B. W. Streeter, M. E. Davis, in *Cell Biology and Translational Medicine, Volume 5*, Springer **2018**, p. 1.

[170] M. E. Davis, *Circulation research* **2016**, 119, 1280.

[171] N. Gurusamy, A. Alsayari, S. Rajasingh, J. Rajasingh, in *Progress in molecular biology and translational science*, Vol. 160, Elsevier **2018**, p. 1.

[172] Y. Sawa, Y. Yoshikawa, K. Toda, S. Fukushima, K. Yamazaki, M. Ono, Y. Sakata, N. Hagiwara, K. Kinugawa, S. Miyagawa, *Circulation Journal* **2015**, 79, 991.

[173] M. Latifpour, S. N. Nematollahi-Mahani, M. Deilamy, B. S. Azimzadeh, S. H. Eftekhar-Vaghefi, F. Nabipour, H. Najafipour, N. Nakhaee, M. Yaghoubi, R. Eftekhar-Vaghefi, *Cardiology* **2011**, 120, 9.

[174] E. C. Martinez, D.-T. Vu, J. Wang, S. Lilyanna, L. H. Ling, S. U. Gan, A. L. Tan, T. T. Phan, C. N. Lee, T. Kofidis, *Stem cells and development* **2013**, 22, 3087.

[175] S. Lilyanna, E. C. Martinez, T. D. Vu, L. H. Ling, S. U. Gan, A. L. Tan, T. T. Phan, T. Kofidis, *Tissue Engineering Part A* **2013**, 19, 1303.

[176] J. Mayourian, R. M. Savizky, E. A. Sobie, K. D. Costa, *PLoS computational biology* **2016**, 12, e1005014.

[177] J. Mayourian, Icahn School of Medicine at Mount Sinai, **2018**.

[178] B. W. Streeter, J. Xue, Y. Xia, M. E. Davis, *ACS applied materials & interfaces* **2019**, 11, 18242.

[179] E. Ruvinov, S. Cohen, *Advanced drug delivery reviews* **2016**, 96, 54.

[180] D. Bejleri, B. W. Streeter, A. L. Nachlas, M. E. Brown, R. Gaetani, K. L. Christman, M. E. Davis, *Advanced healthcare materials* **2018**, 7, 1800672.

[181] Y. Duan, Z. Liu, J. O'Neill, L. Q. Wan, D. O. Freytes, G. Vunjak-Novakovic, *J. Cardiovasc. Transl. Res.* **2011**, *4*, 605.

[182] M. Becker, J. A. Maring, M. Schneider, A. X. Herrera Martin, M. Seifert, O. Klein, T. Braun, V. Falk, C. Stamm, *Int. J. Mol. Sci.* **2018**, *19*, 1032.

[183] C. Williams, E. Budina, W. L. Stoppel, K. E. Sullivan, S. Emani, S. M. Emani, L. D. Black III, *Acta Biomater.* **2015**, *14*, 84-95.

[184] S. Pok, I. V. Stupin, C. Tsao, R. G. Pautler, Y. Gao, R. M. Nieto, Z. W. Tao, C. D. Fraser Jr, A. V. Annapragada, J. G. Jacot, *Adv. Healthcare Mater.* **2017**, *6*, 1600549.

[185] K. E. Pourfarhangi, S. Mashayekhan, S. G. Asl, Z. Hajebrahimi, *Biologicals* **2018**, *53*, 10-18.

[186] Y. Efraim, H. Sarig, N. C. Anavy, U. Sarig, E. de Berardinis, S.-Y. Chaw, M. Krishnamoorthi, J. Kalifa, H. Bogireddi, T. V. Duc, *Acta Biomater.* **2017**, *50*, 220-233.

[187] W. L. Stoppel, D. Hu, I. J. Domian, D. L. Kaplan, L. D. Black III, *Biomed. Mater.* **2015**, *10*, 034105.

[188] W. L. Stoppel, A. E. Gao, A. M. Greaney, B. P. Partlow, R. C. Bretherton, D. L. Kaplan, L. D. Black III, *J. Biomed. Mater. Res., Part A* **2016**, *104*, 3058-3072.

[189] G. N. Grover, N. Rao, K. L. Christman, *Nanotechnology* **2013**, *25*, 014011.

[190] A. E. Jakus, M. M. Laronda, A. S. Rashedi, C. M. Robinson, C. Lee, S. W. Jordan, K. E. Orwig, T. K. Woodruff, R. N. Shah, *Adv. Funct. Mater.* **2017**, *27*, 1700992.

[191] J. Jang, H.-J. Park, S.-W. Kim, H. Kim, J. Y. Park, S. J. Na, H. J. Kim, M. N. Park, S. H. Choi, S. H. Park, *Biomaterials* **2017**, *112*, 264-274.

[192] K. Roshanbinfar, J. Hilborn, O. P. Varghese, O. P. Oommen, *RSC Adv.* **2017**, *7*, 31980-31988.

[193] I. T. Ozbolat, M. Hospodiuk, *Biomaterials* **2016**, 76, 321.

[194] V. Mironov, R. P. Visconti, V. Kasyanov, G. Forgacs, C. J. Drake, R. R. Markwald, *Biomaterials* **2009**, 30, 2164.

[195] X. Cui, T. Boland, *Biomaterials* **2009**, 30, 6221.

[196] M. T. Poldervaart, H. Gremmels, K. van Deventer, J. O. Fledderus, F. C. Öner, M. C. Verhaar, W. J. Dhert, J. Alblas, *Journal of controlled release* **2014**, 184, 58.

[197] D. B. Kolesky, R. L. Truby, A. S. Gladman, T. A. Busbee, K. A. Homan, J. A. Lewis, *Advanced materials* **2014**, 26, 3124.

[198] R. Gaebel, N. Ma, J. Liu, J. Guan, L. Koch, C. Klopsch, M. Gruene, A. Toelk, W. Wang, P. Mark, *Biomaterials* **2011**, 32, 9218.

[199] A. L. Nachlas, S. Li, B. W. Streeter, K. J. D. J. Morales, F. Sulejmani, D. I. Madukauwa-David, D. Bejleri, W. Sun, A. P. Yoganathan, M. E. Davis, *Biomaterials* **2020**, 240, 119838.

[200] T. J. Hinton, Q. Jallerat, R. N. Palchesko, J. H. Park, M. S. Grodzicki, H.-J. Shue, M. H. Ramadan, A. R. Hudson, A. W. Feinberg, *Science advances* **2015**, 1, e1500758.

[201] L. Ouyang, R. Yao, Y. Zhao, W. Sun, *Biofabrication* **2016**, 8, 035020.

[202] V. Hosseini, S. Ahadian, S. Ostrovidov, G. Camci-Unal, S. Chen, H. Kaji, M. Ramalingam, A. Khademhosseini, *Tissue Eng. Pt. A* **2012**, 18, 2453.

[203] T. Billiet, E. Gevaert, T. De Schryver, M. Cornelissen, P. Dubruel, *Biomaterials* **2014**, 35, 49.

[204] G. Gao, A. F. Schilling, K. Hubbell, T. Yonezawa, D. Truong, Y. Hong, G. Dai, X. Cui, *Biotechnol. Lett*. **2015**, 37, 2349.

[205] C. Bahney, T. Lujan, C. Hsu, M. Bottlang, J. West, B. Johnstone, *Eur. Cells Mater.* **2011**, 22, 43.

[206] K. S. Lim, B. S. Schon, N. V. Mekhileri, G. C. Brown, C. M. Chia, S. Prabakar, G. J. Hooper, T. B. Woodfield, *ACS Biomater. Sci. Eng.* **2016**, 2, 1752.

[207] I. Noshadi, S. Hong, K. E. Sullivan, E. Shirzaei Sani, R. Portillo-Lara, A. Tamayol, S. R. Shin, A. E. Gao, W. L. Stoppel, L. D. Black III, A. Khademhosseini, N.

Annabi, *Biomater. Sci.* **2017**, 5, 2093.

[208] C. Colosi, S. R. Shin, V. Manoharan, S. Massa, M. Costantini, A. Barbetta, M. R. Dokmeci, M. Dentini, A. Khademhosseini, *Adv. Mater.* **2016**, 28, 677.

[209] K. Hölzl, S. Lin, L. Tytgat, S. Van Vlierberghe, L. Gu, A. Ovsianikov, *Biofabrication* **2016**, 8, 032002.

[210] J. Li, M. Chen, X. Fan, H. Zhou, *J. Transl. Med.* **2016**, 14, 271.

[211] R. Lev, D. Seliktar, *J. R. Soc. Interface* **2018**, 15, 20170380.

[212] A. Blaeser, D. F. Duarte Campos, U. Puster, W. Richtering, M. M. Stevens, H. Fischer, *Adv. Healthc. Mater.* **2016**, 5, 326.

[213] B. Liu, B. W. Lee, K. Nakanishi, A. Villasante, R. Williamson, J. Metz, J. Kim, M. Kanai, L. Bi, K. Brown, *Nat. Biomed. Eng.* **2018**, 2, 293.

[214] A. Chierchia, N. Chirico, L. Boeri, I. Raimondi, G. A. Riva, M. T. Raimondi, M. Tunesi, C. Giordano, G. Forloni, D. Albani, *Eur. J. Pharm. Biopharm.* **2017**, 121, 113.

[215] A. Skardal, S. V. Murphy, K. Crowell, D. Mack, A. Atala, S. Soker, *J. Biomed. Mater. Res. B* **2017**, 105, 1986.

[216] A. Paul, A. Hasan, H. A. Kindi, A. K. Gaharwar, V. T. Rao, M. Nikkhah, S. R. Shin, D. Krafft, M. R. Dokmeci, D. Shum-Tim, *ACS Nano* **2014**, 8, 8050.

[217] M. Stastna, J. E. Van Eyk, *Circ. Genom. Precis. Med.* **2012**, 5, o8.

[218] S. B. Seif-Naraghi, D Horn, P. A. Schup-Magoffin, K. L. Christman, *Acta Biomater.* **2012**, 8, 3695.

[219] S. Sonnenberg, A. A. Rane, C. J. Liu, N. Rao, G. Agmon, S. Suarez, R. Wang, A. Munoz, V. Bajaj, S. Zhang, R. Braden, P. J. Shup-Magoffin, O. L. Kwan, A. N. DeMaria, J. R. Cochran, K. L. Christman, *Biomaterials* **2015**, 45, 56.

[220] B. Trappmann, J. E. Gautrot, J. T. Connelly, D. G. Strange, Y. Li, M. L. Oyen, M. A. C. Stuart, H. Boehm, B. Li, V. Vogel, *Nat. Mater.* **2012**, 11, 642.

[221] C. Williams, E. Budina, W. L. Stoppel, K. E. Sullivan, S. Emani, S. M. Emani, L. D. Black III, *Acta Biomater.* **2015**, 14, 84.

[222] J. K. Nguyen, D. J. Park, J. L. Skousen, A. E. Hess-Dunning, D. J. Tyler, S. J. Rowan, C. Weder, J. R. Capadona, *J. Neural. Eng.* **2014**, 11, 056014.

[223] E. Bassat, Y. E. Mutlak, A. Genzelinakh, I. Y. Shadrin, K. B. Umansky, O. Yifa, D. Kain, D. Rajchman, J. Leach, D. R. Bassat, *Nature* **2017**, 547, 179.

[224] B. Kühn, F. Del Monte, R. J. Hajjar, Y.-S. Chang, D. Lebeche, S. Arab, M. T. Keating, *Nature medicine* **2007**, 13, 962.

[225] A. J. Zollinger, M. L. Smith, *Matrix Biology* **2017**, 60, 27.

[226] R. W. Burgess, W. C. Skarnes, J. R. Sanes, *The Journal of cell biology* **2000**, 151, 41.

[227] A. Kudo, *Cellular and molecular life sciences* **2017**, 74, 4259.

[228] V. V. Patel, L. Zhao, P. Wong, B. B. Pradhan, H. W. Bae, L. Kanim, R. B. Delamarter, *The Spine Journal* **2006**, 6, 397.

[229] T. Coleman, *American Journal of Physiology-Heart and Circulatory Physiology* **1980**, 238, H515.

[230] A. C. Mitchell, P. S. Briquez, J. A. Hubbell, J. R. Cochran, *Acta biomaterialia* **2016**, 30, 1.

[231] R. M. Wang, T. D. Johnson, J. He, Z. Rong, M. Wong, V. Nigam, A. Behfar, Y. Xu, K. L. Christman, *Biomaterials* **2017**, 129, 98.

[232] Y. Y. Lipsitz, N. E. Timmins, P. W. Zandstra, *Nature Biotechnology* **2016**, 34, 393.

[233] B. L. Levine, J. Miskin, K. Wonnacott, C. Keir, *Molecular Therapy-Methods &*

Clinical Development **2017**, 4, 92.

[234] R. Sanz-Ruiz, F. Fernández-Avilés, *Pharmacological research* **2018**, 127, 92.

[235] K. L. March, C. J. Pepine, Am Heart Assoc, 2017.

[236] H. V. Almeida, K. J. Mulhall, F. J. O'Brien, D. J. Kelly, *Journal of Tissue Engineering and Regenerative Medicine* **2017**, 11, 2979.

[237] S. Gurunathan, M.-H. Kang, M. Jeyaraj, M. Qasim, J.-H. Kim, *Cells* **2019**, 8, 307.